GEORG-AUGUST-UNIVERSITÄT
GÖTTINGEN

Master's Thesis

Phasenkohärenz und Intermittenz eines turbulenten Feldes anhand eines Systems gekoppelter Oszillatoren

Phase coherence and intermittency of a turbulent field based on a system of coupled oscillators

prepared by

José-Agustín Arguedas-Leiva

from San José, Costa Rica

at the
Institut für Nichtlineare Dynamik,
Georg-August-Universität Göttingen
&
Max-Planck-Institut für Dynamik und Selbstorganisation

Submitted: 14. November 2017

Supervisor: Dr. Michael Wilczek

First referee: Dr. Michael Wilczek

Second referee: (apl) Prof. Dr. Ulrich Parlitz

Natural things are midway between the knowledge of God and our knowledge; for we receive knowledge from natural things, of which God is the cause by His knowledge. Hence, as the natural objects of knowledge are prior to our knowledge, and are its measure, so the knowledge of God is prior to natural things and is the measure of them; as, for instance, a house is midway between the knowledge of the builder who made it and the knowledge of the one who gathers his knowledge of the house from the house already built.

St. Tomas Aquinas, *Summa Theologiæ*, Part I, Question 14, Article 8.
Translation by the Fathers of the English Dominican Province.

Abstract

Scale-dependent statistics, i.e. intermittency, are a hallmark of fully developed turbulence. In hydrodynamical turbulence this means a transition from Gaussian statistics on large scales to non-Gaussian statistics on small scales. The Fourier modes of a Gaussian random field are statistically independent. Conversely, it has been shown that, under quite general conditions, Fourier modes with random phases produce approximately Gaussian real-space statistics. This motivates the study of intermittency in turbulent fluids as a scale-dependent coherence phenomenon of the Fourier phases.

To better understand this relation between real-space intermittency and spectral-space coherence, a simple but novel coupled oscillator model is proposed. It is reminiscent of the phase-phase coupling present in the spectral space formulation of the Navier-Stokes equations, in which sets of three phases are coupled in so-called triads.

By studying this model we show that the three-oscillator PDFs can be completely identified with their triad PDFs. A convenient parametrization allows for a very good description of each triad's PDF using only one parameter. Using this parameter we can isolate each triad's contribution to real-space skewness. This establishes a relation between three-oscillator coherence phenomena and real-space intermittency.

Keywords: Intermittency, turbulence, coupled oscillators, triads

Contents

Nomenclature

Latin letters

Symbol	Meaning
a_k	Fourier amplitude of the mode k
$C_{k,p}$	Mixture parameter of a WSM parametrized triad PDF
$C_{3\times3}$	Two-triad correlation function
i	Imaginary unit, $\mathrm{i}^2 = -1$
J	Closed part of the triad PDF equation
k_0	Number low-number oscillators set to zero
$K_n(X)$	nth moment of the centered, standardized random variable X
N	Number of oscillators in model
T_i	Member of the $k_0 = 0$ triad basis
T_i^j	Member of the $k_0 = 4$ triad basis
$f(X)$	PDF of the random variable X
$\hat{f}_1$	Fine-grained one-oscillator PDF
f_1	One-oscillator PDF
$\hat{f}_3$	Fine-grained triad PDF
f_3	Triad PDF
$f_{1\times1\times1}$	Three-oscillator PDF
$f_{3\times3}$	Two-triad PDF
$\hat{f}_n^{k,p}$	nth Fourier coefficient of the triad PDF
$r_{k,p}$	Angular parameter of a WSM parametrized triad PDF
$R_{k,p}$	Triad WC first moment parameter
S^1	Circumference of the unit circle
S	Non-closed part of the triad PDF equation

Greek letters

Symbol	Meaning
α	Spectrum steepness
β	Exponential cutoff coefficient
φ_k	Oscillator k
$\varphi_{k,p}$	Triad $\varphi_p + \varphi_{k-p} - \varphi_k$
$\omega_{k,p}$	Model coupling constants
$\tilde{\omega}_{k,p}$	Triad self-coupling coefficient
$\Omega_{k,p,k',p'}$	Triad-triad coupling coefficients

Abbreviations

Abbreviation	Meaning
c.c.	Complex conjugate
FFT	Fast Fourier transform
PDF	Probability density function
WC	Wrapped Cauchy
WSM	Wrapped Stable and Uniform Mixture

1. Introduction

The study of fluids dates back several centuries, and its growth and development has been intimately related with the development of physics and mathematics. Ideas from fluid dynamics have found their use in other areas of physics, which originally were thought to be of a more abstract nature; for example the electromagnetic fields are described with equations whose interpretation resembles one of a flow. On the side of mathematics, analysis, the theory of differential equations, probability theory, and more recently, dynamical systems and chaos have allowed a deeper and better understanding of the phenomena encountered in fluid dynamics.

Despite the progress obtained, there are still many unanswered questions and open problems in this area of research. One aspect of fluid dynamics is its chaotic nature, which we call turbulence. From the fluid theoretical point of view turbulence is characterized by enhanced mixing and strong velocity fluctuations. These extreme events are several orders of magnitude more probable than for a random Gaussian field, and they distinguish turbulence from diffusion. Additionally, a wide range of scales are coupled yielding a complex problem of energy transfer, stability, and predictability of the given flow. Therefore the physics at a certain length scale depends not only on what happens on the same length scale, but also on larger and smaller ones.

In turbulent flows, near-Gaussian statistics are observed at large scales. The small scales, on the other hand, show heavy tails with respect to a Gaussian distribution. The statistics of the field are hence scale dependent [48]. This is known in turbulence under the term of intermittency. The mechanisms for the appearance of intermittency and its properties contain key information on the subtle underlying physics at work in turbulence, and the interaction between different length scales.

A great deal of work has been done in the context of homogeneous isotropic turbulence [21]. This is the study of turbulent fluids whose statistics are invariant under space translations and rotations. The basic equations of a fluid are called the Navier-Stokes equations. The complexity of these equations makes it challenging to prove

or derive results. Additionally, the numerical integration of the Navier-Stokes equations to reproduce highly turbulent velocity fields to high enough resolution presents technical challenges [54]. For this reason, not all questions can be answered by direct numerical simulations, and direct analytic approaches have a restricted applicability. Many aspects of turbulence have also been modeled through simple dynamical models [4, 10, 39], yielding simplified tractable systems where certain aspects or properties of turbulence are reproduced and can be more easily understood. A full understanding of intermittency and the mechanism generating non-Gaussianity in turbulence remains unresolved. The latter strategy will be followed here, whereby a simplified model for intermittency and its relation to Fourier phase statistics will be studied.

1.1. Intermittency and Fourier phases

Real-space quadratic non-linearities take in spectral space the form of three Fourier mode interaction. Three modes interacting in such a way are called triads. As we will see, on account of the quadratic non-linearity present in the Navier-Stokes equations, the Fourier phases are coupled in triads [16]. Gaussian fields may also be represented in spectral space. All the Fourier phases of a Gaussian field are statistically independent. The strategy for obtaining the real-space statistics from the spectral space statistics relies on the central limit theorem [29]. Nevertheless, this argument need not apply if the spectrum is too steep. In turbulent fields governed by the Navier-Stokes equations, every phase is statistically uniformly distributed and every pair of Fourier phases are uncorrelated. Turbulent fields shown steep enough spectra, so that the central limit theorem argument no longer applies. Hence, although pairs of phases are uncorrelated, turbulent fields have non-trivial real-space statistics. Additionally, the triad coupling produces more complicated higher-order Fourier phase statistics. Therefore, departure from Gaussianity of turbulent fields can be studied in spectral space.
In a recent direct numerical simulation study [58], the emergence of non-Gaussianity from Gaussian initial conditions was revisited. The authors analyzed the single-point statistics for the velocity field and its vorticity field. A rapid development of non-Gaussianity at small-scale statistics was observed, while the velocity statistics themselves remained close to Gaussian. The authors complemented this observation of the real-space statistics with snapshots of phases of the velocity field's Fourier

coefficients. It was observed that Fourier phases in the high wave-number regime present certain coherent events.
Similar coherence events have been observed in two-dimensional turbulent simulations [49] and numerical studies have been done on the triads' role in forced three-dimensional turbulence [20, 40, 55]. Additionally, analytic reformulations of Navier-Stokes equations in spectral space have been recently proposed [16]. These aim at simplifying the study of triad interactions in turbulent fields, easing the derivation of exact results, and deepening the understanding of the role triads play in the dynamics of turbulent fields. Nevertheless, the question of Fourier phases' statistics exact influence in real-space statistics is a still rather unexplored research question. The rapid transition to non-Gaussianity at the small scales and the coherent events of the high wave-number Fourier phases raise the question of which dynamical effect these phases and their statistics have in the generation of non-Gaussianity. This motivates the study of intermittency as a scale-dependent phase correlation phenomenon.
The authors in [58] propose a phase model inspired by the structure of the Navier-Stokes spectral formulation. This model leaves the amplitudes of the Fourier modes constant and concentrates on the phase dynamics. Simplifying from the considerably more complex Navier-Stokes dynamics, this toy model aims to reproduce the dynamical phenomena of the Fourier phases whilst yielding an at least partially tractable model. Interpreting the Fourier phases as a system of coupled oscillators opens the door for ideas and methods already developed in this area. Studying this phase toy model is the goal of the current thesis.

1.2. Coupled oscillators and synchronization

Oscillators have been used extensively in physics as a first step in understanding physical phenomena. From clocks to atoms, many systems are idealized or abstracted to simple oscillators which, retain the relevant physical behavior whilst yielding a much simpler formulation of the original problem. The basic oscillator studied in physics is the harmonic oscillator. It follows the equation of motion

$$\frac{\mathrm{d}^2 x(t)}{\mathrm{d}t^2} = -\omega^2 x(t). \tag{1.1}$$

A system subject to this equation oscillates with frequency ω in time. Once the basic problems have been understood, more complex systems and phenomena can be tackled by generalizing this oscillator. The next step is introduce a viscous term of the form $\propto \mathrm{d}x(t)/\mathrm{d}t$, which dissipates energy. More and more complex phenomena can be described by subsequent generalizations of the harmonic oscillator. Consequently, these become more difficult to solve and understand.
There are, however, other ways to describe complex phenomena without indefinitely complicating the oscillator's equations of motion. A way to do this is to study an ensemble of coupled oscillators. One behavior which can be studied in such systems is synchronization.
Many simple constituents put together may show non-trivial phenomena when coupled to one another, by changing the system size or when some of the system's parameter changes. These systems are sometimes composed of rather simple individual elements with simple defining and evolution equations. Synchronization therefore appears as a property of the system. It is an ubiquitous phenomenon in physics [47], whereby whole systems or parts of systems dynamically evolve into coherent states.
Given the complexity of most physical systems, it is necessary to find simplified models which, however, reproduce the characteristics of the more complex system. This is where coupled oscillators come into play; without indefinitely complicating the equations of motions of oscillators, but rather coupling many of them together, complex phenomena may be studied. A major advance in this direction is due to Kuramoto, who proposed a model, which later took his name [31]. This model consists of a set of N globally coupled oscillators $\varphi_k(t)$. These oscillators follow the equations of motion

$$\frac{\mathrm{d}\varphi_k(t)}{\mathrm{d}t} = \omega_k + \frac{K}{N}\sum_{p=1}^{N}\sin(\varphi_k(t) - \varphi_p(t))\,, \quad k = 1, ..., N. \tag{1.2}$$

The ω_k are the natural frequencies of the oscillators, and K is a coupling constant. In this context, the idea of a mean field was introduced to better understand the dynamics of the system as a whole. Let the mean field $\mathbf{R} \in \mathbb{C}$ be defined as

$$\mathbf{R}(t) = R(t)\exp[\mathrm{i}\Phi(t)] := \frac{1}{N}\sum_{p=1}^{N}\exp[\mathrm{i}\varphi_p(t)], \;\; R, \Phi \in \mathbb{R}. \tag{1.3}$$

With this mean field, the dynamics of the system can be rewritten as

$$\frac{\mathrm{d}\varphi_k(t)}{\mathrm{d}t} = \omega_k + K\, R(t)\, \sin(\varphi_k(t) - \Phi(t)) \quad k = 1, ..., N. \tag{1.4}$$

This model has been intensely studied and among the most notable results is the existence of a phase transitions [7]. That is, there is a critical value K_C of the coupling, such that for $K > K_C$ the system synchronizes after time evolution $R \to 1^-$. For values lower than the critical value the system remains uniformly distributed $R \sim 0$. After this model was understood well enough, several variations have appeared [52]. These aim at deepening the understanding of coupled oscillator systems in general and broadening the scope of physical phenomena which can be modeled by them. For the case of ensembles of identical and usually globally coupled oscillators many interesting phenomena have been explored. For example, the appearance and transition to synchronization [56] or quasi-periodic phenomena [50].

One major advance in the study of coupled oscillators was achieved with the Ott & Antonsen ansatz [42]. This ansatz was proposed for the Kuramoto model in the thermodynamic limit $N \to \infty$. In this limit the distribution of oscillators is described by a probability density function (PDF). The authors then propose a parametrization for the system's PDF. This parametrization is equivalent to the so-called Wrapped Cauchy (WC) distribution. With this ansatz, the PDF is parametrized through one complex variable. This parameter is the equivalent of the finite-N order parameter, and is hence also denoted $\mathbf{R}$. The authors find that the dynamics of the $N \to \infty$ Kuramoto model is contained in a two-dimensional manifold parametrized by this complex variable. The time evolution of the system's PDF can be reduced to the dynamics of the parameter $\mathbf{R}$. By studying this parameter they recover the existence of a phase transition.
This method of analyzing the thermodynamic limit and parametrizing the PDF as a WC distribution is referred to as the Ott & Antonsen ansatz. It has proved to be an useful tool in investigating systems of coupled oscillators. This ansatz has found its place as a standard tool in this research area. Many different results have been derived using this method. For example, results regarding the underlying mathematical properties [17, 28, 36], the study of heterogeneous oscillator systems [1, 32], and turbulent like behavior [59] have been some of the areas where this ansatz has been used.

The main reason this ansatz works, is that it correctly parametrizes the low-dimensional behavior of many coupled oscillator systems. This low-dimensionality is related to the appearance of synchronization phenomena [45]. Additionally, one of their major achievements is that this ansatz is applicable to systems of non-identical oscillators.
To our knowledge, the Ott & Antonsen ansatz brought the WC distribution into the context of oscillators and synchronization. Although some of the assumptions used in the Ott & Antonsen ansatz will not apply to the oscillator system we study here[1], the introduction of the WC distribution leads to the topics of circular statistics and circular distributions. This is the correct concept for studying cyclic variables, of which complex Fourier phases, our oscillators, are a part of.
The complexity of the systems where these methods have been applied has iteratively increased [46]. Nevertheless, this complexity has not yet reached the one encountered in the model to be studied here. For example, to our knowledge, a Kuramoto-like system with triad interaction has never before been studied. In this work a novel type of systems of coupled oscillators is presented. They are of relevance for dynamics stemming from any quadratic non-linearity. This addition should further enrich the reciprocal transfer of ideas and methods from the fields of coupled oscillator systems and turbulence research.

1.3. Thesis outline

Here we will derive and study the coupled oscillator model proposed in [58]. For this, basic ideas and tools of statistics and turbulence will be developed in chapters 2 and 3. Afterwards the derivation of the model itself and its properties will be presented in chapter 4. Subsequently in chapter 5, the phase dynamics and their statistics will be numerically explored. With knowledge of the oscillator statistics, real-space statistics will be discussed in chapter 6. Finally, summary, conclusions, and outlook will be presented in section 7.
The first appendix A presents relevant details of the numerical implementation. In appendices B and C two oscillator systems will be presented. Firstly a simple cosine model, and secondly an ensemble of Josephson junctions. Probability density functions can be derived for these systems. Their similarity to our coupled oscillator

[1] For example, oscillator statistical independence can be explicitly proven in the Kuramoto model [2].

model will be useful when motivating a starting point for a theory of the three-oscillator statistics. The necessary derivations and exposition do not adequately pass in the main text, and are hence presented in these small appendices.

2. Statistical tools

The dynamics of a turbulent velocity field are chaotic in nature, i.e. they show sensitive dependence on initial conditions [34]. As a consequence, the state of the system cannot be precisely predicted after time evolution. One can only speak of probabilities of the events. It is therefore convenient to regard the velocity field $\mathbf{v}(t, \mathbf{x})$ of a turbulent fluid as a random variable [21].
This statistical approach to turbulence requires developing some basic tools, which we will do in section 2.1 for random variables taking values in $\mathbb{R}$, i.e. linear random variables. More concretely, these will allow for a quantitative description of intermittency in turbulence. This will be carried out in the next chapter.
In the present work we will also treat variables which are cyclic in nature and evolve in chaotic dynamics, i.e. the coupled oscillator model. One therefore also treats these oscillators as random variables. Specific tools will be presented for these circular random variables in sections 2.2 and 2.3.

2.1. Linear statistics

Let X be a real random variable and $x \in \mathbb{R}$ belong to its sample space. X could be, for example, a component or the magnitude of a turbulent velocity field $\mathbf{v}(t, \mathbf{x})$. The random variable X is fully characterized by a probability density function (PDF) $f(x)$. Two random variables with the same PDF are therefore said to be statistically identical. Axiomatically, a PDF is derived from the cumulative distribution function $F(x)$ of a given random variable [48] and it has the following defining properties

- $f(x) := \dfrac{\mathrm{d}F(x)}{\mathrm{d}x}$;
- $f(x) \geq 0 \quad \forall x \in \mathbb{R}$;
- $\displaystyle\int_{\mathbb{R}} \mathrm{d}x\, f(x) = 1.$

The expectation value of a random variable can be calculated from its PDF as

$$\langle X \rangle = \int_{\mathbb{R}} \mathrm{d}x \, f(x) \, x. \tag{2.1}$$

This is a weighted average over all possible values of X. Similarly the expectation value of a function of the random variable $H(X)$ can be obtained as

$$\langle H(X) \rangle = \int_{\mathbb{R}} \mathrm{d}x \, f(x) \, H(x). \tag{2.2}$$

The expectation value is said to exist only if these integrals absolutely converge. The expectation value of a complex exponential is of great interest. It can be cast into the form of a Fourier transform of the PDF

$$\hat{f}(k) := \int_{\mathbb{R}} \mathrm{d}x \, f(x) \, \exp[\mathrm{i}kx] \equiv \langle \exp[\mathrm{i}kX] \rangle. \tag{2.3}$$

This function $\hat{f}$ is called the "characteristic function of f". It can be used to simplify derivations and proofs. Additionally, expectation values can be recast as derivatives on $\hat{f}$; the statistical information contained in f is also contained in $\hat{f}$.
The expectation value of X^n is called the nth moment of X. It can be obtained from the PDF itself as a weighted average or from its characteristic function as a derivative

$$\left. \frac{\mathrm{d}^n \hat{f}(k)}{\mathrm{d}(\mathrm{i}k)^n} \right|_{k=0} = \int_{\mathbb{R}} \mathrm{d}x \, f(x) \, x^n \equiv \langle X^n \rangle. \tag{2.4}$$

The mean $\langle X \rangle$ of X is the first moment. Through a redefinition, the random variable can be made to have first moment equal to zero

$$X \to \tilde{X} = X - \langle X \rangle. \tag{2.5}$$

$\tilde{X}$ is known as a centered random variable. $\tilde{X}$ is useful for looking into the fluctuations of X around its mean. The second moment of $\tilde{X}$ is known as the variance

$$\sigma_X^2 = \langle \tilde{X}^2 \rangle = \int_{\mathbb{R}} \mathrm{d}x \, f(x) \, (x - \langle X \rangle)^2. \tag{2.6}$$

σ_X is known as the standard deviation of X and measures dispersion around the mean. With the standard deviation a standardized centered variable $\hat{X}$ can be

defined as

$$\hat{X} := \frac{\tilde{X}}{\sigma_X} = \frac{X - \langle X \rangle}{\sigma_X}. \tag{2.7}$$

This standardized variable has first moment zero and second moment one. We will denote the moments of $\hat{X}$ as

$$K_n(X) := \langle \hat{X}^n \rangle = \frac{\langle (X - \langle X \rangle)^n \rangle}{\langle (X - \langle X \rangle)^2 \rangle^{n/2}}. \tag{2.8}$$

This process of centering and standardizing a random variable yields the correct context for comparing different statistical processes. All standardized and centered random variables have per definition the same first two moments. Deviations in higher moments therefore serve to differentiate between types of random variables. The third moment of $\hat{X}$ is known as the skewness of X

$$K_3(X) = \langle \hat{X}^3 \rangle = \frac{\langle (X - \langle X \rangle)^3 \rangle}{\langle (X - \langle X \rangle)^2 \rangle^{3/2}}. \tag{2.9}$$

The fourth moment of $\hat{X}$ has the name flatness. It is given by

$$K_4(X) = \langle \hat{X}^4 \rangle = \frac{\langle (X - \langle X \rangle)^4 \rangle}{\langle (X - \langle X \rangle)^2 \rangle^2}. \tag{2.10}$$

We will shortly introduce the Gaussian or normal distribution. This distribution is extensively used in statistics. The skewness and flatness receive special attention, because they are frequently used to measure departure of a distribution from Gaussianity. Higher-order moments can also be used, but obtaining accurate high-order statistics is experimentally difficulty. The higher the statistics one is interested in, the bigger the sample size must be. That is, very large samples obtained under similar conditions are necessary to ensure convergence to the expected value. This means that the theory tries to work with the lower-order moments as extensively as possible.

2.1.1. Gaussian distribution

In probability theory, the Gaussian or normal distribution occupies a central role. On the one hand, its importance stems from the central limit theorem. This theorem states that, under certain conditions, averages of observations of random variables taken from different independent processes will converge to a Gaussian distribution

[48].
In physics one encounters this situation often. For example, molecular uncertainty or the error addition in an experiment follow a normal distribution. In the context of fluid dynamics the statistics of a velocity field can be analyzed in a similar way. If it is driven by independently occurring events, i.e. a spatially and temporally uncorrelated field, its statistics are normally distributed.
A random variable X is said to be normal or Gaussian if its PDF has the form [3]

$$f(x) = \frac{1}{(2\pi\sigma^2)^{1/2}} \exp\left[\frac{-(x-\mu)^2}{2\sigma^2}\right]. \tag{2.11}$$

This distribution has mean $\langle X \rangle = \mu$ and standard deviation $\sigma_X = \sigma$. Its characteristic function (2.3) can be explicitly calculated and takes the form

$$\hat{f}(k) = \exp\left[\mathrm{i}\mu k - \frac{(\sigma k)^2}{2}\right]. \tag{2.12}$$

All moments of a Gaussian distribution exist. They are fixed by the mean and variance, and are given by (2.4). Most notably, a Gaussian distribution has zero skewness and a flatness equals to three.

2.2. Circular statistics

In the previous section we introduced basic tools and notions in the context of statistics of linear random variables. We will now do the same for circular random variables. These circular random variables are statistical processes, which are periodic in nature. They may then be rescaled, so that the probability is completely contained in the circumference of a unit circle S^1. The cyclic nature of these random variables requires special treatment, as will be shown in the following example.
Applications where cyclic variables appear are, e.g., statistics of directions, angles, and events happening at different times of the day. The time of the day 23:45 is just as far away from midnight 00:00 as the time 00:15. One would, therefore, intuitively expect their mean to be midnight. A quick calculation yields, however, the time 12:00 as their mean. On the other hand, the mean would give the correct result if our sample were the times 11:45 and 12:15. Correspondingly, where we place the zero (midnight) has an effect on the statistics. This is only an issue because of the cyclic nature of the hours of the day. With larger more irregularly distributed data

sets choosing the zero will be an issue, as well as unequivocally defining their mean and higher moments.
Specific tools need to be set in place to handle these cyclic variables so that, for example, the means and other moments be the same if we take values over $[0, 2\pi)$ or over $[-\pi, \pi)$. This will be done in the next section. Other aspects present in linear statistics will also be derived for these circular statistics, such as characterizing a random variable by its PDF or its characteristic function. Finally, the subsequent section will introduce two concrete circular distributions useful for the current work. We will follow the nomenclature and ideas as they are presented in [27].

2.2.1. Cyclic variables

Let φ be a random variable yielding values in S^1. Let us take a set of measurements $\{\varphi_i\}$ of the random variable. The first quantity of interest is the mean or preferred direction of the random variable φ. As mentioned in the previous section the cyclic nature of φ renders the arithmetic mean inadequate. With the application of oscillators in mind, let us instead define a mean field $\mathbf{R} \in \mathbb{C}$ as

$$\mathbf{R} = R \exp[\mathrm{i}\Phi] := \sum_i \exp[\mathrm{i}\phi_i]. \tag{2.13}$$

The circular mean direction $\overline{\varphi}$ is then the angle argument of $\mathbf{R}$

$$\overline{\varphi} = \arg[\mathbf{R}] = \Phi. \tag{2.14}$$

Consider additionally, that the same set of measurements is taken on two different conventions for the position of the zero. These two conventions are rotated by δ with respect to one another. The two means $\mathbf{R}$ and $\mathbf{R}'$ are then also related by a rotation by δ

$$\mathbf{R}' = \sum_i \exp[\mathrm{i}(\phi_i + \delta)] = \exp[\mathrm{i}\delta]\mathbf{R}. \tag{2.15}$$

With this definition for the mean, the cyclic nature of φ is explicitly implemented. The mean $\mathbf{R}$ is known as the first trigonometric moment. It plays a fundamental role in circular statistics. In physics similar definitions have been used in the study of synchronization of oscillators, most notably in the Kuramoto model [31].
We will now introduce the concept of PDF for circular random variables. Just as for linear random variables, a circular random variable is fully characterized by its

circular PDF.

2.2.2. Circular PDF

Consider a circular random variable with a corresponding PDF. We will focus on continuous random variables and circular distributions. These are continuous functions $f(\phi)$ in S^1 and have the following properties

- $f(\phi) \geq 0$;
- $\int_{S^1} \mathrm{d}\phi\, f(\phi) = 1$;
- $f(\phi) = f(\phi + 2\pi n),\ \forall\, n \in \mathbb{Z}$.

For linear real random variables the PDF can be obtained from a characteristic function, i.e. its Fourier transform. For a cyclic variable φ, however, the situation is different. Following the definition used for a linear variable (2.3), the circular characteristic function $\hat{f}(k)$ is given by

$$\hat{f}(k) = \frac{1}{2\pi} \int_{S^1} \mathrm{d}\phi\, f(\phi)\ \exp[\mathrm{i}k\phi] \equiv \frac{1}{2\pi} \langle \exp[\mathrm{i}k\phi] \rangle. \tag{2.16}$$

Moreover, as a consequence of the periodicity of f

$$\hat{f}(k) \stackrel{!}{=} \exp[2\pi \mathrm{i}k]\ \hat{f}(k) \Rightarrow k \in \mathbb{Z}. \tag{2.17}$$

That is, the characteristic function is only non-zero at integer values for k. That is, on account of the periodicity of f, its Fourier transformation is its Fourier series. We will denote the Fourier coefficients $\hat{f}_n$ using the characteristic function as $\hat{f}_n := 2\pi f(n)\ \forall n \in \mathbb{Z}$. The normalization of $f(\phi)$ implies that

$$\hat{f}(0) = \frac{1}{2\pi} \Rightarrow \hat{f}_0 = 1. \tag{2.18}$$

The reality of $f(\phi)$ implies that the characteristic function is invariant under complex conjugation and inversion $k \to -k$, i.e.

$$\hat{f}(k) = \overline{\hat{f}(-k)}. \tag{2.19}$$

This leads us to the most general form of a circular PDF in terms of its Fourier series given by

$$f(\phi) = \frac{1}{2\pi}\left[1 + \sum_{n\in\mathbb{N}} \hat{f}_n \ \exp[-\mathrm{i}\phi n] + \text{c.c.}\right]. \tag{2.20}$$

Recall that the Fourier coefficients are the values of the characteristic function (2.16) at $k \in \mathbb{Z}$. These values play a special role in the theory, and are called the trigonometric moments of $f(\phi)$. For example, the mean of a circular random variable as a continuous version of equation (2.13) is its first trigonometric moment, i.e.

$$\mathbf{R} = \langle \exp[\mathrm{i}\varphi] \rangle = \hat{f}_1. \tag{2.21}$$

By virtue of de Moivre's formula all powers of trigonometric moments can be rewritten in terms the trigonometric moments. The characteristic function, i.e. the Fourier coefficients, of a circular PDF therefore contains all the statistical information of a cyclic random variable. This establishes the similarity between linear and circular PDFs and their corresponding characteristic functions.

2.3. Circular distributions

In the previous sections we introduced tools for working with circular statistical processes. Here we will present circular distributions useful in the present work and discuss some of their properties. We still follow [27].

2.3.1. Uniform distribution

A distribution which has no preferred direction is called an uniform distribution and it is given by

$$f(\phi) = \frac{1}{2\pi} \quad \phi \in [0, 2\pi). \tag{2.22}$$

The preferred direction of a circular statistical process is usually given by its first trigonometric moment, i.e. its mean. If the first moment is zero, one then usually looks at the next highest non-vanishing moment. Because the argument of the number zero $\arg(0 = z \in \mathbb{C})$ is not defined and all trigonometric moments of this distribution are zero, it follows that the distribution has no preferred direction.

2.3.2. Wrapped distributions

One method for generating circular distributions is known as wrapping. A circular random variable φ may be obtained from a linear random variable X by taking the linear variable modulo 2π. This is equivalent to wrapping the real line around the unit circle. Let g be a linear PDF. Then a circular PDF f is obtained from g through

$$f(\phi) = \sum_{n\in\mathbb{Z}} g(\phi + 2\pi n) \quad \phi \in [0, 2\pi). \tag{2.23}$$

The Fourier coefficients of the circular PDF f are related to the characteristic function of the linear PDF. Let $\hat{g}$ be the characteristic function of g given by

$$\hat{g}(k) = \int_{\mathbb{R}} \mathrm{d}x \exp[\mathrm{i}kx] g(x). \tag{2.24}$$

The relation between the characteristic function and the trigonometric moments may be derived as follows. Take the characteristic function of the circular PDF (2.16) and use the definition of the linear characteristic function (2.24), then plug this into the formula for the wrapping (2.23). This yields the following relation between both characteristic functions

$$\begin{aligned} \hat{f}_k \quad = 2\pi \hat{f}(k) \quad &= \int_{S^1} \mathrm{d}\phi \, f(\phi) \exp[\mathrm{i}k\phi] \\ &= \sum_{n\in\mathbb{Z}} \int_{S^1} \mathrm{d}\phi \, g(\phi + 2\pi n) \exp[\mathrm{i}k\phi] \\ &= \int_{\mathbb{R}} \mathrm{d}\phi \, g(\phi) \exp[\mathrm{i}k\phi]. \end{aligned} \tag{2.25}$$

In short

$$\hat{f}_k = 2\pi \hat{f}(k) = \hat{g}(k). \tag{2.26}$$

Wrapping therefore transfers some of the statistical properties of the linear random variable to the circular one. Namely, the value of the linear characteristic function $\hat{g}(k)$ at integer k fixes the corresponding trigonometric moments $\hat{f}_k$ of the wrapped circular PDF.

2.3.3. Wrapped Cauchy (WC) distribution

On the real line $x \in \mathbb{R}$ the Cauchy distribution $g_{\mathbf{R}}$ can be parametrized as

$$g_{\mathbf{R}}(x) = \frac{1}{\pi} \frac{-\log R}{(\log R)^2 + (x - \Phi)^2}, \quad \mathbf{R} = R \exp[\mathrm{i}\Phi]. \tag{2.27}$$

The Cauchy distribution has characteristic function $\hat{g}_{\mathbf{R}}$ given by

$$\hat{g}_{\mathbf{R}}(k) = R^{|k|} \exp[\mathrm{i}\Phi k]. \tag{2.28}$$

This linear distribution can be wrapped to produce a circular one. Wrapping $g_{\mathbf{R}}$ as in (2.23) yields a circular PDF known as the Wrapped Cauchy (WC) distribution. The WC distribution then takes the form

$$f_{\mathbf{R}}(\phi) = \frac{1}{2\pi} \left[1 + \sum_{n \in \mathbb{N}} \mathbf{R}^n \exp[-\mathrm{i}n\phi] + \text{c.c.} \right]. \tag{2.29}$$

After wrapping $g_{\mathbf{R}}$, the first trigonometric moment of the resulting circular PDF $f_{\mathbf{R}}$ is $\mathbf{R}$. To ensure convergence the condition $R < 1$ is necessary. The sum can be carried out explicitly as a geometric series. The resulting form yields

$$\begin{aligned} f_{\mathbf{R}}(\phi) &= \frac{1}{2\pi} \left[1 + \frac{\mathbf{R} \exp[-\mathrm{i}\phi]}{1 - \mathbf{R} \exp[-\mathrm{i}\phi]} + \text{c.c.} \right], \\ f_{\mathbf{R}}(\phi) &= \frac{1}{2\pi} \frac{1 - R^2}{1 + R^2 - 2R\cos(\Phi - \phi)}. \end{aligned} \tag{2.30}$$

The WC distribution is symmetric with respect to Φ, i.e. $f_{\mathbf{R}}(\Phi + \phi) = f_{\mathbf{R}}(\Phi - \phi) \forall \phi$. Using equation (2.30) we consider its at extrema

$$\frac{\mathrm{d} f_{\mathbf{R}}(\phi)}{\mathrm{d}\phi} \stackrel{!}{=} 0 \Rightarrow \phi = \Phi, \Phi + \pi. \tag{2.31}$$

The concavity at the extrema will define if they are a maximum or minimum

$$\begin{aligned} \left. \frac{\mathrm{d}^2 f_{\mathbf{R}}(\phi)}{\mathrm{d}\phi^2} \right|_{\phi=\Phi} &= \frac{-R}{\pi (1 - R)^2} < 0, \qquad \forall R \in [0, 1), \\ \left. \frac{\mathrm{d}^2 f_{\mathbf{R}}(\phi)}{\mathrm{d}\phi^2} \right|_{\phi=\Phi+\pi} &= \frac{R}{\pi} \frac{1 - R}{(1 + R)^3} > 0, \quad \forall R \in [0, 1). \end{aligned} \tag{2.32}$$

The distribution is therefore unimodal and it accumulates at $\phi = \Phi$. This means it has only Φ as a preferred direction. The role of R is further understood by taking the ratio of f at its maximum and minimum

$$\frac{f_{\mathbf{R}}(\Phi)}{f_{\mathbf{R}}(\Phi + \pi)} = \left(\frac{1+R}{1-R}\right)^2 . \tag{2.33}$$

$R = 0$ corresponds to an uniform distribution, as can also be seen from (2.29). A higher value of R means a more peaked PDF around Φ. As will be shortly seen, the limit $R \to 1^-$ leads to a δ-distribution.

Note that the parameters Φ and R correspond to the angle argument and magnitude of the first trigonometric moment $\mathbf{R} = \hat{f}_1$. Additionally, all higher trigonometric moments are given through this first moment by the relation $\hat{f}_n = \hat{f}_1^n = \mathbf{R}^n$. As expected for wrapped distributions (2.26), the trigonometric moments of the circular variable correspond to the characteristic function of the linear variable (2.28) at $k \in \mathbb{Z}$.

Another remarkable property of the WC distribution is that it is α-stable, i.e. its functional form is invariant under convolution with another WC distribution. Let $f_{\mathbf{R}_f}$ and $h_{\mathbf{R}_h}$ be WC distributions with first moments $\mathbf{R}_f$ and $\mathbf{R}_h$, respectively. Their convolution can be computed using their series form (2.29). This yields

$$\begin{aligned}
(f_{\mathbf{R}_f} * h_{\mathbf{R}_h})(\phi) &= \int_{S^1} \mathrm{d}\theta \, f_{\mathbf{R}_f}(\theta) \, h_{\mathbf{R}_h}(\phi - \theta) \\
&= \frac{1}{2\pi} \left[1 + \sum_{n \in \mathbb{N}} \sum_{m \in \mathbb{N}} \mathbf{R}_f^n \mathbf{R}_h^m \exp[-\mathrm{i}m\phi] \delta_{m,n} + \text{c.c.} \right] \\
&= \frac{1}{2\pi} \left[1 + \sum_{n \in \mathbb{N}} (\mathbf{R}_f \mathbf{R}_h)^n \exp[-\mathrm{i}n\phi] + \text{c.c.} \right] .
\end{aligned} \tag{2.34}$$

Therefore, a convolution of two WC distributions yields another WC distribution. The first moment of the resulting distribution $\mathbf{R}_{f*h}$ is the product of the first moments of the original distributions, i.e. $\mathbf{R}_{f*h} = \mathbf{R}_f \mathbf{R}_h$. Finally, because convergence of the original sums requires that $R_f < 1$ and $R_h < 1$, it follows that $R_{f*h} < 1$. This ensures convergence of the resulting sum to a WC distribution.

Poisson kernel

Consider the WC distribution given in the series form (2.29). In the limit $R \to 1^-$ this expression is known as the Poisson kernel, i.e., it is an integral kernel to solve the two-dimensional Laplace equation with Dirichlet boundary conditions on the unit disc $\mathbb{D}$ [5]. It is known[1] that equation (2.29) being a sum of orthogonal functions converges in the limit $R \to 1^-$ in the sense of distributions to a δ-distribution

$$\lim_{R\to 1^-} f_{\mathbf{R}}(\phi) = \delta(\phi - \Phi). \tag{2.35}$$

Let g be a Lebesgue integrable function on the boundary of the unit disc, $g \in \mathbb{L}^1(\partial\mathbb{D})$. Let u be a function in the unit disc $\mathbb{D}$ given by

$$u(\mathbf{R}) = \int_{\partial\mathbb{D}} \mathrm{d}\phi f_{\mathbf{R}}(\phi) g(\exp[\mathrm{i}\phi]). \tag{2.36}$$

Then $u(\mathbf{R})$ is harmonic in $\mathbb{D}$ and given (2.35) it fulfills the boundary condition

$$\lim_{R\to 1^-} u(\mathbf{R}) = g(\exp[\mathrm{i}\Phi]).$$

Recall circular PDFs can be used to compute ensemble averages of circular random variables. For example, a function h of a circular random variable φ has the expected value

$$v(\mathbf{R}) := \int_{S^1} \mathrm{d}\phi \, f_{\mathbf{R}}(\phi) \, h(\phi) \equiv \langle h(\varphi) \rangle. \tag{2.37}$$

By comparing this equation with equation (2.36) it is clear, that ensemble averages of a function h over circular random variables distributed as a WC distribution are analytic in $\mathbf{R}$.

2.3.4. Wrapped Stable and Uniform Mixture (WSM)

The WC distribution is not the most general α-stable distribution. It nevertheless provides a good starting point for modeling the functional form of circular PDFs. More general functional forms of α-stable distributions become however too complicated and intractable [27]. One therefore looks for simple generalizations of this distribution. This may be easily done by combining the WC distribution, with first moment $\mathbf{r} = r \exp[\mathrm{i}\Phi] \in \mathbb{C}$, with the uniform distribution. This introduces an additional parameter $C \in \mathbb{R}$, which yields a more general distribution, which is

[1] See e.g. in [3] exercise 14.3.11.

still α-stable, as will be shown below. This Wrapped Stable and Uniform Mixture distribution (WSM) can be parametrized as

$$f_{C,\mathbf{r}}(\phi) = \frac{1}{2\pi}\left[1 + C\sum_{n\in\mathbb{N}}\mathbf{r}^n \exp[-in\phi] + \text{c.c.}\right]. \tag{2.38}$$

We will call C the mixture parameter. C controls the relative weight of the angular part with respect to the uniform part. The sum can be carried out just like for the WC distribution. This yields

$$f_{C,\mathbf{r}}(\phi) = \frac{1-C}{2\pi} + \frac{C}{2\pi}\frac{1-r^2}{1+r^2-2r\cos(\Phi-\phi)}. \tag{2.39}$$

Looking for extrema and studying their concavity follows like in the case of the WC distribution. For $C > 0$, the result is the same. The WSM distribution is unimodal, symmetric around Φ, with maximum at Φ and minimum at $\Phi + \pi$. In the case of $C < 0$ the maximum and minimum are swapped. To ensure that $f_{C,\mathbf{r}}$ is a positive function, the condition

$$\frac{r-1}{2r} \leq C \leq \frac{r+1}{2r} \tag{2.40}$$

must be imposed. A modified version of the Poisson kernel result also applies here: Expectation values are also analytic in $\mathbf{r}$.

The α-stability of the WSM distribution is easily verifiable using (2.38). Let $f_{C_f,\mathbf{r}_f}$ and $h_{C_f,\mathbf{r}_h}$ be WSM distributions. Convolving them yields another WSM distribution, namely $g_{C_fC_h,\mathbf{r}_f\mathbf{r}_h} = (f_{C_f,\mathbf{r}_f} * h_{C_f,\mathbf{r}_h})$.

Further generality could be introduced by taking the case $C \in \mathbb{C}$. Most notably this would break the reflection symmetry around $\phi = \Phi$. In the present work, however, $C \in \mathbb{R}$ provides the sufficient generalitz framework for modeling circular PDFs, and we will therefore remain on the level of generality supplied by the WSM distribution. For mathematical literature on statistics and fits using this distribution we refer the reader to [44, 51].

3. Basic notions of turbulence

In this section we will present basic notions of Navier-Stokes turbulence. General properties and the phenomenon of intermittency will be presented. In depth treatment and results can be found in the literature, such as in [21, 48]. Additionally, the Burgers equation will be introduced. This equation served historically as a toy model for turbulence and in the next chapter this will be our starting point for deriving a coupled oscillator model for phase dynamics. As before, only a minimal exposition is made, and we refer to the literature [9, 12] for further information.

3.1. Navier-Stokes turbulence

The basic equations of an incompressible fluid read [48]

$$\begin{aligned} &\partial_t \mathbf{v} + (\mathbf{v}\cdot\nabla)\mathbf{v} = -\frac{\nabla P}{\rho} + \nu\nabla^2\mathbf{v} + \mathbf{f}, \\ &\nabla\cdot\mathbf{v} = 0. \end{aligned} \tag{3.1}$$

These are called the incompressible Navier-Stokes equations for a velocity field $\mathbf{v}(t,\mathbf{x})$. Here ρ is the flow density, $P(t,\mathbf{x})$ the pressure field, ν the viscous damping, and $\mathbf{f}(t,\mathbf{x})$ are the external forces acting on the fluid.
In a $(2\pi)^3$ periodic box we may write the velocity field as a Fourier series

$$\mathbf{v}(t,\mathbf{x}) = \sum_{\mathbf{k}\in\mathbb{Z}^3} \hat{\mathbf{v}}(t,\mathbf{k}) \exp[\mathrm{i}\mathbf{x}\cdot\mathbf{k}] = \sum_{\mathbf{k}\in\mathbb{Z}^3} \sum_{i=1,2,3} \hat{\mathbf{e}}_i \, \hat{v}_i(t,\mathbf{k}) \, \exp[\mathrm{i}\mathbf{x}\cdot\mathbf{k}], \tag{3.2}$$

where $\hat{\mathbf{e}}_i$ are the elements of an orthonormal vector basis. To avoid confusion with indices, a comment is in order. Subindices indicate the vectorial component, whereas the Fourier mode in question is denoted in the argument. The dynamics in spectral space can then be formulated. In the case without external forces we may rewrite

the Navier-Stokes equations as [30]

$$(\partial_t + \nu \mathbf{k}^2)\hat{v}_i(t,\mathbf{k}) = \sum_{m,n} \frac{-\mathrm{i}}{2} P_{imn}(\mathbf{k}) \sum_{\mathbf{p}+\mathbf{q}=\mathbf{k}} \hat{v}_m(t,\mathbf{p})\hat{v}_n(t,\mathbf{q}). \tag{3.3}$$

Note that the last sum on the right hand side is a convolution of the different Fourier modes. The P_{imn} is a projector and is defined as

$$P_{imn}(\mathbf{k}) := k_m P_{in}(\mathbf{k}) + k_n P_{im}(\mathbf{k}) \text{ , with } \quad P_{im}(\mathbf{k}) := \delta_{im} - \frac{k_i k_m}{\mathbf{k}^2}.$$

The incompressibility of the flow $\mathbf{k}\cdot\hat{\mathbf{v}}(t,\mathbf{k}) = 0$ is already incorporated into equation (3.3).

In both the real-space and the spectral space formulations, the complexity of these equations may be observed. On the one hand, pressure makes the equations non-local and leads to complicated projection operations in spectral space. On the other hand, the quadratic non-linearity in real-space leads to convolutions in spectral space. This has as consequence, that the Fourier modes couple three at a time. This may be more clearly seen by considering the equations of motion for the phase φ_i of the Fourier mode $\hat{v}_i(t,\mathbf{k}) = a_i(t,\mathbf{k})\exp[\mathrm{i}\varphi_i(t,\mathbf{k})]$. Taking the imaginary part of (3.3) we read

$$\partial_t \varphi_i(t,\mathbf{k}) = \sum_{m,n} P_{imn} \sum_{\mathbf{p}+\mathbf{q}=\mathbf{k}} \frac{-a_m(t,\mathbf{p})a_n(t,\mathbf{q})}{2\, a_i(t,\mathbf{k})} \cos[\varphi_m(t,\mathbf{p}) + \varphi_n(t,\mathbf{q}) - \varphi_i(t,\mathbf{k})]. \tag{3.4}$$

Fourier modes satisfying the condition $\mathbf{p}+\mathbf{q}=\mathbf{k}$ are coupled to one another, and this coupling involves their amplitudes and phases with a convolution sum. Fourier modes coupled in this way are called triads. Additionally, the projector operator makes the Fourier mode coupling more complicated by mixing different components in a non-trivial manner. It is notable that the phase dynamics does not directly depend on the viscosity ν. This dependence enters the phase dynamics indirectly through the amplitudes $a_i(t,\mathbf{k})$.

Existence and uniqueness of particular forms of the solutions of equations (3.1) or (3.3) are still open questions in mathematics [19, 33]. Although deterministic, these equations show chaotic behavior [34]. That is, among others, extreme sensitivity to initial conditions; infinitesimal perturbations in the initial conditions will grow exponentially fast with time evolution. This, together with the innate complexity of the Navier-Stokes equations, leads to the problem of looking for adequate tools

and well-defined objects of study for turbulent phenomena. Even though individual realizations of a velocity field, satisfying the Navier-Stokes equations, might appear different to one another, statistical objects are well defined within an ensemble of realizations of solutions to these equations [26]. A statistical theory for turbulent flows can be hence derived, whereby the velocity field $\mathbf{v}(t, \mathbf{x})$ is taken as a random variable of time t and position $\mathbf{x}$.

The study of the statistical properties of fully developed homogeneous isotropic turbulence of incompressible fluids is an active field of research [41]. Much work has been done from this statistical perspective in explaining scaling laws and the energy transfer mechanisms at work in turbulence. One of the hallmarks of three-dimensional homogeneous turbulent flows is the appearance of scale-dependent statistics. Explaining the underlying mechanisms why small scales depart from Gaussianity whereas large scales remain near normal has been an open research question for some time [57]. This phenomenon of scale-dependent statistics is known in turbulence research as intermittency.

3.1.1. Intermittency in turbulent flows

In a three-dimensional homogeneous turbulent field, the single-point statistics of the velocity field are close to Gaussian [48]. On the other hand, by looking at the velocity gradient and vorticity fields, one observes departure from Gaussianity with super-Gaussian tails. These latter quantities are obtained from differential operators on the velocity field; they probe smaller scales than the velocity field itself. These observations point to the fact, that the statistics of a turbulent field are scale dependent. Additionally, the single-point statistics are not enough to characterize the system; we cannot distinguish between global Gaussian and locally uncorrelated Gaussian velocity fields.

For a better understanding of the statistics of a turbulent flow, it is hence of interest to study the many-point statistics. We look specifically into the two-point statistics. These can be explored, for example, via the so-called velocity increments. These have been studied not only because of experimental reasons, but also because they present two-point statistics which interpolate between large and small scales. Additionally they play an important role in the statistical theory of turbulence, as they appear in the theory for the two-point velocity PDF. We refer to [21] for further details.

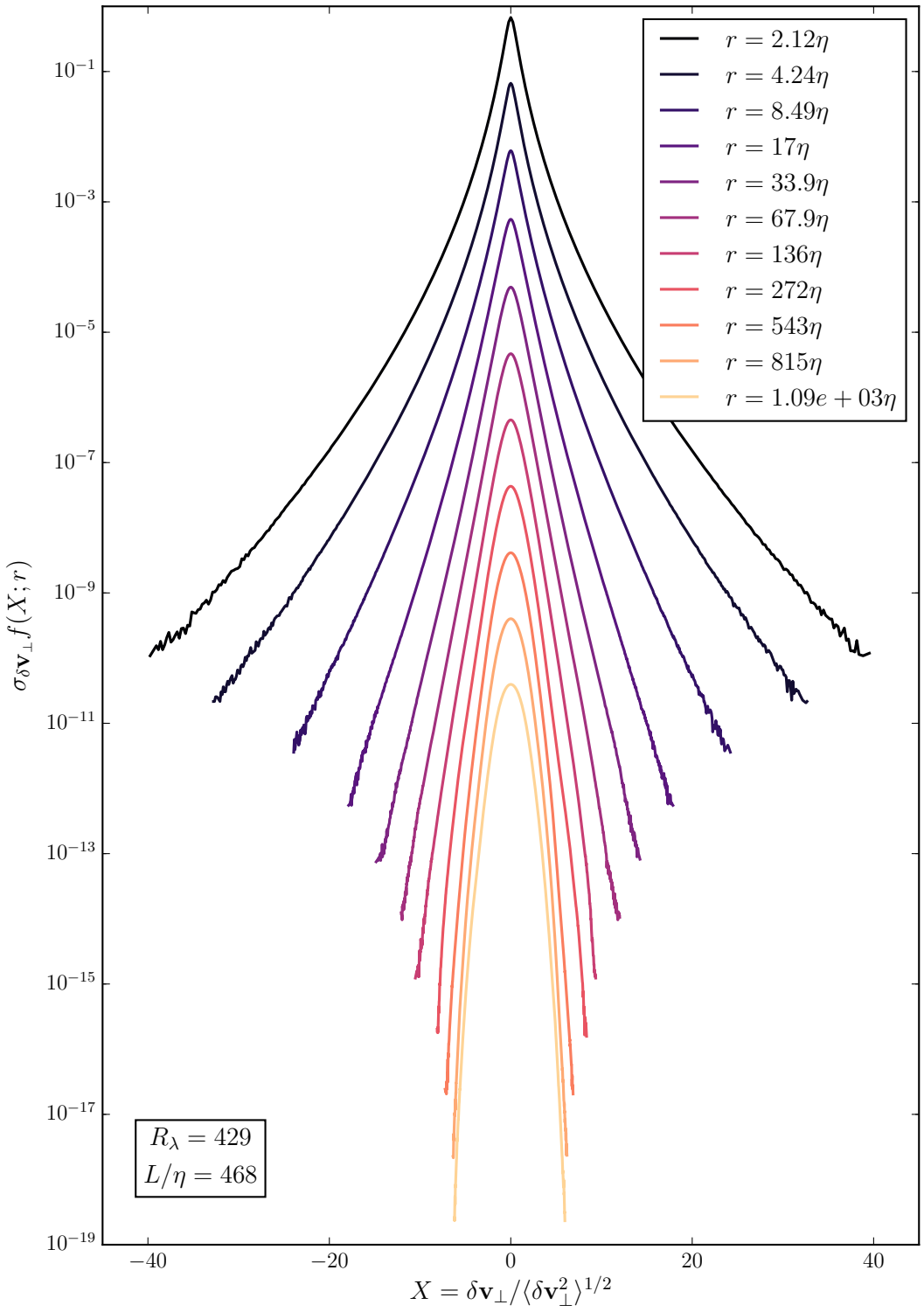

Figure 3.1.: PDFs of the Eulerian transverse velocity increments (3.5) obtained from the direct numerical simulations [18] of three-dimensional Navier-Stokes turbulence, averaged over all directions. The small increments probe the small-scale statistics of the field. These show super-Gaussian tails. As the r increases the statistics become close to normal. L/η is the ratio of the box edge to the Kolmogorov scale of the simulation and R_λ is the Taylor-scale Reynolds number [48].

Velocity increments are defined as

$$\delta\mathbf{v}(\mathbf{r}) := \mathbf{v}(t, \mathbf{x} + \mathbf{r}) - \mathbf{v}(t, \mathbf{x}). \tag{3.5}$$

In an homogeneous turbulent field the velocity increment may be taken as a random variable. In the case of isotropic turbulence the statistics of this variable are parametrized by $|\mathbf{r}|$. For $|\mathbf{r}|$ of the order of the system's size the PDF of $\delta\mathbf{v}(\mathbf{r})$ is almost Gaussian. In this case, $\delta\mathbf{v}(\mathbf{r})$ is a sum of the velocity field at points far away from one another. These are highly uncorrelated. Therefore $\delta\mathbf{v}(\mathbf{r})$ is in this case a sum of two Gaussian uncorrelated variables, and the PDF of $\delta\mathbf{v}(\mathbf{r})$ reflects the large-scale near-Gaussianity of turbulent fields. Furthermore, in the limit $\mathbf{r} \to 0$ the centered standardized moments of $\delta\mathbf{v}(\mathbf{r})$ converge towards the corresponding moments of the velocity gradient

$$\lim_{|\mathbf{r}|\to 0} K_n(\delta\mathbf{v}(\mathbf{r})) = K_n(\nabla\mathbf{v}). \tag{3.6}$$

By probing the small-scale velocity increments we are hence probing the small scales through the gradient statistics. As $|\mathbf{r}|$ decreases velocity increment's PDF becomes intermittent and skewed [21]; the third centered standardized moment (2.8) $K_3(\delta\mathbf{v}(\mathbf{r}))$ is slightly non-zero. Additionally flatness $K_4(\delta\mathbf{v}(\mathbf{r}))$ increases. By studying the $|\mathbf{r}|$ dependence of the moments of the velocity increment we can therefore quantitatively measure the scale-dependence of the PDFs. Additionally, these statistical moments are related in the context of turbulence to certain phenomena. Non-zero skewness of the velocity increments is related to vortex stretching and to the non-linear energy transfer from large to small scales, i.e. the so-called energy cascade [21]. Higher than Gaussian flatness, on the other hand, implies that large deviation events are more probable than for a Gaussian distribution. This indicates a departure from a Gaussian distribution in the small scales and the appearance of extreme events. By varying $|\mathbf{r}|$ we therefore probe the different scales of the turbulent flow and its corresponding PDFs. To illustrate these phenomenological observations of turbulent flows we will present PDFs obtained from direct numerical simulations.

By numerically integrating the three-dimensional Navier-Stokes equations the velocity field's statistics can be calculated. PDFs of the transverse component of the velocity increments are shown in Figure 3.1. Here can be seen how the small-scale PDFs show super-Gaussian tails. These foretell the presence of extreme events, and

consequently departure from Gaussianity in these scales. As the increment becomes larger, the tails are gradually regularized, and the statistics become normally distributed.
Finally, a quick note regarding length scales is in order. The typical picture of energy transfer in turbulence is as follows. Energy is injected in the largest scales. It is then transferred through several length scales, until it arrives at the small scales in the flow. There it is dissipated as heat. This middle range in which energy is transferred scale by scale is known as the inertial range. Much of the research of homogeneous isotropic turbulence has dedicated itself to finding universal quantities in the inertial range. This universality would be broken if the statistics were scale dependent. It is hence necessary to note that the intermittent phenomena are observed below the inertial range, wherefore self-similar statistics of the inertial range are still found [21].

The mathematical complexity of the Navier-Stokes equations means that exact derivations are rare. A full understanding of all mechanisms present in turbulent flows is far from being attained. On the other hand, numerical approaches also have their limitations. The Navier-Stokes equations can be numerically integrated, but it is technically challenging and increasingly difficult to obtain intense turbulent flows to high enough resolution. Non-dimensionalizing the Navier-Stokes equations leads to the definition of a control parameter known as the Reynolds number $Re = vL/\nu$; L and v are the length and velocity scales of the problem at hand. It measures the ratio between the non-linear advection term and the viscous damping. This control parameter regulates the transition of a flow's behavior from laminar to turbulent, whereas higher Reynolds numbers correspond to more turbulent fields [34]. Additionally, the number of degrees of freedom needed to take into account for a good description of turbulent flows dramatically increases at high Reynolds numbers [10]. This means that it is computationally very expensive to integrate high resolution and high Reynolds numbers flows. It is because of this reason that simplified models have been proposed over the years. These present a simpler mathematical structure, where results may be derived or at least better understood. One of these was the Burgers equation.

3.2. Burgers turbulence

The Burgers equation was introduced in the 1930's as a one-dimensional simplified toy model for Navier-Stokes turbulence. This equation reads [12]

$$\partial_t u(t,x) + \frac{1}{2}\partial_x u(t,x)^2 = \nu \partial_x^2 u(t,x). \tag{3.7}$$

In one dimension, incompressibility is not imposed; it would imply a constant velocity field. The pressure term is also absent from the Burgers equation, but apart from this, it has all terms present in the Navier-Stokes equation; it has a quadratic advective non-linearity compensated by diffusion. Additionally, this equation possesses some of the symmetries present in the Navier-Stokes equation. Namely it is invariant under space and time translations, and it conserves energy and momentum in the non-diffusive case $\nu = 0$. Space translations

$$x \to x + x_0 \tag{3.8}$$

will later play an important role in spectral space, where our coupled oscillator model will be defined. Let us rewrite the Burgers equation in spectral space. For this we take periodic boundary conditions $u(t,x) = u(t, x + 2\pi)$. Then the Burgers velocity field can be expressed as a Fourier series

$$u(t,x) = \sum_{k\in\mathbb{Z}} \hat{u}_k(t) \exp[\mathrm{i}kx]. \tag{3.9}$$

Plugging this series representation into equation (3.7) leads to the dynamics of the Fourier coefficients $\hat{u}_k(t)$, which read

$$\frac{\mathrm{d}\hat{u}_k(t)}{\mathrm{d}t} + \frac{\mathrm{i}k}{2}\sum_{p\in\mathbb{Z}} \hat{u}_p(t)\hat{u}_{k-p}(t) = -\nu k^2 \hat{u}_k(t). \tag{3.10}$$

The translation symmetry in real-space (3.8) in spectral space becomes multiplication by a complex phase

$$\hat{u}_k(t) \to \hat{u}_k(t) \exp[\mathrm{i}kx_0]. \tag{3.11}$$

This symmetry has as consequence the existence of a conserved quantity. In the present work we will use this system's symmetry, but we will not need to explicitly calculate its conserved quantity.

The original motivation to study the Burgers equation was the assumption, that its dynamics were reminiscent of the chaotic Navier-Stokes turbulence. This was, however, proven to be false with the Cole-Hopf transformation [12]

$$u(t,x) = -2\nu\,\partial_x \log \tau(t,x). \tag{3.12}$$

This transforms the Burgers equation into the heat equation $\partial_t \tau = \nu \partial_x^2 \tau$. This is equation is not chaotic. Sensitivity to initial conditions as in chaotic systems is consequently not present in the Burgers equation. Therefore a typical characteristic of turbulence, namely the introduction of randomness through chaotic dynamics, is missing.
The Burgers equation is nevertheless still being studied, specially because of its relevance in fields apart from fluid dynamics [9]. In the context of turbulence it is still used as a simple toy model, usually under stochastic forcing [15, 37]. For example, its properties in spectral space have been studied in order to shed light on the full Navier-Stokes system [13, 14, 22]. Notably, there exist exact analytic results for statistics and intermittency in Burgers systems [6, 8, 25]. Among the typical observations of driven Burgers turbulence is its inertial range scaling $E(k) \propto k^{-2}$ [24]. Another example of a mechanism understood in Burgers turbulence is the appearance of shocks in the inviscid limit. This has explicitly been proven for this simpler model, but remains an open mathematical question for the Navier-Stokes equations.

Directly studying aspects of fully-developed homogeneous isotropic Navier-Stokes turbulence is experimentally, numerically, as well as theoretically difficult; therefore having a simple model to test ideas and understand basic properties is helpful. In the present thesis we will follow this strategy to study the influence of the Fourier phase dynamics in real-space intermittency. By using the Burgers equation as a starting point, a simplified coupled oscillator model will be derived. This model will have a resemblance to the full Fourier phase equation (3.4). Nevertheless its mathematical complexity is notably less. We may therefore use this simplified model to investigate which effect phase space coherence events have in the real-space intermittency of a turbulent field.

4. Coupled oscillator model

We have until now presented tools describing the statistics of linear and circular random variables. Additionally, basic notions of Navier-Stokes turbulence and intermittency were discussed. The Navier-Stokes system is not analytically tractable, and the mechanism of generation of intermittency is an open question.
As we saw in the introductory chapter 1, there appears to be a relation between phase coherence in spectral space and real-space intermittency. In essence, coherent phase phenomena are observed on the same length scales where non-Gaussianity originates. This raises the question of the role of phase coherence phenomena in the statistics of real-space quantities. The Fourier phase equations (3.4) are convoluted, and studying them directly is not feasible.
In this section we will derive from the Burgers equation a coupled oscillator model. This model simplifies the Fourier phase dynamics and aims at easing the understanding of the phases' coherence phenomena and their effect on the real-space intermittency. Although this is a simplified model and neglects much of the complexity present in Navier-Stokes equations, it nevertheless retains the main phase-phase coupling structure. The derivation will follow a previously proposed toy model [58]. In the following, general properties of the model will be presented, such as its coupling through triad interaction and the construction of triad bases. Next, oscillator PDFs will be defined. The one-oscillator PDFs will be shown to be uniform. Additionally, on account of a system's symmetry it will be shown that the triad PDFs have the same information as the three-oscillator PDFs, and vice versa. Finally, a semi-analytic theory for the PDFs will give a starting point for studying the triad's statistical behavior.

4.1. Derivation of the model

Consider the one-dimensional inviscid Burgers equation in a periodic one-dimensional box of length 2π. Let us begin with the spectral formulation (3.10)

$$\frac{\mathrm{d}\hat{u}_k(t)}{\mathrm{d}t} + \frac{\mathrm{i}k}{2}\sum_{p\in\mathbb{Z}}\hat{u}_p(t)\ \hat{u}_{k-p}(t) = 0\ , \quad k \in \mathbb{Z}. \tag{4.1}$$

This equation is a simpler, one-dimensional version of the equation for the Navier-Stokes Fourier phases (3.4), but it retains certain similarities to it. Notably, the dynamics of Navier-Stokes Fourier phases (3.4) are also independent of viscocity. This motivates modeling the simplified phase dynamics starting from an inviscid Burgers equation.

Equation (4.1) still describes the same dynamics as in the original inviscid Burgers equation (3.7). Consider now the amplitude and phase of a Burgers Fourier mode as $\hat{u}_k(t) = a_k(t)\exp[\mathrm{i}\varphi_k(t)]$. We will derive a toy model to study the synchronization of the phases $\varphi_k(t)$ of the different modes. The dynamics of the amplitudes will be neglected so as to concentrate on the dynamics of the phases. We then keep the amplitudes of the Fourier modes fixed and allow only their phases to be dynamical quantities, i.e. $\hat{u}_k(t) = a_k\exp[\mathrm{i}\varphi_k(t)]$. The reality of the velocity field $\hat{u}(t,x)$ implies for the Fourier amplitudes and phases the relations

$$a_k = a_{-k} \quad \text{and} \quad \varphi_k(t) = -\varphi_{-k}(t). \tag{4.2}$$

Applying this to equation (4.1) yields equations of motion for the phases

$$\frac{\mathrm{d}\varphi_k(t)}{\mathrm{d}t} = \sum_{p\in\mathbb{Z}}\frac{-k\ a_p\ a_{k-p}}{2\ a_k}\ \exp\left[\mathrm{i}(\varphi_p(t) + \varphi_{k-p}(t) - \varphi_k(t)\right]\ , \ \text{for}\ k \in \mathbb{Z}/\{0\}. \tag{4.3}$$

The $k = 0$ oscillator is zero because of the field is real. That is, $\varphi_0 = -\varphi_0 \Rightarrow \varphi_0 = 0$. Taking only the real part of the last equation establishes the similarity with the equations of motion for the Navier-Stokes Fourier phases (3.4). The number of modes will be truncated, so that we are left with N modes. We are hence left with oscillators φ_k, where the index k takes values $|k| \leq N$. We set oscillators outside this range, that is $|k| > N$, to zero. Finally, we define coupling coefficients $\omega_{k,p}$ as

$$\omega_{k,p} = \frac{-k\ a_p\ a_{k,p}}{a_k}. \tag{4.4}$$

The equations of motion of N coupled oscillators are then obtained from equation (4.3)

$$\frac{\mathrm{d}\varphi_k(t)}{\mathrm{d}t} = \sum_{p=-N}^{N} \omega_{k,p} \, \cos(\varphi_p + \varphi_{k-p} - \varphi_k) \, , \quad k = 1, ..., N. \tag{4.5}$$

The 1/2 numerical factor from (4.3) has been absorbed in a time rescaling. The elements in the sum for which $p > N$ are ignored. It is this system of coupled oscillators which we will study here. It constitutes a system of non-identical, globally coupled oscillators with three-oscillator sinusoidal coupling.
This system of ordinary differential equations (4.5) inherits the Burgers equation translation symmetry (3.11). It is hence invariant under the transformation

$$\varphi_k \to \varphi_k + kx_0 \, , \quad x_0 \in \mathbb{R}. \tag{4.6}$$

This symmetry has as consequence the existence of a conserved quantity. The system (4.5) has therefore formally $N - 1$ degrees of freedom. Although we will use this symmetry to derive statistical properties of the system, the conserved quantity itself will not be used to reduce the dimension of the system.

4.1.1. Numerical implementation of the coupled oscillator system

Equation (4.5) can be numerically implemented and time series integrated. Let $\Re(z) = x$ be the real part of $z = x + \mathrm{i}y \in \mathbb{C}$. The sum in equation (4.5) may then be written as a convolution

$$\frac{\mathrm{d}\varphi_k}{\mathrm{d}t} = \Re \left[\frac{-k \exp(-\mathrm{i}\varphi_k)}{a_k} \sum_{p=-N}^{N} (a_p \, \exp[\mathrm{i}\varphi_p]) \, (a_{k-p} \, \exp[\mathrm{i}\varphi_{k-p}]) \right] . \tag{4.7}$$

For N-tuples the convolution is a computation which requires numerical operations in the order of $\mathcal{O}(N^2)$. On the other hand, convolutions can be easily implemented using a fast Fourier fransform algorithm (FFT)[1]. With this algorithm, the convolution can be reduced from an operation costing $\mathcal{O}(N^2)$ numerical operations to one costing $\mathcal{O}(N \log N)$. Therefore, equation (4.5) was implemented using a FFT algorithm. Further details and validation of this implementation will be presented in appendix A.

[1]For general mathematical properties of the FFT as well as the discrete Fourier transform we refer to [3] and in the context of turbulence and numerical simulations to [48].

Additionally, an equivalent formulation of equation (4.7) will be derived. This new formulation is useful, because the reality condition, i.e. $\varphi_k = -\varphi_{-k}$, is explicitly taken into account. This makes stability analysis and rewriting of the dynamical equations in terms of triads much easier.
As we will see in section 5.1, to obtain non-trivial dynamics, systems with the first k_0 modes set to zero will be numerically integrated. With this in mind, we implement the reality condition of $u(t,x)$ into equation (4.5). We then separate the sum in positive and negative p, and leave only the terms for which the oscillators φ_k are in the set $k_0 < |p| \leq N$. Finally, the summation indices are changed as shown

$$\begin{aligned}
\frac{\mathrm{d}\varphi_k}{\mathrm{d}t} &= \sum_{p=-N}^{N} \omega_{k,p} \cos(\varphi_p + \varphi_{k+p} - \varphi_k) \\
&= \underbrace{\sum_{p=-N+k}^{-1-k_0} \omega_{k,p} \cos(\varphi_p + \varphi_{k+p} - \varphi_k)}_{p \to -p} + \sum_{p=1+k_0}^{k-1-k_0} \omega_{k,p} \cos(\varphi_p + \varphi_{k+p} - \varphi_k) \\
&\quad + \underbrace{\sum_{p=k+1+k_0}^{N} \omega_{k,p} \cos(\varphi_p + \varphi_{k+p} - \varphi_k)}_{p \to p+k} .
\end{aligned} \tag{4.8}$$

Changing the indices allows to identify the first and last sums. A reformulation of equation (4.5) is thus obtained

$$\frac{\mathrm{d}\varphi_k(t)}{\mathrm{d}t} = 2 \sum_{p=k_0+1}^{N-k} \omega_{k,k+p} \cos(\varphi_p + \varphi_k - \varphi_{k+p}) + \sum_{p=k_0+1}^{k-1-k_0} \omega_{k,p} \cos(\varphi_p + \varphi_{k-p} - \varphi_k). \tag{4.9}$$

The main advantage of this reformulation is that the oscillator index is nowhere negative. One needs therefore not worry about double counting because of oscillators with negative index. The basic structure of equation (4.7) is sill found here, because the sums can again be written as convolutions.
The dynamics of our model (4.5) is given in Fourier space. Recall that the oscillators are interpreted as Fourier phases of a Burgers field. To relate spectral space coherence and intermitency we need then the real-space velocity field. A numerical implementation uses a finite number of modes, so that the inverse transformation of (3.9) becomes an inverse discrete Fourier transform. This discrete transform will allow us to obtain the real-space velocity field. Given a system of oscillators $\{\varphi_k\}$

the inverse discrete Fourier transform takes then the form

$$u(t,x) = \frac{1}{2N}\sum_{k=-N}^{N} a_k\, e^{\mathrm{i}(\varphi_k(t)+kx)} = \frac{1}{N}\sum_{k=k_0+1}^{N} a_k\, \cos(\varphi_k(t)+kx). \tag{4.10}$$

The $\frac{1}{2N}$ factor stems from the normalization of the discrete Fourier transform. The second equality is obtained by use of the reality condition on the Fourier coefficients. The velocity gradient statistics are also of interest, as they probe the small scales of the velocity field. As is standard in spectral analysis, the gradient of the velocity field is obtained by multiplication in spectral space. This yields a formula for the velocity gradient. It reads

$$\partial_x u(t,x) = \frac{1}{2N}\sum_{k=-N}^{N} a_k\, \mathrm{i}k\, e^{\mathrm{i}(\varphi_k(t)+kx)} = \frac{1}{N}\sum_{k=k_0+1}^{N} -a_k\, k\, \sin(\varphi_k(t)+kx). \tag{4.11}$$

This finite element implementation fulfills a modified version of the Parseval identity for Fourier series [3] given by

$$\frac{1}{\pi}\int_0^{2\pi} [u(t,x)]^2 dx = \frac{1}{N^2}\sum_{k=k_0+1}^{N} a_k^2. \tag{4.12}$$

With (4.7), (4.10) and (4.11) at hand we can numerically implement our system, and study oscillator, velocity and velocity gradient statistics. Numerical results will be explored later in the text. In the next chapter oscillator statistics will be discussed and in the chapter thereafter real-space statistics.

4.2. Triad interaction in the oscillator model

Equations (4.5) or (4.9) constitute the whole dynamics of our model. Each oscillator is coupled to all others. This coupling appears as cosine of combinations of three oscillators. These combinations are of the form $\varphi_p + \varphi_{k-p} - \varphi_k$. We call linear combinations of this form in general a triad. In this section we will try to shed some light on our system by studying the structure and dynamics of this system in terms of triads.

A convention must be met in order to categorize all triads without repetitions. We call the linear combination $\varphi_p + \varphi_{k-p} - \varphi_k$ the triad $\varphi_{k,p}$ if $k > p$ and $k - p \geq p$. We are thus naming each triad by identifying its oscillators with highest and lowest wave

number, k and p respectively. This convention also allows a useful representation of all triads, by displaying them in the region $0 < p < k/2, 0 < k < N$. In this region each and every triad is uniquely shown.
Numerically integrating the case where the first k_0 oscillators are set to zero (see section 5.1) produces non-trivial dynamics. For even N, the total number of triads without repetitions formed from oscillators $\{\phi_k | k \in \{k_0, ..., N\}\}$ is given by $(N/2 - k_0)^2$. The whole dynamics (4.5) can be reformulated in terms of these triads. Equation (4.5) then takes the form

$$\begin{aligned}\frac{\mathrm{d}\varphi_k}{\mathrm{d}t} = & \sum_{p=k_0+1}^{k} 2\,\omega_{k,k+p}\cos(\varphi_{k+p,p}) + \sum_{p=2k+1}^{N} 2\,\omega_{k,p}\cos(\varphi_{p,k}) \\ & + \sum_{p=k_0+1}^{\lfloor k/2\rfloor - 1} 2\,\omega_{k,p}\cos(\varphi_{k,p}) + \omega_{k,k/2}\cos(\varphi_{k,k/2}).\end{aligned} \tag{4.13}$$

The last term in this equation is taken into account only if k is an even number. This formulation has the advantage that it describes coupling of oscillator to triads. From equation (4.5) we know that each oscillator is coupled all others. On the other hand, equation (4.13) shows that each oscillator is only coupled to a small number of all possible triads. The triads on the right hand side of this equation are highlighted in Figure 4.1 and each sum is identified with a different region in $k - p$ space. The first, second and third sums correspond to the red, blue, and green lines in the figures, respectively.
Both the oscillator (4.5) and triad (4.13) formulations show that each oscillator and triad couples to all oscillators. If we try to reformulate the system only in terms of triads by taking linear combinations of the oscillators' equations of motion, the situation changes. Let the equation of motion of triad $\varphi_{k,p}$ be given through (4.13) as

$$\frac{\mathrm{d}\varphi_{k,p}}{\mathrm{d}t} = \frac{\mathrm{d}\varphi_p}{\mathrm{d}t} + \frac{\mathrm{d}\varphi_{k-p}}{\mathrm{d}t} - \frac{\mathrm{d}\varphi_k}{\mathrm{d}t}\,, \quad k \in \{2(k_0+1), ..., N\},\ p \in \{k_0+1, \lfloor k/2\rfloor\}. \tag{4.14}$$

Writing the equations of motion in terms of triads yields a system which resembles the equations found when studying arrays of coupled Josephson junctions [53], albeit with non-identical oscillators. Explicitly, every triad has equations of motion of the form

$$\frac{\mathrm{d}\varphi_{k,p}}{\mathrm{d}t} = \tilde{\omega}_{k,p}\cos(\varphi_{k,p}) + \sum_{\{k',p'\}} \Omega_{k,p,k',p'}\ \cos(\varphi_{k',p'}). \tag{4.15}$$

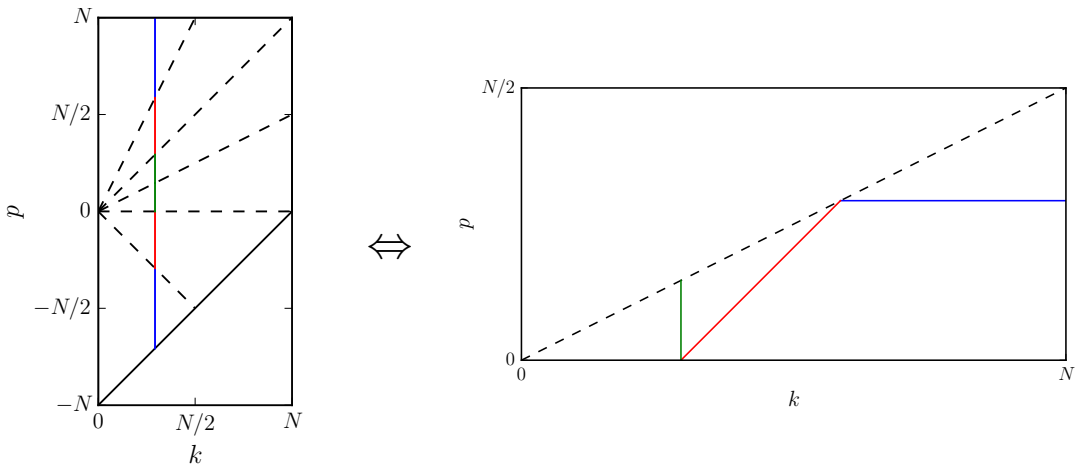

Figure 4.1.: We present a visual representation of the elements of the sum from the right hand side of equation (4.5) on the left. For a given k, the sum on the right hand side goes from $p = -N + k$ to $p = N$. On the right are shown the same elements but sorted according to triads, as in equation (4.13). For a given k, the oscillator φ_k is coupled to all triads that contain that oscillator. The first, second and third sums from equation (4.13) correspond in the figures to the red, blue, and green lines, respectively.

The triad is coupled to itself with coupling coefficient $\tilde{\omega}_{k,p} = 2(\omega_{p,k} + \omega_{k-p,k} - \omega_{k,p})$. The terms in the sum do not explicitly include the triad itself. The coupling coefficients $\Omega_{k,p,k',p'}$ are in principle known, albeit complicated; they contain information regarding which triad is coupled to which others.

This reformulation in terms of only triads seems to lead to a system with many more degrees of freedom than the original system. For $\mathcal{O}(N)$ oscillators there are $\mathcal{O}(N^2)$ triads. Each oscillator is coupled to $\mathcal{O}(N)$ triads, as seen from the sum in equation (4.13). Because the triad equations of motion are composed of linear combinations of the equations of motion from three oscillators, each triad is coupled to $\mathcal{O}(N)$ triads. Triads are therefore coupled through the dynamics (4.14) only to few other triads. As an example take Figure 4.2. Here through (4.14) a generic triad will only be coupled to the highlighted triads; this is only a minute fraction of the total number of triads. In other words, the dynamics (4.14) alone has less structure than the original system (4.5), if we do not know how the triads were constructed or how they depended on one another. This information is contained in the structure given by finding a basis of $N - k_0$ triads and how to construct all other triads from them. This means that writing the system in terms of triads will also yield $N - k_0$ degrees

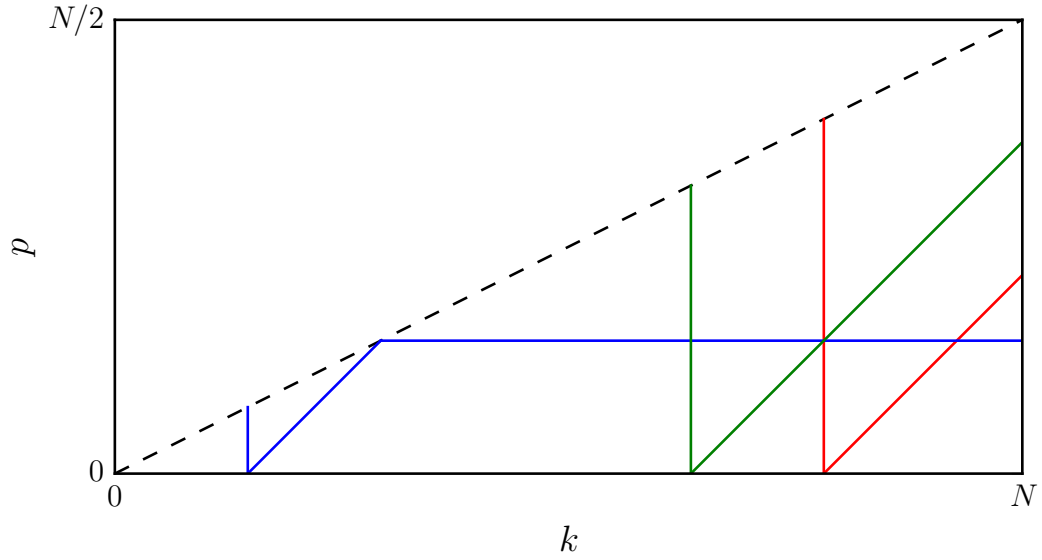

Figure 4.2.: The triads each oscillator is coupled to can be visually presented, as was shown in Figure 4.1. By taking linear combinations of three oscillators and their equations of motion, a similar visualization can be obtained for the triads themselves. the triads to wich a triad is coupled to may also be visually presented in this manner. In color are shown the triads which couple to the oscillators φ_p, φ_{k-p}, and φ_k. These oscillators form the triad $\varphi_{k,p}$. Hence, this triad is coupled to all triads marked by the colored lines. The triad itself is found at the crossing point of the three colored lines.

of freedom, with all other triads being linear combinations of these base triads. In the next section we will derive triad bases and explain how to write all other triads in terms of them to support this claim.

4.2.1. Triad basis

In reformulating the dynamics from the oscillators (4.5) to triads (4.14) additional information is necessary to ensure the same dynamics are being described. The dependence of triads on one another through linear combinations must also be supplied to avoid spurious degrees of freedom.

In general, systems which interact with a quadratic non-linearity are coupled via triads in spectral space. In previous work triads and triad bases have been found and studied in other systems, e.g. in [13], or similar to the one studied here, e.g. in [38]. In this section triad bases will be constructed for the cases $k_0 = 0$ and $k_0 = 4$.

Additionally, a formula for writing any triad in terms of the triad basis will be given.

Case $k_0 = 0$:

In this case we consider a system with oscillators $\varphi_1, ..., \varphi_N$ as dynamical variables. We define the triad basis $\{T_i\}$ given by the first oscillator and the $p = 1$ triads. That is

$$T_1 := \varphi_1, \quad T_i := \varphi_{i,1} \text{ for } i \in \{2, ..., N\}.$$

We have then N oscillators $\{\varphi_1, ..., \varphi_N\}$ and N elements in our triad basis $\{T_1, ..., T_N\}$. A transformation matrix between these two sets is given by

$$\begin{pmatrix} T_1 \\ T_2 \\ T_3 \\ T_4 \\ T_5 \\ T_6 \\ \vdots \end{pmatrix} = \begin{pmatrix} 1 & 0 & 0 & 0 & 0 & 0 & \cdots \\ 2 & -1 & 0 & 0 & 0 & 0 & \cdots \\ 1 & 1 & -1 & 0 & 0 & 0 & \cdots \\ 1 & 0 & 1 & -1 & 0 & 0 & \cdots \\ 1 & 0 & 0 & 1 & -1 & 0 & \cdots \\ 1 & 0 & 0 & 0 & 1 & -1 & \cdots \\ \vdots & \vdots & \vdots & \vdots & \vdots & \vdots & \ddots \end{pmatrix} \cdot \begin{pmatrix} \varphi_1 \\ \varphi_2 \\ \varphi_3 \\ \varphi_4 \\ \varphi_5 \\ \varphi_6 \\ \vdots \end{pmatrix}.$$

The inverse transformation takes the form

$$\begin{pmatrix} \varphi_1 \\ \varphi_2 \\ \varphi_3 \\ \varphi_4 \\ \varphi_5 \\ \varphi_6 \\ \vdots \end{pmatrix} = \begin{pmatrix} 1 & 0 & 0 & 0 & 0 & 0 & \cdots \\ 2 & -1 & 0 & 0 & 0 & 0 & \cdots \\ 3 & -1 & -1 & 0 & 0 & 0 & \cdots \\ 4 & -1 & -1 & -1 & 0 & 0 & \cdots \\ 5 & -1 & -1 & -1 & -1 & 0 & \cdots \\ 6 & -1 & -1 & -1 & -1 & -1 & \cdots \\ \vdots & \vdots & \vdots & \vdots & \vdots & \vdots & \ddots \end{pmatrix} \cdot \begin{pmatrix} T_1 \\ T_2 \\ T_3 \\ T_4 \\ T_5 \\ T_6 \\ \vdots \end{pmatrix}.$$

All other triads are obtained from linear combinations of these N basis triads. By summing and subtracting rows from the inverse transformation matrix we obtain the relation

$$\varphi_{k,p} = -T_2 - \cdots - T_p + T_{k-p+1} + \cdots + T_k \,, \quad p \neq 1.$$

With this formula we can rewrite any triad in terms of the basis triads Note that the case $p = 1$ is not treated, as these are per definition the base triads themselves.

Case $k_0 = 4$:

Let us now consider a system with $N = 1024$ and where the first $k_0 = 4$ modes are set to zero. This system is of interest because it is used for the numerical implementation. For details and justification of this choice we refer to section 5.1. For this system the situation is slightly more complicated than the previous case $k_0 = 0$.
The easiest way which we found to iteratively construct a basis relies in two indices, i and j; our basis will be a set of the form $\{T^i_j\}$.
The first $k_0 + 1$ non-zero oscillators themselves will be part of the base. We will call them T^i_1, so that

$$T^i_1 := \varphi_i \quad i \in \{5, 6, 7, 8, 9\}.$$

The rest of basistriads will be the $p = 5$ triads, such that

$$T^i_j := \varphi_5 + \varphi_{i+5\,(j-2)} - \varphi_{i+5\,(j-1)} = \varphi_{i+5\,(j-1),5}, \quad i \in \{5, 6, 7, 8, 9\},\ \ j \in \{2, ..., 204\}.$$

Note that we now have 1020 oscillators $\{\varphi_5, ..., \varphi_{1024}\}$ and 1020 triad basiselements

$$\{T^i_j\} = \{T^5_1, T^6_1, T^7_1, T^8_1, T^9_1, ..., T^5_{204}, T^6_{204}, T^7_{204}, T^8_{204}, T^9_{204}\}.$$

These bases have also transformation matrices. For $i = 5$ it reads

$$\begin{pmatrix} T^5_1 \\ T^5_2 \\ T^5_3 \\ T^5_4 \\ T^5_5 \\ T^5_6 \\ \vdots \end{pmatrix} = \begin{pmatrix} 1 & 0 & 0 & 0 & 0 & 0 & \cdots \\ 2 & -1 & 0 & 0 & 0 & 0 & \cdots \\ 1 & 1 & -1 & 0 & 0 & 0 & \cdots \\ 1 & 0 & 1 & -1 & 0 & 0 & \cdots \\ 1 & 0 & 0 & 1 & -1 & 0 & \cdots \\ 1 & 0 & 0 & 0 & 1 & -1 & \cdots \\ \vdots & \vdots & \vdots & \vdots & \vdots & \vdots & \ddots \end{pmatrix} \cdot \begin{pmatrix} \varphi_5 \\ \varphi_{5+5} \\ \varphi_{5+10} \\ \varphi_{5+15} \\ \varphi_{5+20} \\ \varphi_{5+25} \\ \vdots \end{pmatrix}.$$

For $i \in \{6,7,8,9\}$ the transformation matrix reads

$$\begin{pmatrix} T_1^5 \\ T_1^i \\ T_2^i \\ T_3^i \\ T_4^i \\ T_5^i \\ \vdots \end{pmatrix} = \begin{pmatrix} 1 & 0 & 0 & 0 & 0 & 0 & \cdots \\ 0 & 1 & 0 & 0 & 0 & 0 & \cdots \\ 1 & 1 & -1 & 0 & 0 & 0 & \cdots \\ 1 & 0 & 1 & -1 & 0 & 0 & \cdots \\ 1 & 0 & 0 & 1 & -1 & 0 & \cdots \\ 1 & 0 & 0 & 0 & 1 & -1 & \cdots \\ \vdots & \vdots & \vdots & \vdots & \vdots & \vdots & \ddots \end{pmatrix} \cdot \begin{pmatrix} \varphi_5 \\ \varphi_i \\ \varphi_{i+5} \\ \varphi_{i+10} \\ \varphi_{i+15} \\ \varphi_{i+20} \\ \vdots \end{pmatrix}.$$

By recursively subtracting rows from these matrices from the bottom up, a relation for the inverse is found. This relation reads

$$\varphi_{i+5\,(j-1)} = -\sum_{n=2}^{j} T_n^i + T_1^i + (j-1)\, T_1^5 \quad j \neq 1. \tag{4.16}$$

This relation also allows one to write the inverse transformation as matrices. For $i = 5$ we have

$$\begin{pmatrix} \varphi_5 \\ \varphi_{5+5} \\ \varphi_{5+10} \\ \varphi_{5+15} \\ \varphi_{5+20} \\ \varphi_{5+25} \\ \vdots \end{pmatrix} = \begin{pmatrix} 1 & 0 & 0 & 0 & 0 & 0 & \cdots \\ 2 & -1 & 0 & 0 & 0 & 0 & \cdots \\ 3 & -1 & -1 & 0 & 0 & 0 & \cdots \\ 4 & -1 & -1 & -1 & 0 & 0 & \cdots \\ 5 & -1 & -1 & -1 & -1 & 0 & \cdots \\ 6 & -1 & -1 & -1 & -1 & -1 & \cdots \\ \vdots & \vdots & \vdots & \vdots & \vdots & \vdots & \ddots \end{pmatrix} \cdot \begin{pmatrix} T_1^5 \\ T_2^5 \\ T_3^5 \\ T_4^5 \\ T_5^5 \\ T_6^5 \\ \vdots \end{pmatrix}.$$

For $i \in \{6,7,8,9\}$ we have similarly

$$\begin{pmatrix} \varphi_5 \\ \varphi_i \\ \varphi_{i+5} \\ \varphi_{i+10} \\ \varphi_{i+15} \\ \varphi_{i+20} \\ \vdots \end{pmatrix} = \begin{pmatrix} 1 & 0 & 0 & 0 & 0 & 0 & \cdots \\ 0 & 1 & 0 & 0 & 0 & 0 & \cdots \\ 1 & 1 & -1 & 0 & 0 & 0 & \cdots \\ 2 & 1 & -1 & -1 & 0 & 0 & \cdots \\ 3 & 1 & -1 & -1 & -1 & 0 & \cdots \\ 4 & 1 & -1 & -1 & -1 & -1 & \cdots \\ \vdots & \vdots & \vdots & \vdots & \vdots & \vdots & \ddots \end{pmatrix} \cdot \begin{pmatrix} T_1^5 \\ T_1^i \\ T_2^i \\ T_3^i \\ T_4^i \\ T_5^i \\ \vdots \end{pmatrix}.$$

Using (4.16) we can write any triad as a linear combination of the basis triads. This justifies working either with oscillators or with triads without loss of generality or generation of spurious degrees of freedom. All the matrices presented in this section are triangular matrices, with diagonal elements ± 1. Therefore they have det $= \pm 1$. These transformations are hence phase-space volume preserving. This means that when transforming PDFs defined in terms of triads to PDFs defined in terms of oscillators the Jacobian of the transformation is unity.

4.3. Oscillator PDFs

By considering the oscillators as random variables we may study their statistical properties with the tools presented in chapter 2. The oscillators are in this sense cyclic random variables and their PDFs will hence be circular PDFs. In the next section PDFs will be defined for the oscillator and triad statistics. Subsequently the Fourier coefficients of the three-oscillator PDF will be shown to be the same as the one-triad trigonometric moments. Afterwards the PDF equation will be introduced and it will be shown that it does not produce any defining equations for the triad PDFs. Finally, a semi-analytic theory for the triad PDF will be proposed by comparing the triad equations of motion with much simpler systems for which the PDFs are known.

4.3.1. Definition of the PDFs

Consider the oscillators $\varphi_k(t)$ as circular random variables parametrized by time t. Let then the fine-grained PDF $\hat{f}_1$ of this random variable be defined as

$$\hat{f}_1(\phi; k) := \delta(\phi - \varphi_k(t)). \tag{4.17}$$

Averaging over the fine-grained PDF yields the one-oscillator PDF f_1

$$f_1(\phi; k) \equiv \langle \hat{f}_1(\phi; k) \rangle. \tag{4.18}$$

All other higher-order oscillator PDFs can be obtained by use of the one-oscillator fine-grained PDFs. Let the n-oscillator PDF be defined as

$$f_{\underbrace{1\times ...\times 1}_{n}}(\phi_1,...,\phi_n;p_1,...,p_n) := \left\langle \prod_{i=1}^{n} \hat{f}_1(\phi_i;p_i) \right\rangle . \tag{4.19}$$

The notation used implies that we explicitly indicate the order of the statistics described by each PDF. So, for example, f_1 is a one-oscillator PDF, $f_{1\times 1}$ is a two-oscillator PDF, $f_{1\times 1\times 1}$ is a three-oscillator PDF, and so on. The oscillator PDFs contain all the oscillator statistical information. This means that ensemble averages can be rewritten as weighted averages with the PDFs. Let $g(\varphi_{p_1},...,\varphi_{p_n})$ be a function of n of the oscillators. The n-order PDF may then be used to express ensemble averages of g through a weighted average as

$$\int_{S^1} f_{1\times ...\times 1}(\phi_1,...,\phi_n;p_1,...,p_n)\; g(\phi_1,..,\phi_n)\mathrm{d}\phi_1...\mathrm{d}\phi_n \equiv \langle g(\varphi_{p_1},...,\varphi_{p_n})\rangle. \tag{4.20}$$

These higher-order PDFs contain therefore the full statistical information of the n-oscillator system. Describing the full statistics of a coupled oscillator system, like the one we are studying, is a major task. We therefore concentrate on the low-order statistics. The lowest-order statistics of interest are the three-oscillator statistics. Because oscillators couple in triads we will also define PDFs for the triads.
Consider now one triad $\varphi_{k,p}$ as a random variable. Conditioning three one-oscillator fine-grained PDFs, a fine-grained triad PDF $\hat{f}_3$ can be defined as

$$\begin{aligned} \hat{f}_3(\phi;k,p) = &\int_{S^1} \mathrm{d}\beta \int_{S^1} \mathrm{d}\gamma \int_{S^1} \mathrm{d}\omega\; \hat{f}_1(\beta;p)\; \hat{f}_1(\gamma;k-p)\; \hat{f}_1(\omega;k)\; \delta(\beta+\gamma-\omega-\phi) \\ = &\; \delta(\varphi_p+\varphi_{k-p}-\varphi_k-\phi). \end{aligned} \tag{4.21}$$

Let a triad's PDF be denoted by f_3. A relation between the triad PDF and the three-oscillator PDF $f_{1\times 1\times 1}$ is obtained by averaging the fine-grained triad PDF

$$\begin{aligned} f_3(\phi;k,p) = &\int_{S^1} \mathrm{d}\beta \int_{S^1} \mathrm{d}\gamma \int_{S^1} \mathrm{d}\omega\; f_{1\times 1\times 1}(\beta,\gamma,\omega;p,k-p,k)\; \delta(\beta+\gamma-\omega-\phi) \\ = &\; \langle \delta(\varphi_p+\varphi_{k-p}-\varphi_k-\phi)\rangle. \end{aligned} \tag{4.22}$$

By comparison with equation (4.20) we identify, that the triad PDF is the expectation value of the three-oscillator function $\delta(\varphi_p + \varphi_{k-p} - \varphi_k - \phi)$. Just as for the oscillators, the triad's PDF can be used to calculate ensemble averages.
Finally, we also look into the two-triad statistics. This should give some insight into the triad-triad coupling, and how they dynamically influence one another. The PDF for the two-triad joint statistics $f_{3\times3}$ is defined as

$$\begin{aligned} f_{3\times3}(\phi,\theta;k_1,p_1,k_2,p_2) = &\ \langle\delta(\varphi_{p_1}+\varphi_{k_1-p_1}-\varphi_{k_1}-\phi)\,\delta(\varphi_{p_2}+\varphi_{k_2-p_2}-\varphi_{k_2}-\theta)\rangle \\ = &\ \langle\hat{f}_3(\phi;k_1,p_1)\,\hat{f}_3(\theta;k_2,p_2)\rangle. \end{aligned} \tag{4.23}$$

Additionally, let a correlation function $C_{3\times3}$ measure departure from statistical independence

$$\begin{aligned} f_{3\times3}(\phi,\theta;k_1,p_1,k_2,p_2) = &\ f_3(\phi;k_1,p_1)\,f_3(\theta;k_2,p_2) \\ &+C_{3\times3}(\phi,\theta;k_1,p_1,k_2,p_2). \end{aligned} \tag{4.24}$$

Note that the one-triad PDFs can be recovered by integrating out one of the variables. That is

$$\int_{S^1} \mathrm{d}\theta\, f_{3\times3}(\phi,\theta;k_1,p_1,k_2,p_2) = f_3(\phi;k_1,p_1). \tag{4.25}$$

This means that the correlation function is subject to the condition

$$\int_{S^1} \mathrm{d}\theta\, C_{3\times3}(\phi,\theta;k_1,p_1,k_2,p_2) = 0 = \int_{S^1} \mathrm{d}\phi\, C_{3\times3}(\phi,\theta;k_1,p_1,k_2,p_2). \tag{4.26}$$

4.3.2. Translation symmetry and oscillator statistics

As was previously shown, the coupled oscillator model is invariant under translations (4.6). This has implications for the oscillator statistics. In terms of the n-oscillator PDF, this symmetry is generated by the following vector field

$$\sum_{i=1}^{n} p_i\,\partial_{\phi_i}\, f_{1\times\ldots\times1}(\phi_1,\ldots,\phi_n;p_1,\ldots,p_n) = 0 \tag{4.27}$$

We will solve this condition for the one- and three-oscillator cases. To solve this vector field we use an exponential ansatz for the PDFs. As a consequence of this

symmetry all one-oscillator PDFs f_1 are uniform

$$k\,\partial_\phi\, f_1(\phi;k) = k\,\mathrm{i}m\,\exp[\mathrm{i}m\phi] \stackrel{!}{=} 0 \Rightarrow m = 0 \Rightarrow f_1(\phi;k) = \frac{1}{2\pi}\,\forall\, k. \tag{4.28}$$

Now consider the three-oscillator PDFs $f_{1\times1\times1}$ of three oscillators forming a triad. These PDFs are subject to the symmetry generated by the vector field

$$\begin{pmatrix} p \\ k-p \\ k \end{pmatrix} \cdot \begin{pmatrix} \partial_\beta \\ \partial_\gamma \\ \partial_\phi \end{pmatrix} f_{1\times1\times1}(\beta,\gamma,\phi;p,k-p,k) = 0. \tag{4.29}$$

To solve the vector field we will make the ansatz $f_{1\times1\times1}(\beta,\gamma,\phi;p,k-p,k) = \exp[\mathrm{i}(n_\beta\beta + n_\gamma\gamma + n_\phi\phi)]$. This ansatz leads to

$$pn_\beta + (k-p)n_\gamma + kn_\phi \stackrel{!}{=} 0 \;\;\Rightarrow\;\; n = n_\beta = n_\gamma = -n_\phi\,, \quad n \in \mathbb{Z}. \tag{4.30}$$

Periodicity of $f_{1\times1\times1}$ requires n to be an integer number. The three-oscillator PDF then takes the form of a Fourier series as

$$f_{1\times1\times1}(\beta,\gamma,\phi;p,k-p,k) = \frac{1}{(2\pi)^3}\left[1 + \sum_{n\in\mathbb{N}} \hat{f}_n^{k,p}\exp[-\mathrm{i}n(\beta+\gamma-\phi)] + \text{c.c.}\right]. \tag{4.31}$$

Plugging equation this equation into the definition of the triad PDF (4.22) we obtain the triad PDF as

$$f_3(\phi;k,p) = \frac{1}{2\pi}\left[1 + \sum_{n\in\mathbb{N}} \hat{f}_n^{k,p}\exp[-\mathrm{i}n\phi] + \text{c.c.}\right]. \tag{4.32}$$

We come, hence, to the conclusion that the triad Fourier coefficients are the same as the three-oscillator Fourier coefficients. That is, speaking of three-oscillator joint statistics is the same as of triad statistics. No additional information is contained in the three-oscillator joint PDF which is not present in the triad PDF and vice versa.

4.3.3. PDF equation

PDFs fulfill a continuity equation for probability of the form [48]

$$\partial_t f(t,\phi) + \partial_\phi J(t,\phi) = 0, \tag{4.33}$$

where J is a probability density current. We seek a theory for the triad PDFs. This should shed some light into the different synchronization properties of different triads. Equation (4.33) is the typical starting point for yielding defining equations for the PDFs.

In this work we look into the statistically stationary case, and not the dynamical evolution of the PDFs. In one dimension with stationary statistics $\partial_t f = 0$, equation (4.33) leads to a divergence-free (constant) probability density current J; thus the PDF equation usually yields no defining equations for the PDF. This may be true because either J is constant, or because it involves higher-order PDFs. We will exemplify this explicitly with the one-oscillator PDF equation. Take the fine-grained one-oscillator PDF $\hat{f}_1(\phi; k)$. The fine-grained PDF depends on the specific realization used, and is therefore differentiable in time. Differentiating in time and using the sifting property[2] of the δ-distribution one then obtains

$$\partial_t \hat{f}_1(\phi; k) = -\partial_\phi \hat{f}_1(\phi; k)\dot{\varphi}_k = -\partial_\phi \hat{f}_1(\phi; k) \sum_{p=-N}^{N} \omega_{k,p} \cos(\varphi_p + \varphi_{k-p} - \phi). \tag{4.34}$$

In order to obtain an equation only for PDFs, the φ_p and $\varphi_{k,p}$ oscillators must be rewritten in terms of their PDFs. For this we insert unity twice as

$$1 \equiv \int_{S^1} \mathrm{d}\beta\, \hat{f}_1(\beta; p) \qquad \text{and} \qquad 1 \equiv \int_{S^1} \mathrm{d}\gamma\, \hat{f}_1(\gamma; k-p).$$

Subsequently, the the sifting property is used again. We then average and obtain the probability conservation equation for $f_1(\phi; k)$

$$\partial_t f_1(\phi; k) = 0 = -\partial_\phi \sum_{p=-N}^{N} \omega_{k,p} \int_{S^1} \mathrm{d}\beta \int_{S^1} \mathrm{d}\gamma \cos(\beta + \gamma - \phi) f_{1\times1\times1}(\beta, \gamma, \phi; p, k-p, k). \tag{4.35}$$

We have, however, knowledge on the functional form of the three-oscillator PDF of oscillators forming a triad. By plugging in equation (4.31) into the above equation we obtain

$$0 = \partial_\phi \sum_{p=-N}^{N} \omega_{k,p}\, \Re(\hat{f}_1^{k,p}), \tag{4.36}$$

which is trivially fulfilled. As argued in section 4.3.2, f_1 itself is trivial. That equation (4.35) is therefore automatically fulfilled is not a surprise. We, however,

[2]For general properties of the δ-distribution we refer to [3] and in the context of turbulence appendix C in [48].

used the one-oscillator equation to highlight several points. On the one hand, as already noted, one-dimensional statistically stationary PDF equations can lead to trivial continuity equations. These don't yield any defining equations for the PDFs. On the other hand, even though PDF equations for higher-order statistics may be non-trivial, it is considerably more difficult handling these higher dimensional cases. Apart from the technical difficulty of solving a high dimensional partial differential equation, PDF equations have in general the problem of closure. Note that the right hand side of equation (4.35) involves a higher-order PDF than the one on the left hand side. Equations such as (4.33) lead to a coupling between low- and high-order statistics. This produces the known closure problem. That is, to solve for the one-oscillator PDF we need the three-oscillator PDF, and to solve the three-oscillator PDF we need the six-oscillator PDF, and so on.
Deriving an exact theory for the triad PDFs is a difficult endeavor, and although we know the triad PDF equation will not be closed, treating it will elucidate which level of complexity is to be explained by such a theory. In the following, we will derive an exact relation between the two-triad correlation function and the triad PDF. Consider the PDF equation of the fine-grained triad PDF. It is given by

$$\partial_t \hat{f}_3(\phi; k, p) = -\partial_\phi \left[\hat{f}_3(\phi; k, p) \dot{\varphi}_{k,p} \right], \tag{4.37}$$

where we use the triad equations of motion as given in (4.15). We will now average to obtain in the stationary case

$$0 = \partial_\phi \left\langle \hat{f}_3(\phi; k, p) \left(\tilde{\omega}_{k,p} \cos(\varphi_{k,p}) + \sum_{\{k',p'\}} \Omega_{k,p,k',p'} \cos(\varphi_{k',p'}) \right) \right\rangle. \tag{4.38}$$

Subsequently, the sifting property of the δ-distribution is used and unity

$$1 \equiv \int_{S^1} \mathrm{d}\theta \; \hat{f}_3(\theta; k', p')$$

will be inserted to obtain the two-triad PDF

$$0 = \partial_\phi \left\langle \hat{f}_3(\phi; k, p) \left(\tilde{\omega}_{k,p} \cos(\phi) + \sum_{\{k',p'\}} \Omega_{k,p,k',p'} \int_{S^1} d\theta \; \hat{f}_3(\theta; k', p') \cos(\theta) \right) \right\rangle. \tag{4.39}$$

Finally, using the two-triad PDF with the correlation function factorization (4.24) we are led to the equation

$$0 = \partial_\phi \left[f_3(\phi; k, p) J(\phi; k, p) + S(\phi; k, p) \right]. \tag{4.40}$$

$J(\phi; k, p)$ is defined as

$$J(\phi; k, p) := \tilde{\omega}_{k,p} \cos\phi + \sum_{\{k',p'\}} \Omega_{k,p,k',p'} \, \Re(\hat{f}_1^{k,p}), \tag{4.41}$$

where we denote a triad's k, p first trigonometric moment as $\hat{f}_1^{k,p}$. The S term contains the non-closed part of the PDF equation as it involves higher-order statistics, and it is given by

$$S(\phi; k, p) := \sum_{\{k',p'\}} \Omega_{k,p,k',p'} \int_{S^1} \mathrm{d}\theta \cos\theta \, C_{3\times 3}(\phi, \theta; k, p, k', p'). \tag{4.42}$$

This derivation is exact and equation (4.40) yields a formula for f_3

$$f_3(\phi; k, p) = \frac{\mathcal{K} - S(\phi; k, p)}{J(\phi; k, p)} \tag{4.43}$$

for a constant $\mathcal{K}$. Recall that the equations of motion (4.5) and (4.15) are invariant under spectrum and time rescaling

$$\begin{cases} t \to t/A \\ a_k \to a_k \, A \end{cases} \quad \forall A \in \mathbb{R}_{/\{0\}}. \tag{4.44}$$

This leaves statistical objects such as PDFs and trigonometric moments invariant, whilst it scales quantities such as $\tilde{\omega}_{k,p}$ and $\Omega_{k,p,k',p'}$. S and J therefore scale with this transformation. On the other hand, once $\mathcal{K}$ has been found for a choice of spectrum it remains the same for all choices of spectra. With this in mind, we come to the conclusion that for f_3 to be invariant under this transformation it is necessary that $\mathcal{K} = 0$. We are hence left with the relation

$$f_3(\phi; k, p) = \frac{-S(\phi; k, p)}{J(\phi; k, p)}. \tag{4.45}$$

This is an exact relation between the correlation function and the one-triad PDF. Note that S sums over the correlation functions of all triads coupled to the triad k, p.

This means that we must have information on the whole system to carry out the sum. Additionally, this makes it explicit that the triad PDF involves the statistical dependence between the different triads in a non-trivial manner.
The one-oscillator and triad PDF equations are the starting point to search for defining equations for the triad PDF. However, as we have seen, the PDF equations have non-closed terms or they are trivially fulfilled on account of a system's symmetry. We hence look at further simplifications of the equations of motion (4.5) to look for a starting point for a theory for the triad PDFs.

4.4. Semi-analytic theory for the triad PDFs

The unclosed terms in the PDF equation means it will not lead us to a defining equation for f_3. We will therefore take an alternative approach and compare the oscillator system to simpler systems whose behavior is known, and in this way motivate a theory for the triad PDFs, without deriving it from first principles.
Consider the triad equations of motion as given in (4.15). We may summarize the terms which do not explicitly contain the triad itself as a function $\alpha_{k,p}(t)$. Each triad has, with this formulation, equations of motion of the form

$$\frac{\mathrm{d}\varphi_{k,p}}{\mathrm{d}t} = \tilde{\omega}_{k,p}\cos(\varphi_{k,p}) + \alpha_{k,p}(t). \tag{4.46}$$

Let us consider $\alpha_{k,p}$ as a stochastic forcing. This may be justified by arguing that it contains a sum of many different triads summed in a non-trivial manner. This combination of triads covers a wide range of time scales. When summed, these act on the triad $\varphi_{k,p}$ in a manner appearing stochastic. This leads us to consider the triad equation of motion in an equivalent way as

$$\frac{\mathrm{d}\varphi_{k,p}}{\mathrm{d}t} = 1 + \gamma\cos\varphi_{k,p} + \alpha'_{k,p}(t). \tag{4.47}$$

This system has similarity with the simpler system

$$\frac{\mathrm{d}\varphi}{\mathrm{d}t} = 1 + \gamma\cos\varphi \tag{4.48}$$

which can be shown in to have a WC distributed PDF[3]. The forcing should therefore homogenize the variable φ, driving it towards a more uniformly distributed PDF and

[3]See appendix B for details.

possibly changing its preferred direction.
Consider additionally, that the triad equation of motion resembles that of an array of Josephson junctions [53]. Because we know there is a triad basis and not all triads are independent, the triad $\varphi_{k,p}$ may appear implicitly in $\alpha(t)$, but always in linear combinations with other triads. This means that the triad equations of motion have much more structure than identical Josephson junction array systems. Nevertheless, comparison with the simpler system also sheds light on the possible form of the triad PDFs. It has been shown that in the thermodynamic limit Josephson junctions show low-dimensional behavior, synchronizing with a PDF parametrized by a WC distribution[4]. Furthermore, the similarity between triad equations (4.15) and Josephson array equations can be made clearer by setting a flat spectrum. That is, for example, by setting $a_k = 1$. This yields the possibility of continuously transforming a Josephson system into our triad system, given we ignore the linear dependence between triads.
These results together motivate starting the study of triad PDFs not in full generality, but in concrete with the special case of a WSM, which offers an interpolation between a WC and a uniform distribution. Every triad PDF would then be parametrizable as

$$f_3(\phi; k, p) = \frac{1}{2\pi}\left[1 + C_{k,p}\sum_{n\in\mathbb{N}} \mathbf{r}_{k,p}^n \exp[-in\phi] + \text{c.c.}\right]. \tag{4.49}$$

The triad equations of motion are coupled through the real-part of different triads' first trigonometric moments. This is consistent with a theory for the PDFs where these first moments play a determining role. Note that we have changed the notation from (2.38). Since we assume that we can reduce every triad's statistics to two parameters, we directly label the PDF by the triad's k and p. Additionally, this ansatz for the PDF can be corroborated directly by comparing the triads' trigonometric moments; these in turn are obtainable from integrated time series. It is hence not necessary to implement fitting algorithms for the numerical PDFs.
In summary, comparing our system in broad terms with Josephson junctions and a simple cosine model leads to a starting point for modeling the triad PDFs. On the other hand we know that the triad system has much more structure than these simple models, as exemplified by the dependence between the two-triad correlation functions and the one-triad PDF. Nevertheless, a phenomenological theory for the

[4]See appendix C for details.

triad PDFs is a good place to start investigating this system, relegating more complex statistics for a future study. It serves therefore as a starting semi-analytic theory to describe the triad statistics.

A numerical exploration of the triad statistics will be presented in next chapter, along with general numerical observations from our model. A verification of our proposal for the triad PDF will be numerically done and consequences thereof will be explored.

5. Numerics of the model

In the previous chapter we showed a couple of exact results; the one-oscillator PDFs are uniform and the three-oscillator Fourier coefficients are the same as the triad trigonometric moments. The non-closed triad PDF equation means that it does not determine the triad PDFs. A semi-analytic theory was hence proposed. This gives a starting point to model the PDF, but it does not fix any parameters.
This motivates the numerical study of model (4.5) and verification of the semi-analytic theory from the empirical observations thereof.
Here we comment on results obtained by numerically integrating equation (4.5) through a direct implementation of equation (4.7). We use overall $N = 1024$ as the maximum oscillator index. The choice of spectrum, the existence of a fixed point and stability analysis are shown in the next section. Subsequently numerical PDFs will be presented. Finally we will verify the accuracy of the semi-analytic approach and its consequences. Real-space numerics and statistics will be presented in detail in the next chapter.

5.1. Spectrum and fixed point

Before starting numerical integration of equation (4.5) it is necessary to fix the spectrum a_k. The typical toy model for one-dimensional turbulence is the Burgers equation, and it was also our starting point. We want to keep some of its known phenomenology. We therefore implement the $E_k \propto a_k^2 \propto k^{-2}$ inertial range spectrum and a Gaussian cutoff to signify the dissipative length scale. The spectrum was implemented as

$$a_k = A\,|k|^{-\alpha}\,\exp\left[-\beta\,\left(\frac{k}{N/2}\right)^2\right], \tag{5.1}$$

with $\beta = 1$ and $\alpha = 1$. The amplitude A can be set with time rescaling. A log-log plot of this spectrum is shown in Figure 5.1.
Integrating the model with all oscillators $\{\varphi_k\}$ as dynamical variables we observe

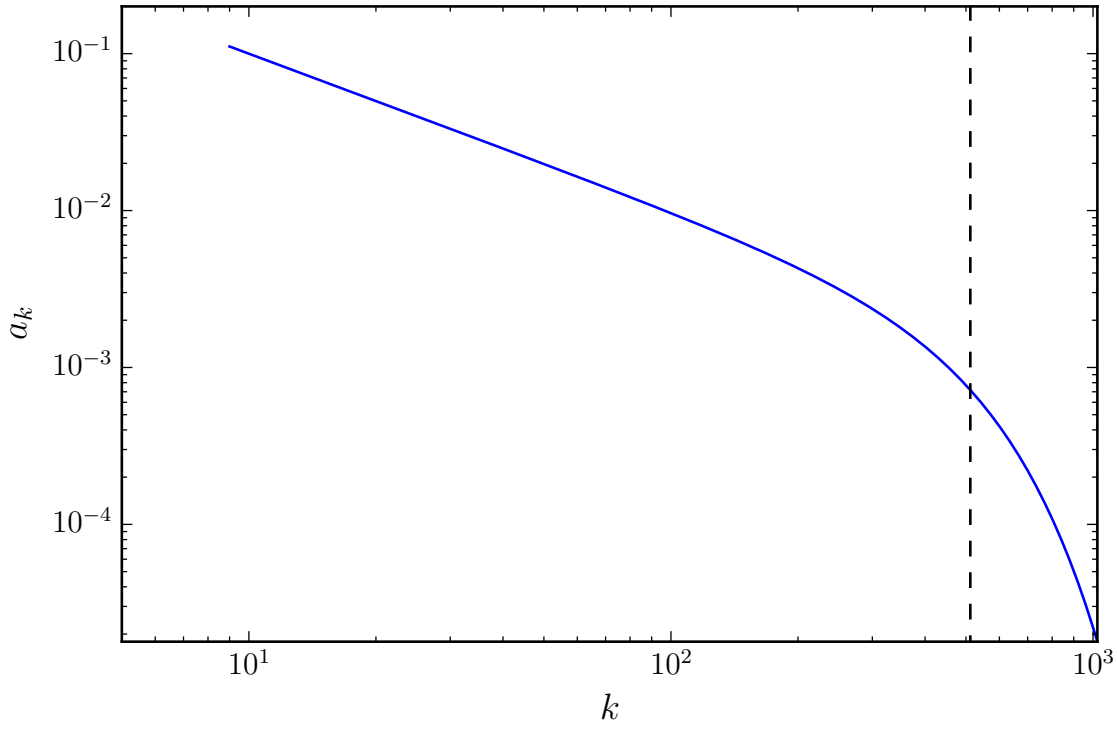

Figure 5.1.: Numerically implemented spectrum (5.1) with $\beta = \alpha = 1$. The dashed lines are at $k = N/2$ and indicate the Gaussian cutoff. The inertial range has Burgers like $a_k \sim k^{-1}$.

convergence to a fixed point. Figure 5.2 shows a snapshot of two different velocity profiles. Both are obtained from our model (4.5) after the same number of integrated time steps for the same spectrum, but with different number of oscillators. We removed in one case the first k_0 oscillators from the dynamics. In blue a system is shown where all oscillators are dynamical variables. This system converges towards a fixed point. In green is a system where the first $k_0 = 4$ modes are set to zero. Removing the first produces a velocity profile typical of the known Burgers one-dimensional turbulence. If this really destabilizes the fixed point or only makes the transient longer will be answered below.

Equations of the form (4.5) have fixed points for all configurations of the oscillators $\{\varphi_k\}$ which produce triads $\varphi_{k,p} = \pm\pi/2$. Because of the symmetry under (4.6) not all configurations which lie on a fixed point $\varphi_{k,p} = \pm\pi/2$ are independent. We observe numerically that the configurations which converge to this fixed point for $k_0 = 0$ are the ones equivalent to those in which every oscillator is at $\pi/2$.

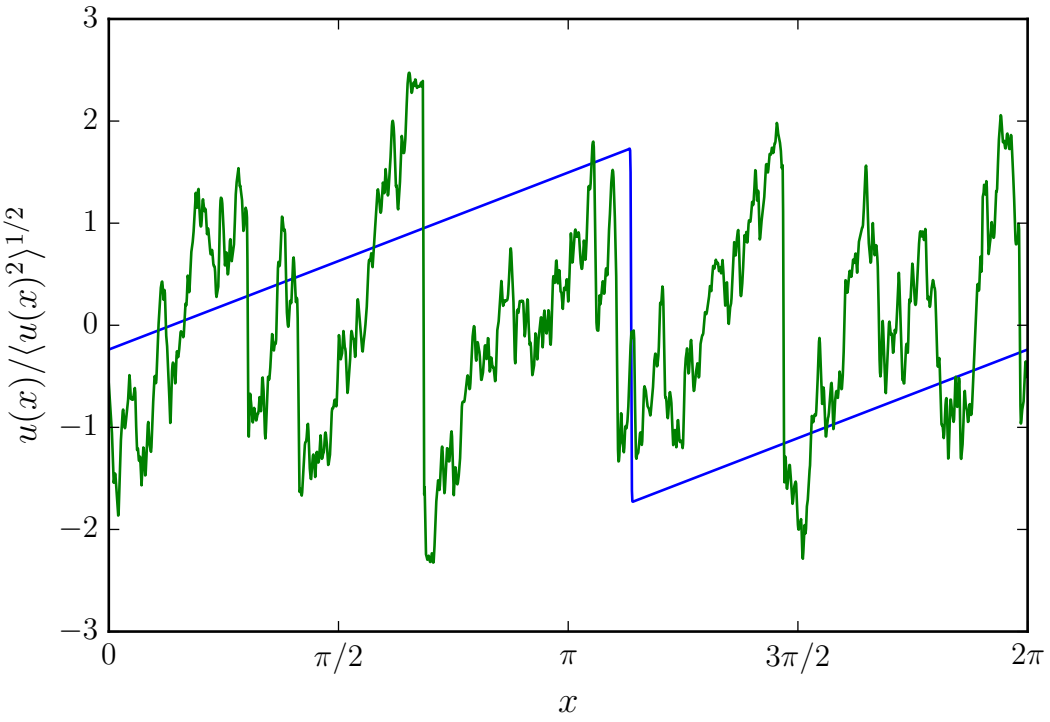

Figure 5.2.: The system (4.5) converges to a fixed point (blue). If the first modes are set to zero (green) this fixed point is destabilized and the real-space velocity profile look similar to typical Burgers velocity profile. For the numerics we used $N = 1024$ and we set the first $k_0 = 4$ modes to zero. A linear stability analysis showed that $k_0 = 4$ is not a long-lived transient of the $k_0 = 0$ fixed point.

The convergence to a saw tooth function in the fixed point is explainable. A generic velocity field takes the form (4.10)

$$u(x) = \frac{1}{N} \sum_{k=k_0+1}^{N} a_k \cos(\varphi_k + kx + kx_0). \tag{5.2}$$

We will now translate the system by $\varphi_k \to \varphi_k - kx_0$. This moves the shock to the origin

$$u(x) = \frac{1}{N} \sum_{k=k_0+1}^{N} a_k \cos(\varphi_k + kx). \tag{5.3}$$

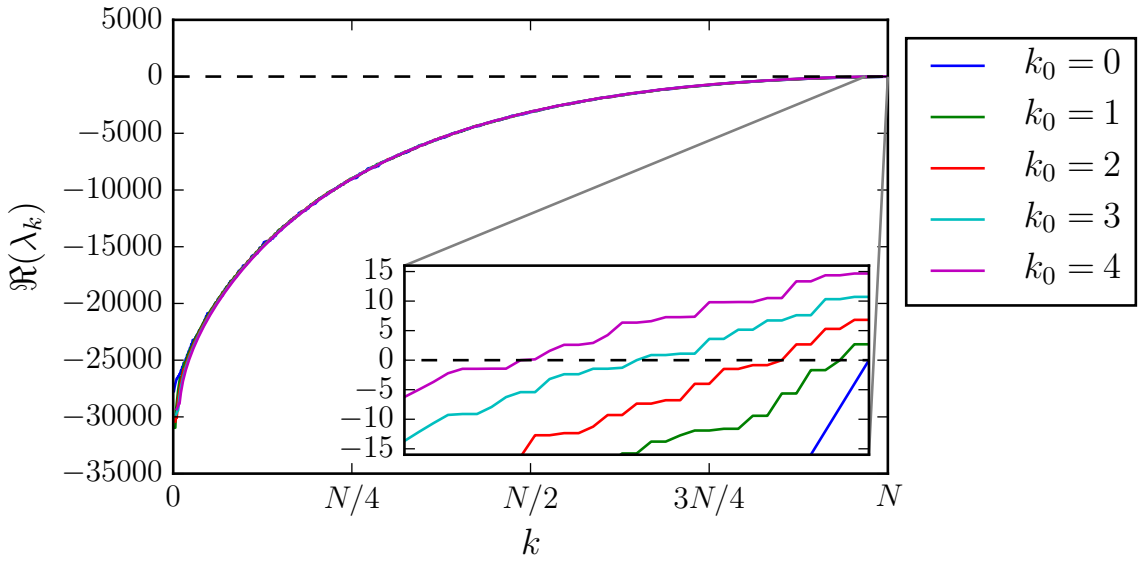

Figure 5.3.: Real part of the eigenvalues of the Jacobi matrix (5.8). The fixed point is only stable for $k_0 = 0$. The $\lambda_k = 0$ eigenvalue is always present as a consequence of the conserved quantity.

In the fixed point $\varphi_k \to \frac{\pi}{2}$

$$u(x) = -\frac{1}{N} \sum_{k=k_0+1}^{N} a_k \, \sin(kx). \tag{5.4}$$

For $k_0 = 0$ and in the limit $N \to \infty$ the asymptotic relation for the spectrum reads $a_k \sim k^{-1}$. We recall that the $1/N$ factor fulfills the role of normalization, so that applying the transformation twice is equals to the identity transformation. With this in mind, in the limit $N \to \infty$ this prefactor can be reabsorbed into the coefficients a_k. With the above considerations we take the $N \to \infty$ limit, and we exchange the discrete Fourier transform by a Fourier series. This yields

$$u(x) \sim -\sum_{k \in \mathbb{N}} \frac{\sin(kx)}{k} \quad , \quad N \to \infty. \tag{5.5}$$

This series can be summed using standard methods[1]. The resulting expression for the velocity field reads

$$u(x) = \frac{x - \pi}{2} \quad , \quad x \in [0, 2\pi). \tag{5.6}$$

[1]See e.g. in [3] example 14.1.1 .

The convergence to a saw tooth function in real-space is therefore consistent with the fixed point in oscillator space.
The question remains, whether setting the first modes to zero destabilizes the fixed point or if the system has a longer transient. To resolve this question we perform a linear stability analysis of equation (4.5). As noted in section 4.1.1, equation (4.9) is more adequate for deriving the Jacobi matrix. From this equation the system's Jacobi matrix $J_{k,q} := \partial\dot{\varphi}_k/\partial\varphi_q$ follows

$$\begin{aligned} J_{k,q} = \quad & \delta_{k,q} \sum_{p=-N}^{N} \omega_{k,p} \ \sin(\varphi_p + \varphi_{k-p} - \varphi_k) \\ & -2\,\omega_{k,q} \ \sin(\varphi_q + \varphi_{k-q} - \varphi_k) - 2\,\omega_{k,k+q} \ \sin(\varphi_q + \varphi_k - \varphi_{k+q}). \end{aligned} \tag{5.7}$$

We have assumed that terms that contain oscillators φ_k for $|k| > N$ are not taken into account in this expression. At the fixed point $\varphi_k = \pi/2$ the Jacobi matrix takes the form

$$\begin{aligned} J_{k,q} = \quad & \delta_{k,q} \sum_{p=-N}^{N} \omega_{k,p} \ \mathrm{sgn}(p) \ \mathrm{sgn}(k-p) \\ & -2\,\omega_{k,q} \ \mathrm{sgn}(k-q) - 2\,\omega_{k,k+q}. \end{aligned} \tag{5.8}$$

We may now carry out a linear stability analysis[2] around the fixed point for different k_0. This requires computing the eigenvalues λ_k of the Jacobi matrix (5.8). The eigenvalue with the largest real part defines stability of the fixed point . If the real part of this eigenvalue is larger than zero it is an unstable fixed point; infinitesimal perturbations will grow exponentially fast. On the other hand, if all eigenvalues have negative real part, the fixed point is stable. We calculated numerically the eigenvalues of the Jacobi matrix. These are shown for different k_0 in Figure 5.3. As a consequence of the conserved quantity we always have a $\lambda_k = 0$. We verify numerically that for $N = 1024$ and $k_0 = 0$ the fixed point is stable, whereas for $k_0 > 0$ it is unstable. This explains why setting the first modes to zero produces non-trivial dynamics, and, more importantly, shows that the dynamics for $k_0 \geq 1$ are not a long lived transient of this fixed point.
We can thus produce Burgers-like non-trivial dynamics with our model (4.5) by removing the first k_0 modes from the dynamics.

[2]Linear stability analysis is presented in the context of turbulence in [34].

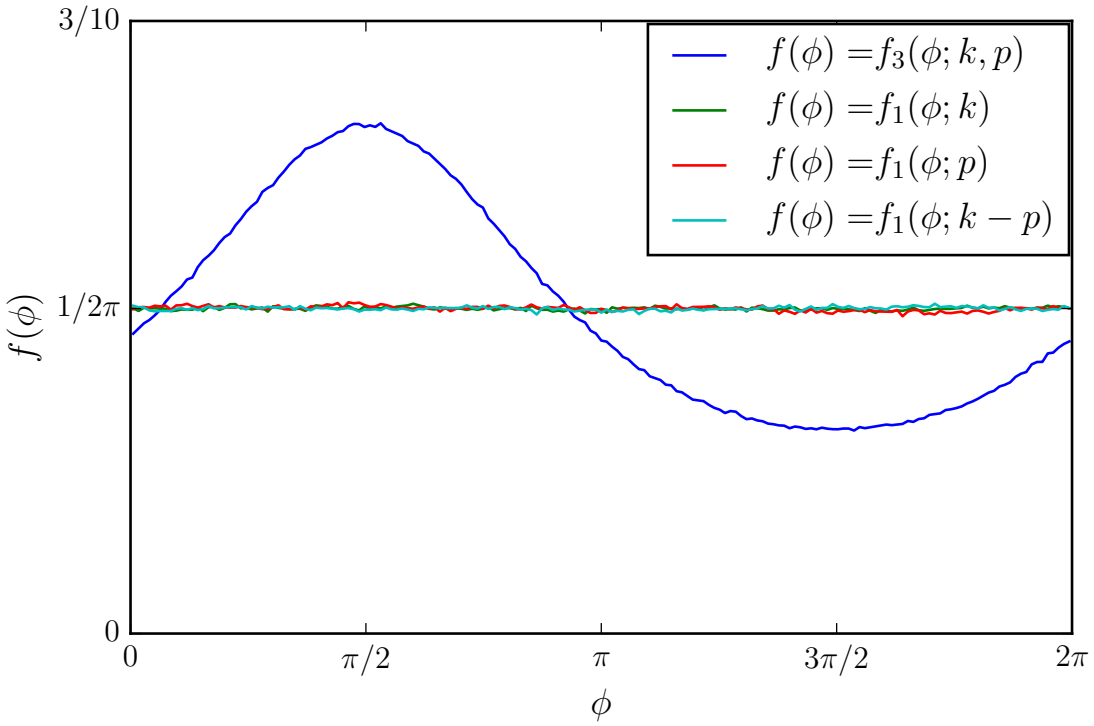

Figure 5.4.: Typical one-oscillator and triad PDFs from the numerics. The one-oscillator PDFs are trivial, whereas the triad's peaks around $\pi/2$. Shown here is the triad $\varphi_{500,100}$ for a time series $\sim 10^7$ units of time long.

5.2. Numerical oscillator PDFs

We now have our model (4.5) for the dynamical quantities φ_k, $k \in \{k_0, ..., N\}$, and a convenient choice of spectrum. With this in place we may numerically integrate it and observe non-trivial oscillator dynamics. We start our analysis by looking into the oscillator PDFs.

We first consider the one-oscillator (4.18) and triad (4.22) PDFs . In Figure 5.4 we show the one-oscillator PDF f_1 for three different oscillators and the triad PDF f_3 of the triad they form. As we observe, the one-oscillator PDFs are uniformly distributed. This supports numerically the invariance of the system under (4.6). The behavior shown in Figure 5.4 is the typical situation observed in all oscillators and triads. Oscillator PDFs are uniformly distributed, whereas the triads peak around $\pi/2$. Indeed a consequence of the triad labeling convention from section 4.2 is that triads peak around $\pi/2$ and have a minimum at $3\pi/2$. The behavior and form of the PDF is similar for all triads, but the height depends on the individual

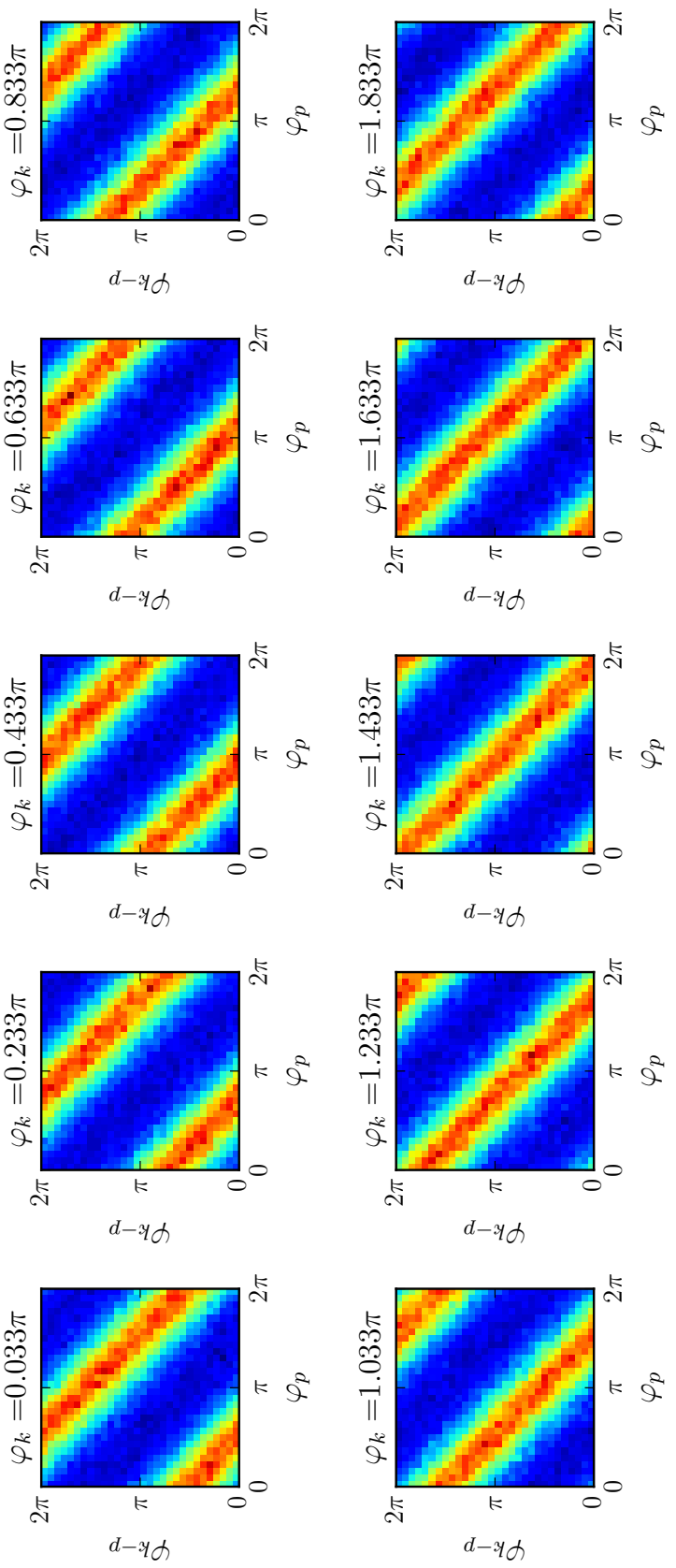

Figure 5.5.: Three-oscillator PDF $f_{1\times1\times1}$ at constant φ_k cuts. The observation that the oscillators accumulate at the plane $\phi_{k-p} = \pi/2 + \phi_k - \phi_p$ is a consequence of the correspondence between the triad and three-oscillator PDFs. The same color scale has been used for all cuts.

triad.
If we consider the full three-oscillator PDF $f_{1\times1\times1}$ we observe the behavior shown in Figure 5.5. Shown in this figure are slices at constant ϕ_k. As we observe, the maximum is found along the $\phi_p + \phi_{k-p} - \phi_k = \pi/2$ plane and the minimum along the $\phi_p + \phi_{k-p} - \phi_k = 3\pi/2$ plane. This observation can also be cast in the form of an invariance of the three-oscillator PDF. This invariance takes the form

$$\begin{aligned} f_{1\times1\times1}(\beta,\gamma,\omega+\delta;p,k-p,k) = &\quad f_{1\times1\times1}(\beta,\gamma-\delta,\omega;p,k-p,k) \\ = &\quad f_{1\times1\times1}(\beta-\delta,\gamma,\omega;p,k-p,k) \end{aligned} \tag{5.9}$$

and is the numerical equivalent of the infinitesimal (4.29). Note additionally, that the fact that the maximum and the minimum of the three-oscillator PDF are found at the corresponding planes is a consequence of the correspondence between the triad and the three-oscillator PDF.
These are numerical observations, which verify results obtained in the last chapter. The fact that triads accumulate at $\pi/2$ is interpreted as the presence of coherence phenomena, whereby a linear combination of random variables has non-trivial statistics, while the individual oscillators are uniformly distributed. Let us now concentrate on the triad PDFs and how to describe their statistics. By comparing the triad system with simpler systems, we proposed in the last chapter a parametrization for the PDF. We now proceed to numerically probe the trigonometric moments in order to verify this assertion.

5.3. Oscillator statistics

From the numerical integration we obtained triad PDFs. Although we did not develop a theory for obtaining the PDFs directly from the dynamics, studying the numerical results allows us to verify the semi-analytic theory for the triad PDFs. In this section we will look into the trigonometric moments of triads. This will allow us to find relations between the different trigonometric moments and probe the validity of the semi-analytic theory. A verification of this theory for the triad PDFs will be done and its consequences presented.

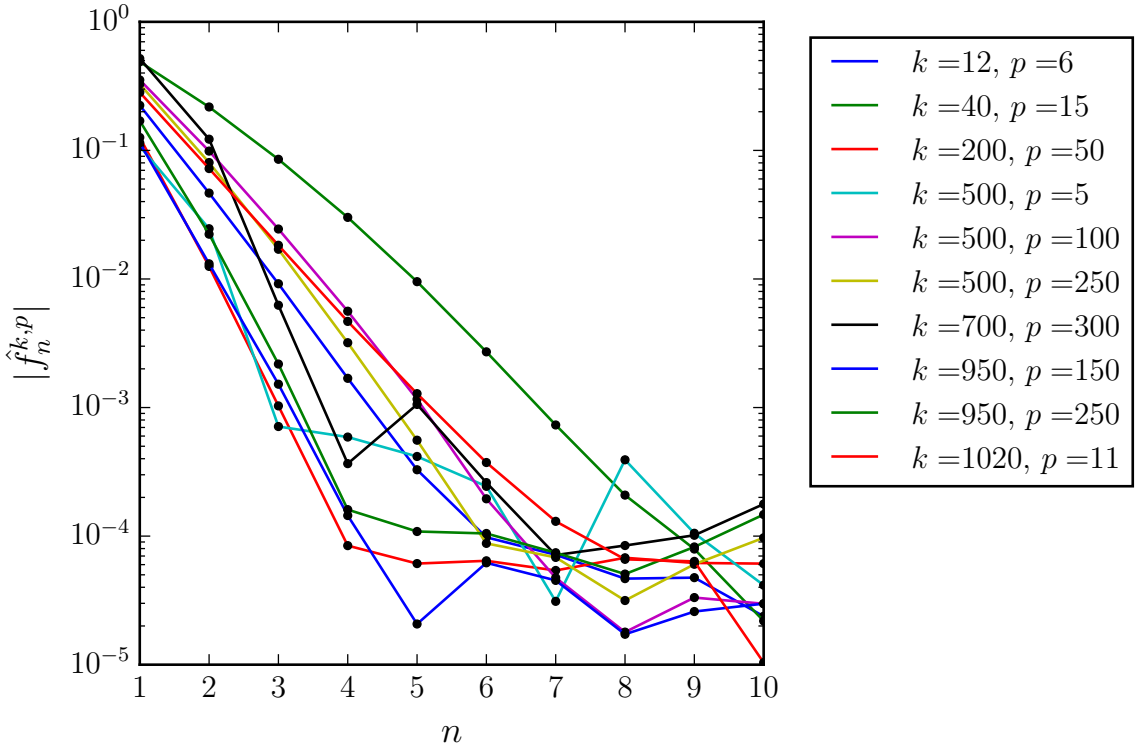

Figure 5.6.: Linear-log plot of the first ten Fourier coefficients of triad PDFs as in (5.10). A linear behavior is observed, which reassures the approach of modeling the triad PDFs as WSM distributions (5.13). Averaged over sample size $\sim 10^{10}$. To resolve moments with numerical value below $|\hat{f}_n^{k,p}| \sim 10^4$ longer time series are necessary.

5.3.1. Parametrization for the triad PDF

Let our starting point be the triad PDF f_3 as defined in (4.22). As we saw in section 2.2.2 a general Fourier series for a 2π-periodic real function f_3 satisfying the normalization $\int_{S^1} f_3(\phi)\,\mathrm{d}\phi = 1$ may be written as

$$f_3(\phi; k, p) = \frac{1}{2\pi}\left[1 + \sum_{n\in\mathbb{N}} \hat{f}_n^{k,p}\ \exp(-\mathrm{i}n\phi) + c.c.\right]. \tag{5.10}$$

Given a triad $\varphi_{k,p}$ we seek its trigonometric moments, i.e. the Fourier coefficients $\hat{f}_n^{k,p}$. These are parametrized by k and p; each triad has different trigonometric moments and consequently different PDFs. Knowing all trigonometric moments completely characterizes the circular PDF and hence the triad as a circular random variable. In terms of circular statistics, we will calculate the trigonometric moments.

These can be identified as equivalent to ensemble averages, and, in ergodic systems, as time averages. We work under the conjecture that our system is ergodic. This yields an empirical way of obtaining the coefficients $\hat{f}_n^{k,p}$ given by

$$\hat{f}_n^{k,p} \equiv \langle \exp\left[\mathrm{i}n\varphi_{k,p}(t)\right]\rangle = \lim_{N\to\infty}\frac{1}{N}\sum_{j=1}^{N}\exp\left[\mathrm{i}n\varphi_{k,p}(t_j)\right] \ , \quad n\in\mathbb{N}. \tag{5.11}$$

We can now empirically explore the behavior of the Fourier coefficients for the triads by integrating a time series and taking expectation values (5.11). In Figure 5.6 the magnitude of the first ten Fourier Coefficients for a sample of triads is shown. This is a small subset of all triads, but shows the general behavior. Triads have Fourier coefficients following a linear-log behavior

$$\log|\hat{f}_n^{k,p}| = \alpha_0\, n + \alpha_0, \tag{5.12}$$

where α_0 and α_1 are constant coefficients. Numerical precision becomes an issue at around $|\hat{f}_n^{k,p}| \sim 10^{-4}$. Additionally, the high frequency of the higher moments on the one side and triads with slow oscillators on the other require much larger sample sizes for convergence. Nevertheless, a general linear behavior is observed at least at the lowest modes.

Observing the behavior of the trigonometric moments and based on our starting hypothesis (4.49) we propose coefficients of the form

$$\hat{f}_n^{k,p} = C_{k,p}\ \exp[\mathrm{i}\, n\,\pi/2]\ r_{k,p}^n\ , \quad n\in\mathbb{N}\ , \quad C_{k,p}\in\mathbb{R}^+ \quad , |r_{k,p}|<1. \tag{5.13}$$

The phase of $\hat{f}_n^{k,p}$ is set to capture the preferred direction of the triads around $\pi/2$ (see e.g. Figure 5.4). Parametrization (5.13) allows us then to rewrite the triad PDF (5.10) as

$$f_3(\phi;k,p) = \frac{1}{2\pi}\left[1 + C_{k,p}\sum_{n\in\mathbb{N}} r_{k,p}^n\ \exp\left[\mathrm{i}n\ (\pi/2-\phi)\right] + \text{c.c.}\right]. \tag{5.14}$$

This parametrization for the PDF is consistent with Figure 5.4 and represents a WSM circular distribution. It is an unimodal circular PDF which accumulates at $\pi/2$. Just as in equation (2.39) the sum in equation (5.14) can be explicitly carried

out using the geometric series

$$f(\phi;k,p) = \frac{C_{k,p}}{2\pi}\left[\frac{1-r_{k,p}^2}{1+r_{k,p}^2-2r_{k,p}\,\sin\phi}\right] + \frac{1-C_{k,p}}{2\pi}. \tag{5.15}$$

Convergence is assured by the condition $|r_{k,p}| < 1$. The parameters $r_{k,p}$ and $C_{k,p}$ themselves can be expressed through trigonometric moments by ensemble averages. Using the first two moments and the relation between them we obtain from (5.11) and (5.13)

$$\begin{aligned} C_{k,p} &= \frac{(\hat{f}_1^{k,p})^2}{\hat{f}_2^{k,p}} = \frac{\langle \exp\left[\mathrm{i}\,\varphi_{k,p}(t)\right]\rangle^2}{\langle \exp\left[2\mathrm{i}\,\varphi_{k,p}(t)\right]\rangle}, \\ r_{k,p} &= \frac{\hat{f}_2^{k,p}}{\mathrm{i}\,\hat{f}_1^{k,p}} = \frac{\langle \exp\left[2\mathrm{i}\,\varphi_{k,p}(t)\right]\rangle}{\mathrm{i}\,\langle \exp\left[\mathrm{i}\,\varphi_{k,p}(t)\right]\rangle}. \end{aligned} \tag{5.16}$$

Furthermore, this functional form for the PDFs has as a consequence that we can describe every triad PDF by only two parameters. This shall be explored in detail in the next sections.

5.3.2. Triad parameters $r_{k,p}$ and $C_{k,p}$

Recall that in section 4.4 a comparison of the triad dynamics with a stochastically forced simple model and a similarity to arrays of Josephson junctions led to the proposition that the triad PDF could be described by a WSM distribution. This was numerically verified by comparison of the different trigonometric moments. We hence parametrized the triad PDF as a WSM distribution. This reduced the study of triad PDFs to two parameters. Comparison of these parameters simplifies the study of triad PDFs. Instead of having to compare numerical PDFs we only need to look at these parameters to know the triads' complete statistical information. The value $r_{k,p} = 0$ leads to an uniform distribution, i.e. $f_3(\phi;k,p) = 1/2\pi$. Larger $r_{k,p}$ implies a higher peak at $\pi/2$. $C_{k,p}$ is a mixture parameter, and modulates the magnitude of the angular part of the distribution with respect to the uniform part.

As commented in section 4.2, we hold to a convention which avoids double counting of triads. This leads to displaying triads in a two-dimensional plot, with axis k and p, whereby the region defined by $k - p \geq p \cup p \geq 0$ includes all possible triads without repetitions. The magnitude of the triads' first trigonometric moment is shown in Figure 5.7. Using the second trigonometric moment and equation (5.16) we obtain $r_{k,p}$ and $C_{k,p}$, which are shown in Figures 5.8 and 5.9, respectively. We

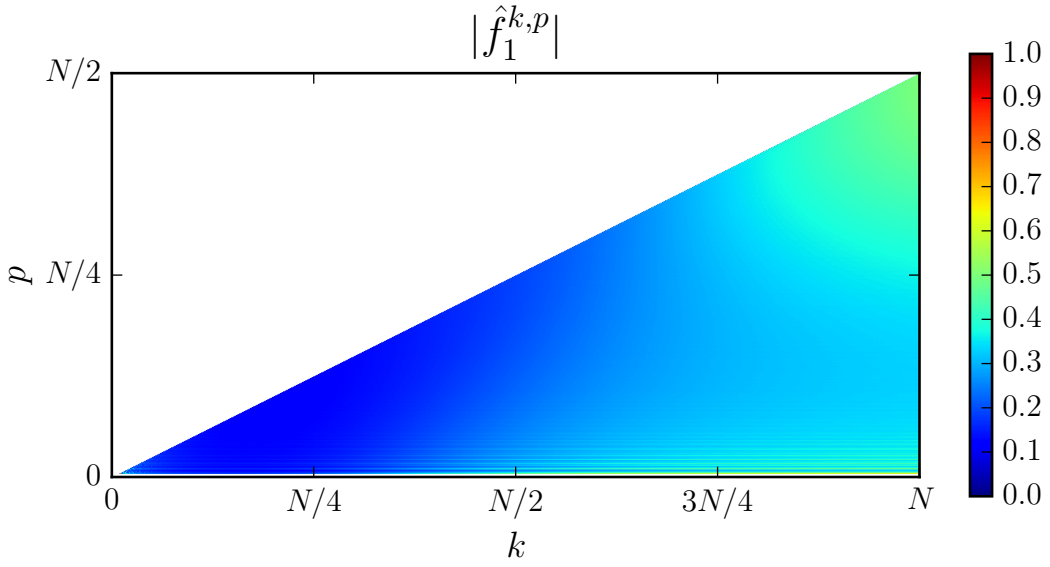

Figure 5.7.: The first trigonometric moment for all triads. The general observation is that higher k leads to a larger first trigonometric moment.

verified that the condition for positive PDFs (2.40) was fulfilled for all triads.

The interpretation of these results is the following. The parameter $r_{k,p}$ tells us how peaked the distribution is. The mixture parameter $C_{k,p}$ also influences the height of the PDF, but its main purpose is to parametrize departure from pure WC distribution. In Figure 5.8 we observe a tendency of high k triads to peak higher than ones with lower k; this is especially so for triads with both high k and p. In Figure 5.9 we observe that high k triads with low p have a marked departure from uniform distribution. Triads with both k and p low also show a high mixture parameter, but their $r_{k,p}$ parameter is rather low. This indicates that although the angular part of the distribution is higher than the uniform one, the angular part is relatively small in comparison with other triads.
Identifying the triad PDFs as WSM distribution means that all one-triad statistical information is contained in these plots.

5.3.3. Reduction to a WC distribution

As we see from Figure 5.9, the bulk of triads has mixture parameter $C_{k,p}$ in the range $[1, 1.4]$. This is also shown in the distribution of the values of the mixture parameter $C_{k,p}$ in Figure 5.10. Recall that a WSM distribution with $C = 1$ is a

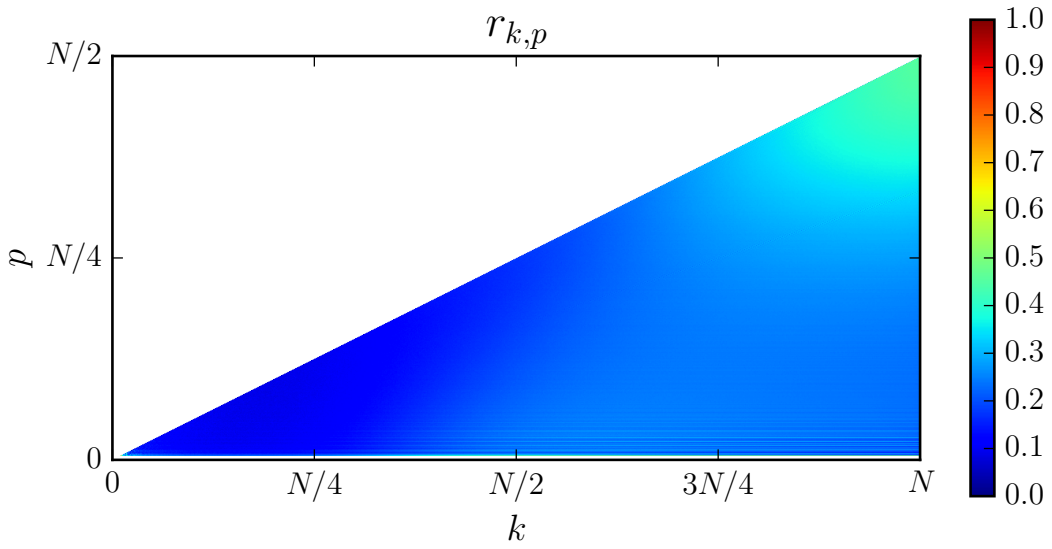

Figure 5.8.: The triad parameter $r_{k,p}$ for all triads. This parameter measures how peaked the PDF is. Convergence of the sum requires that $|r_{k,p}| \leq 1$.

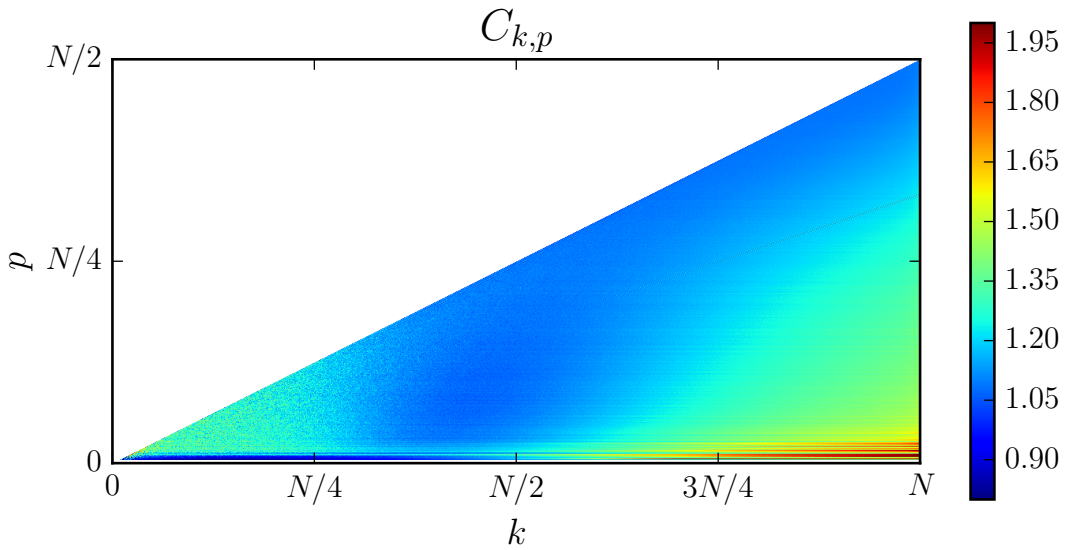

Figure 5.9.: Using (5.16) we calculate the mixture parameter $C_{k,p}$ for all triads. It measures the relative weight of the angular part in the PDF (5.14) with respect to the uniform part. The condition for positive PDFs (2.40) is fulfilled.

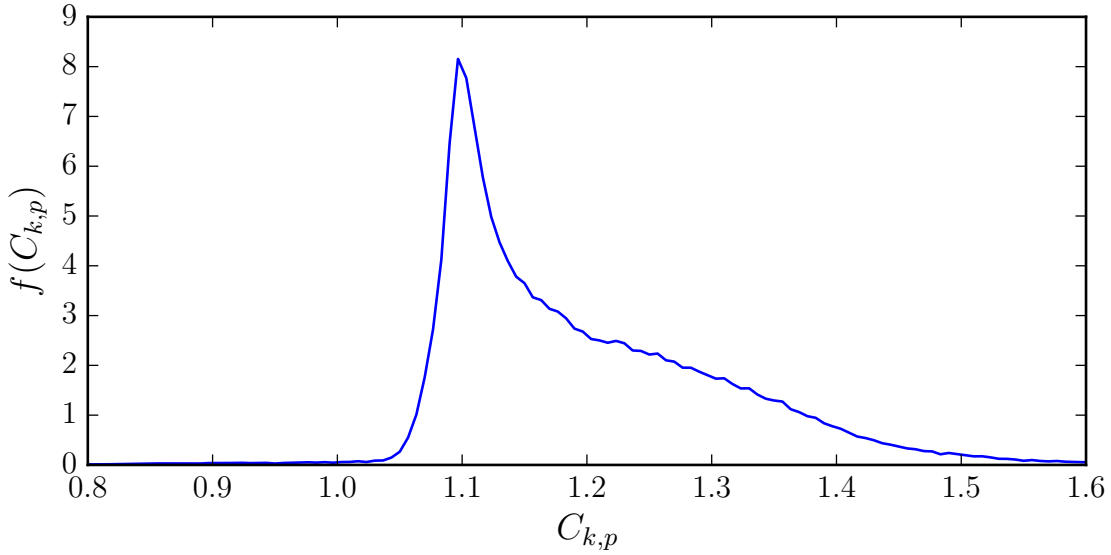

Figure 5.10.: Distribution of the $C_{k,p}$ parameter values for all triads. The bulk of triads has $C_{k,p}$ value around 1.1. This motivates modeling the triad PDF with the simpler WC distribution. The angular part of the PDF is mixed with parameter near one, whereby it is possible to reduce our theory to a simpler one-parameter WC distribution.

WC distribution. The values for $C_{k,p}$ accumulate around ~ 1.1. This poses the question of how well the simpler WC distribution describes the triad PDFs. This would leave only one parameter for each triad PDF. A simpler ansatz than (5.13) for the trigonometric moments reads

$$\hat{f}_n^{k,p} = \exp[\mathrm{i}\, n\, \pi/2]\; R_{k,p}^n\,, \quad n \in \mathbb{N}\,, \quad |R_{k,p}| < 1. \tag{5.17}$$

This is equivalent to a WC distribution (2.29) with first trigonometric moment $\mathbf{R} = R_{k,p} \exp[\mathrm{i}\pi]$. Following equations (2.29) and (2.30), in this simplified theory the triad PDFs take the form

$$\begin{aligned} f_3(\phi; k, p) = &\quad \frac{1}{2\pi}\left[1 + \sum_{n\in\mathbb{N}} R_{k,p}^n \, \exp\left[\mathrm{i}n\,(\pi/2 - \phi)\right] + c.c\right] \\ = &\quad \frac{1}{2\pi}\frac{1 - R_{k,p}^2}{1 + R_{k,p}^2 - 2\, R_{k,p}\, \sin\phi}. \end{aligned} \tag{5.18}$$

As was previously the case (5.16), we now also have a relation between the first moment $R_{k,p}$ and ensemble averages given by

$$R_{k,p} = -\mathrm{i}\, \hat{f}_1^{k,p} = -\mathrm{i}\, \langle \exp\left[\mathrm{i}\, \varphi_{k,p}(t)\right] \rangle. \tag{5.19}$$

Analytic property of the expected values

In section 2.3.3 we introduced the WC distribution and commented on some of its properties. One of these is the identification of the WC distribution with the Poisson kernel. As noted there, this property has the consequence that expectation values of functions of triads are analytic in the complex variable $\mathbf{R}$. This property yields a considerable amount of structure to triad statistical quantities, and might provide in the future provide means to justify existence of differential equations defining the $R_{k,p}$.

5.3.4. Comparison of the WSM and WC distributions for the triad PDF

We have motivated a WSM parametrization (5.14) for the PDF by comparing it to a simpler system subject to stochastic driving. Numerical study of the behavior of the first coefficients of the Fourier series confirmed this. The observation that the bulk of triads has $C_{k,p}$ near 1 then led to a simpler WC parametrization (5.18). Here we will compare these two parametrization.

In Figure 5.11 we show triad PDFs obtained from integrated time series, as well as the corresponding WSM (5.14) and WC (5.18) distributions for four different triads. For the bulk of triads, the WC ansatz (5.18) yields results with up to 5% error, with the advantage of reducing the whole description of the PDF to one parameter. Only very few triads, usually the ones with high-k and low-p, show errors of more than 5% when describing their PDF as a WC distribution. This motivates a general study of the triads with this distribution, considering the high-k and low-p triads as a minority of special cases.

A more global analysis is provided in Figure 5.12. Here the cumulative error was calculated for all triads. Let $f_{\mathrm{num}}(\phi; k, p)$ be the numerical PDF of the k, p triad. We will then define the cumulative error in percentage as

$$\mathrm{Error}(\%) = \int_{S^1} \mathrm{d}\phi \left| 1 - \frac{f_3(\phi; k, p)}{f_{\mathrm{num}}(\phi; k, p)} \right| \times 100. \tag{5.20}$$

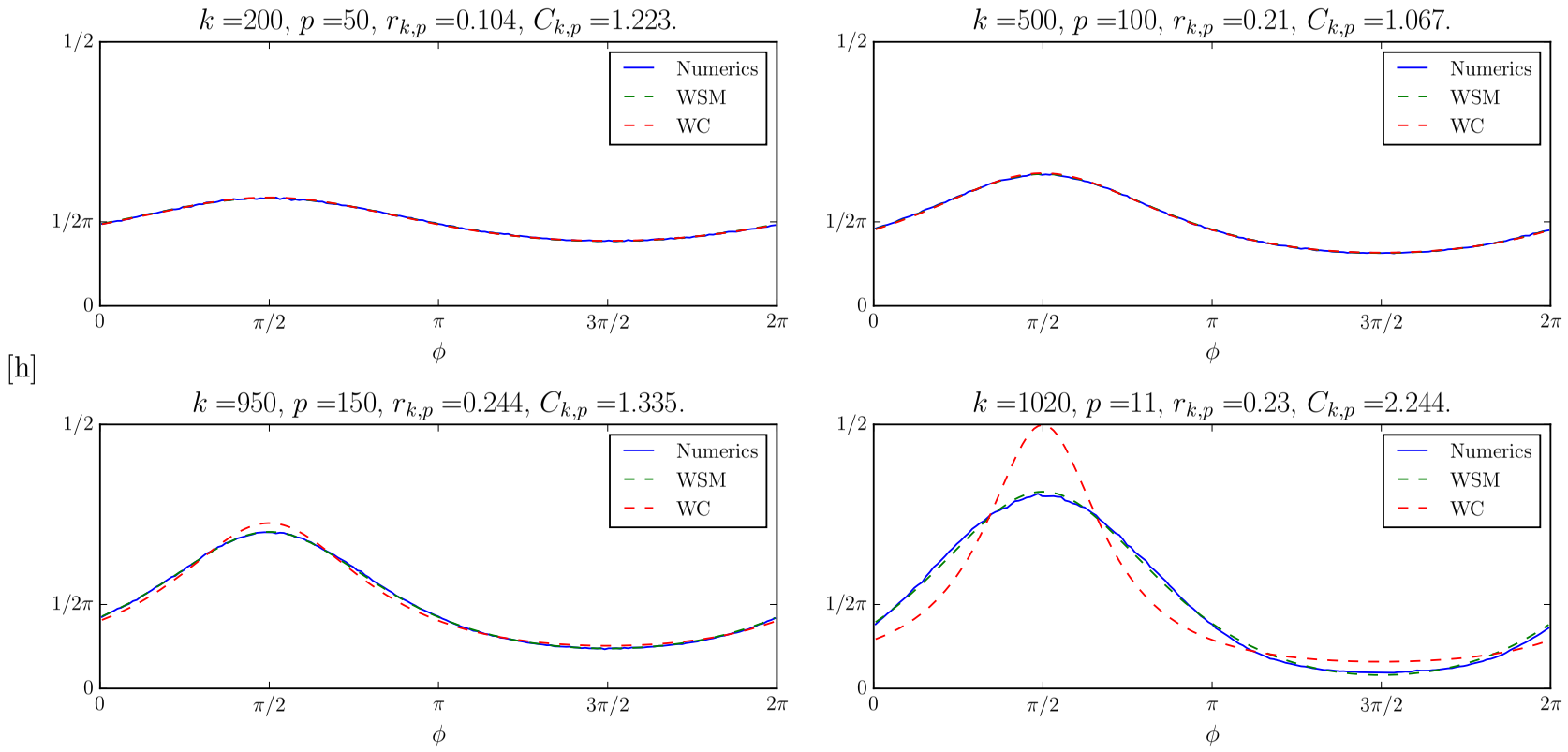

[h]

Figure 5.11.: Numerical integration and the WSM and WC distributions for different triads. Only the triads with $C_{k,p}$ much higher than ~ 1.4 are not well described by the WC distribution. This accounts for a minority of the triads. The result is reducing study of triad PDFs for the bulk of triads to one parameter, $r_{k,p}$ as defined in (5.19).

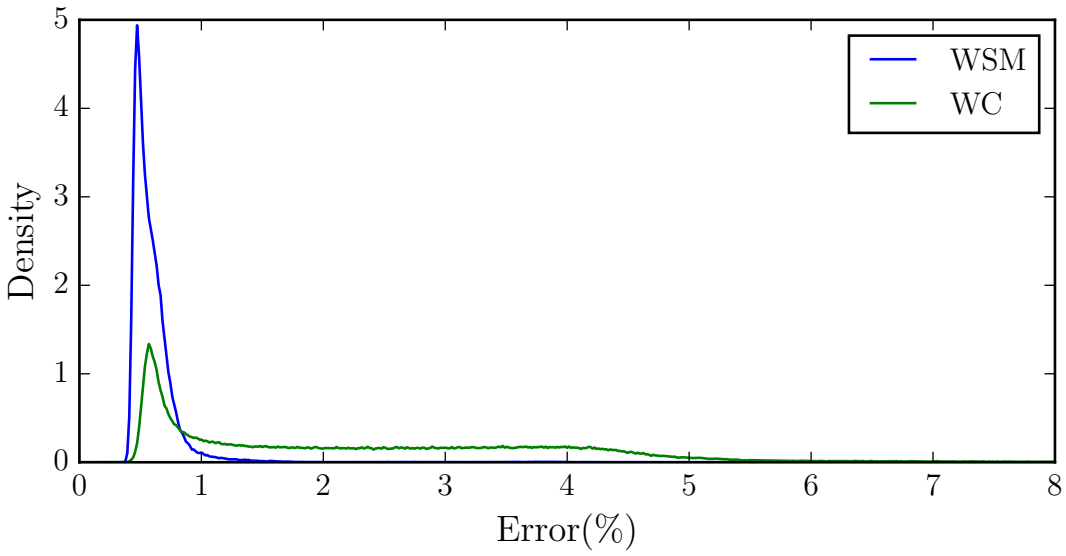

Figure 5.12.: Distribution of the cumulative error (5.20) for the WC and WSM functional forms of the triad PDF. The WSM PDF has error with mean 0.605% and variance 0.128%. The WC PDF has mean 2.40% and variance 4.78%. By reducing the theory for the triad PDFs to the simpler WC distribution we work with only one parameter, whilst keeping error relatively low.

The error was calculated for all triads using both the WC and WSM distributions for $f_3(\phi; k, p)$. The resulting error distributions are shown in Figure 5.12. The WSM distribution ansatz for f_3 has lower error. This distribution has error with mean 0.605% and variance 0.128%. The WC distribution ansatz on the other hand has mean 2.40% and variance 4.78%. Although the WSM distribution is better at describing the triad PDFs than the WC distribution, cumulative error (5.20) for the WC distribution is typically under 5% with the advantage of reducing the study of triad PDFs to a simpler one parameter distribution. We will therefore reduce our theory for the triad PDFs to a simpler WC distribution, whereby for the bulk of triads the first trigonometric moment completely determines all other trigonometric moments.

5.4. Kuramoto-like order parameter

Previous considerations have given a fine-grained description of the system. A more global analysis of the system leads to an order parameter in the mean field sense.

Let the order parameter at time t be defined as a Kuramoto-like parameter

$$R(t)\exp(\mathrm{i}\Phi(t)) := \langle \exp(\mathrm{i}\varphi_{k,p}(t))\rangle_{k,p}\,. \tag{5.21}$$

This parameter contains general information on the synchronization state of triads. Similar definitions have been used in the literature to study the time-depentent triad synchronization in a similar system [38]. In terms of circular statistics, this order parameter is the mean over all triads. This time dependent order parameter serves to evaluate the triad synchronization in time. Averaging in time yields information regarding the average triad behavior. This time average may then be expressed in terms of the parameter $R_{k,p}$ using (5.19). An averaged order parameter then takes the form

$$R\exp(\mathrm{i}\Phi) := \langle R(t)\exp(\mathrm{i}\Phi(t))\rangle_t = \left\langle \langle \exp(\mathrm{i}\varphi_{k,p}(t))\rangle_{k,p}\right\rangle_t . \tag{5.22}$$

We identify these expectation values as the first trigonometric moments of the individual triads, which can be rewritten in terms of the distribution parameters

$$R\exp(\mathrm{i}\Phi) \equiv \mathrm{i}\,\langle R_{k,p}\rangle_{k,p} \tag{5.23}$$

The numerics confirm the expectation that $\Phi = \pi/2$. R is shown in Figure 5.13 for different spectra (5.1). This gives a means of analyzing the effect of the choice of spectrum on the average synchronization properties of the triads. This mean Kuramoto-like order parameter (5.23) gives a global overview of the system.
On the other hand, the triads' first trigonometric moment contains finer information regarding which parts of the system accumulate more or less sharply at $\pi/2$. The triads' first trigonometric moment is shown for several choices of spectra in Figure 5.14. As can be seen, a very quick overview of the system as a whole is easily attainable. This might prove useful in future studies, while investigating the effect of the choice of spectrum on the triad parameters $R_{k,p}$.
Averaging also allows one to establish a comparison point to divide triads into a slow or fast category. In this context fast is meant in the sense that more coherent events take place, and therefore the PDF is more peaked. In Figure 5.15 we show the $R_{k,p}$ value for all triads with the same value $R_{k,p} = R$ marked in red. The transition to fast triads happens in the range $[N/2, 3N/4]$. A similar comparison is shown in Figure 5.16 for selected PDFs. Note that this approach also identifies the triads with larger k as those which accumulate most around $\pi/2$; it is the fastest oscillator

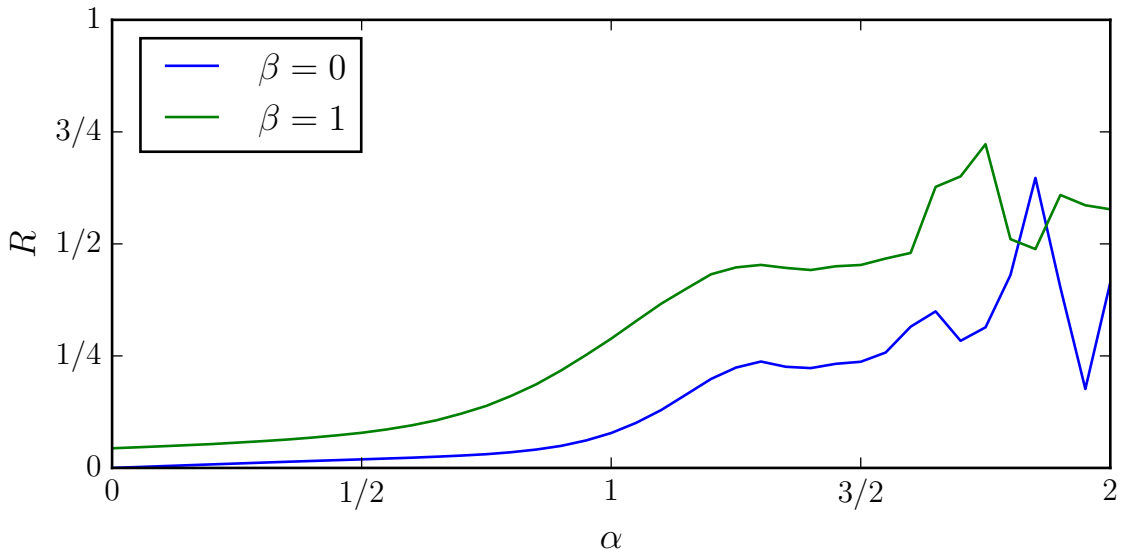

Figure 5.13.: Different spectra, and their averaged triad Kuramoto-like order parameter. This order parameter contains information of the average synchronization state of the triad system. Recall from equation (5.1) that α is the algebraic steepness of the spectrum, and β indicates the Gaussian cutoff.

in a triad the one which determines if the triad is slow or fast.

5.5. Two-triad PDFs

In Figure 4.2 we saw that the triads are not coupled dynamically to all other triads. Two triads are only coupled, if they share one or more oscillators in common. An example of two-triad PDFs (4.23) is shown in Figure 5.17. On the left side is the joint statistics $f_{3\times3}$ and on the right side is the direct product of one-triad statistics $f_3\, f_3$. Comparing the difference between the left and right sides of Figure 5.17 yields the correlation function $C_{3\times3}$. This behavior is quite general; triads which share lowest mode oscillator, i.e. same p, have a much more pronounced correlation than others which share their k or $k-p$ oscillator.
Recall that the triads are distributed as unimodal circular distributions with first moment at $\pi/2$, i.e. $\hat{f}_1 \propto \mathrm{i}$ for all triads. Hence we obtain from equation (4.45)

$$f_3(\phi; k, p) = \frac{-S(\phi; k, p)}{\tilde{\omega}_{k,p} \cos\phi}. \tag{5.24}$$

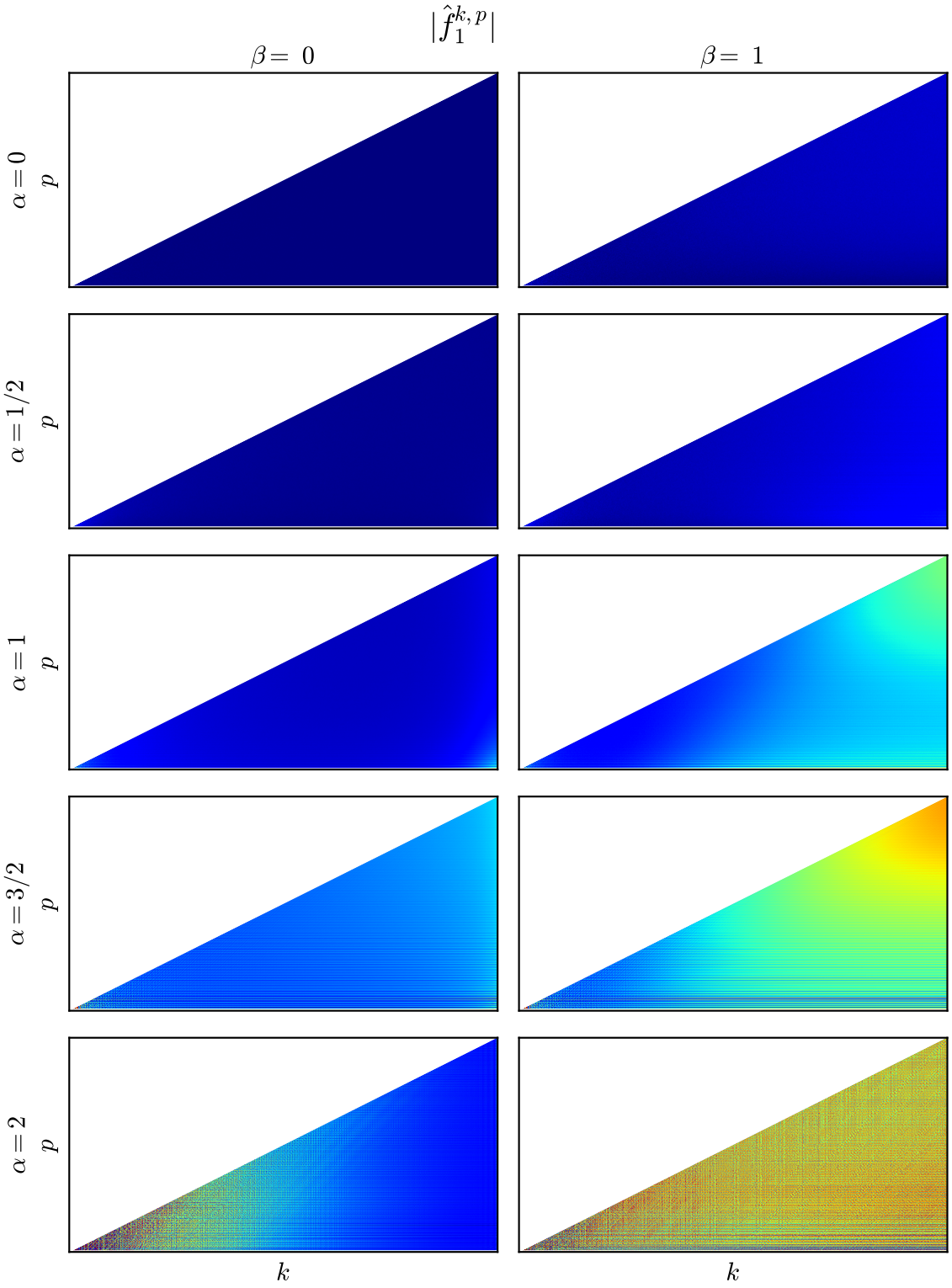

Figure 5.14.: The first trigonometric moments $|\hat{f}_1^{k,p}|$ for different choices of α and β producing different spectra (5.1). This is a high resolution version of Figure 5.13. Same color scale as in Figure 5.7, blue is at 0 and red at 1.

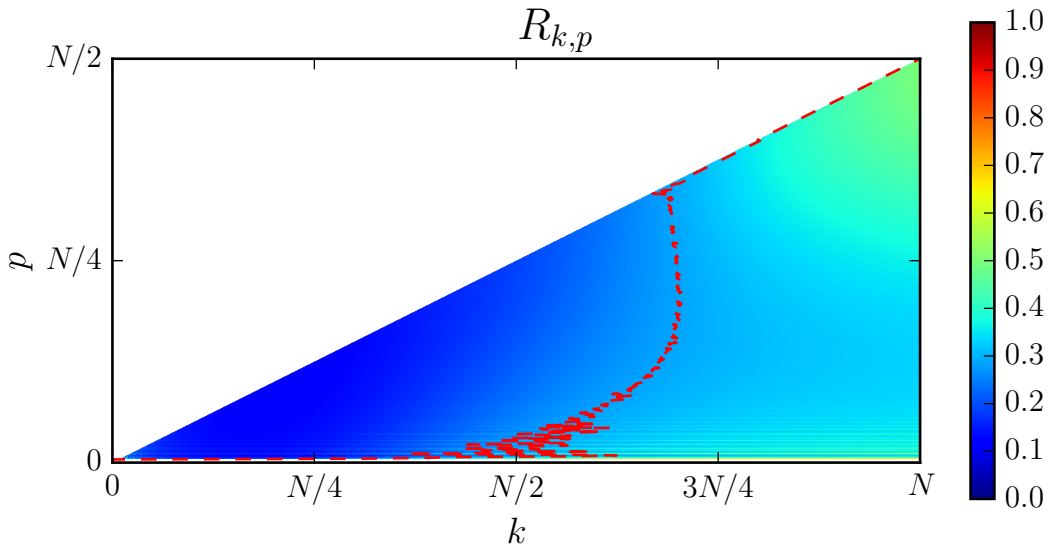

Figure 5.15.: Same as in Figure 5.7, but with the equipotential of the Kuramoto parameter (5.22) shown in red. This allows to differentiate between triads which accumulate more or less at the peak in $\pi/2$. The PDFs of four chosen triads can be compared in Figure 5.16. The transition from slow to fast triads happens in the range $N/2 < k < 3N/4$. Fast triads have k oscillator above the Gaussian cutoff at $\sim N/2$.

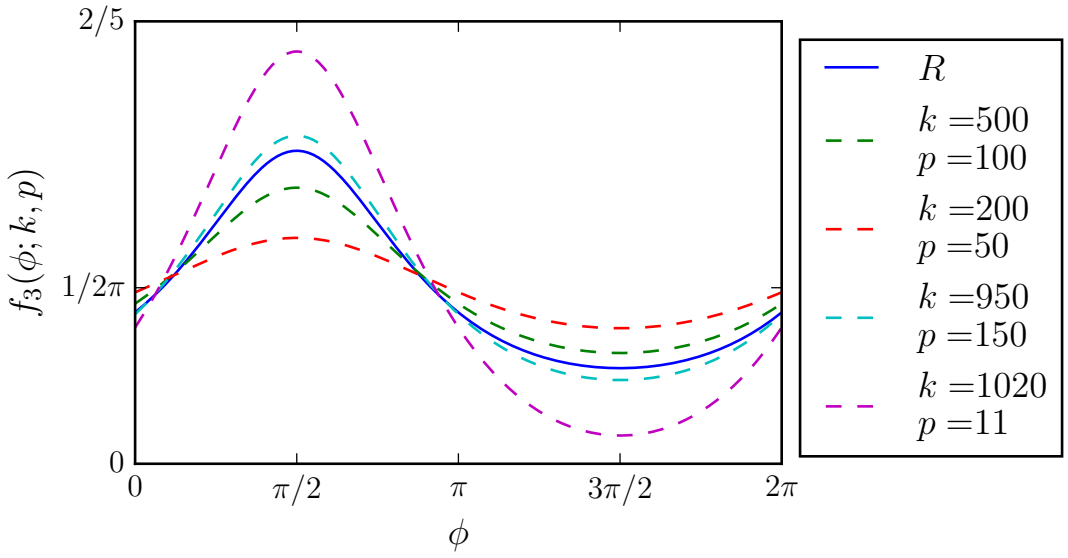

Figure 5.16.: The same triads from Figure 5.11, here compared to the average triad PDF, given by a WC distribution with the Kuramoto R.

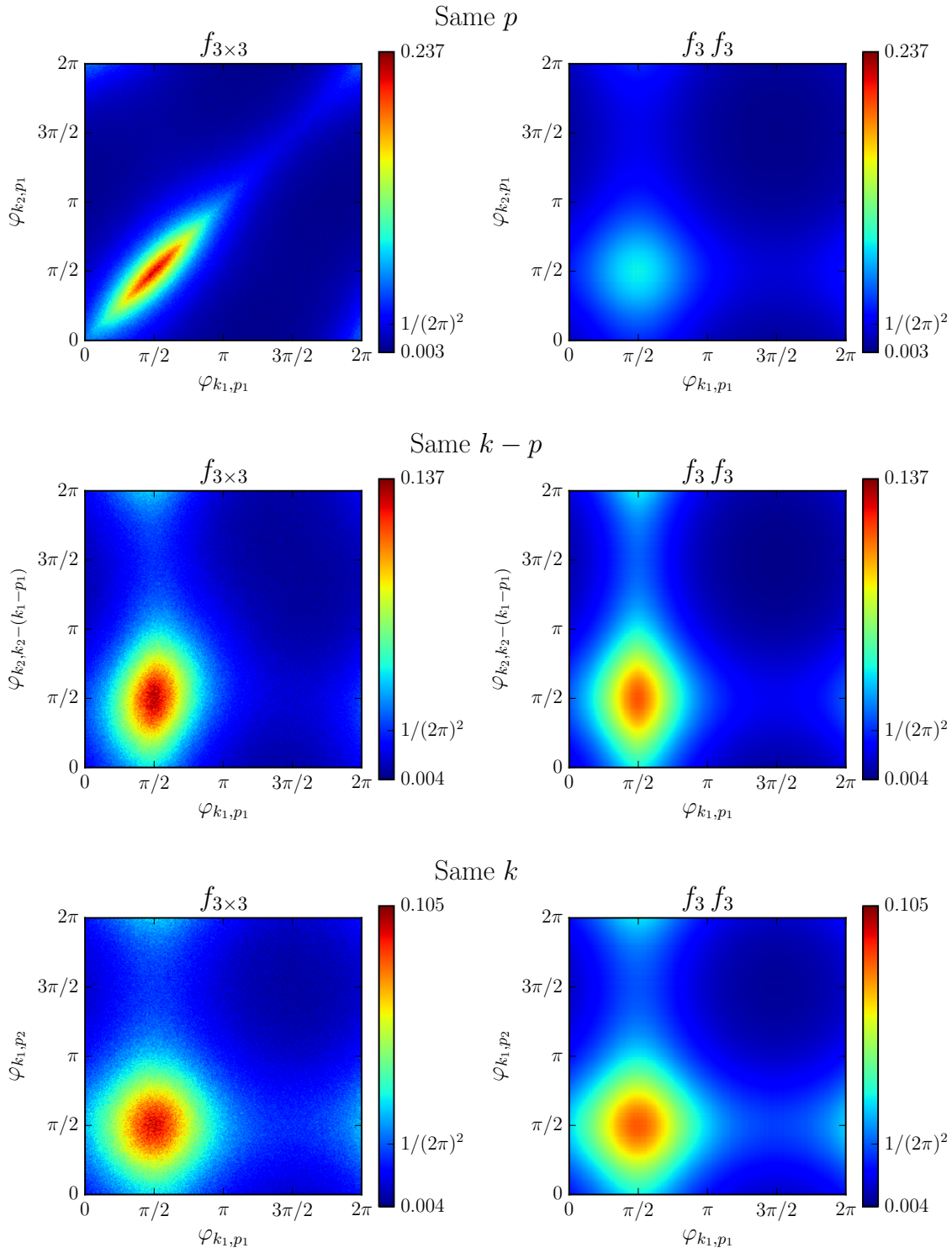

Figure 5.17.: Given k_1, k_2, p_1, p_2 we construct different triads, with the same p, $k-p$ or k and build their joint PDF from an integrated time series. The joint PDF is on the left side. On the right side is a direct product of the two one-triad PDFs. Comparing the two one can judge departure from statistical independence. Each row uses the same color scale.

As previously seen, the triad PDFs depend explicitly on the statistically dependent part of the two-triad PDFs. This means that a full theory for the triad PDFs must necessarily describe the two-triad PDFs in detail. A theory for these two-triad PDFs is not presented here; nevertheless, this may be a good starting point for a theory of the many-oscillator PDFs. For example, parametrizing the triad PDF as a WC distribution means we obtain from equation (5.24)

$$S(\phi; k, p) = \cos\phi \, \frac{\widetilde{\omega}_{k,p}}{2\pi} \left[1 + \sum_{n \in \mathbb{N}} R_{k,p}^{n} \, \exp\left[in \left(\pi/2 - \phi \right) \right] + c.c \right]. \tag{5.25}$$

Recall that S is defined through the correlation function $C_{3\times3}$ as

$$S(\phi; k, p) = \sum_{\{k', p'\}} \Omega_{k,p,k',p'} \int_{S^1} \mathrm{d}\theta \cos\theta \, C_{3\times3}(\phi, \theta; k, p, k', p'). \tag{5.26}$$

Comparing equations (5.25) and (5.26) yields conditions for the correlation function. This could be a starting point for a future theory for the many-oscillator PDF. Additionally, these equations might be used to express two-triad expectation values through the triad PDF and its moments. These ideas require however further development, and we will not treat them here.

In this chapter we have obtained a theory for the triad PDFs, whereby all statistical information of a triad is given through its first trigonometric moment. Three-oscillator coherence effects are seen as peaking of triad PDFs at $\pi/2$, and this is completely described by the triad's first trigonometric moment. In the following chapter the connection between this parameter and real-space statistics will be discussed.

6. Real-space statistics

We have until now worked in the spectral space with the system of oscillators (4.5). This model stems from the Fourier modes of a Burgers velocity field. By virtue of the inverse discrete Fourier transform, the velocity field (4.10) and its gradient (4.11) can be recovered from the oscillators. The effect of the dynamics of the oscillators in real-space can then be investigated.
Studying the oscillator statistics, we reduced the study of triad PDFs to through the WC distribution to one parameter $R_{k,p}$ per triad. By virtue of the WC distribution, all triads' trigonometric moments and expectation values are known, if the corresponding first moment is given. Triad accumulation at $\pi/2$ occurs because of three-oscillator coherence events, and this is completely described by this one parameter.
In this chapter the relation between oscillator coherence and real-space intermittency is discussed. First, general numerical phenomenology of integrated time series in real-space is presented. Afterwards, we explain some of the observed phenomenology with our knowledge of oscillator statistics. Finally, by looking at the velocity increments, the direct influence of the oscillator coherence phenomena on the skewness is derived. Each triad's individual contribution to the skewness will be isolated.

6.1. Velocity and gradient PDFs

Velocity and gradient statistics are a central tool in turbulence; the single-point velocity and gradient statistics provide information about the statistics of the large and small scales, respectively. Our investigations into the oscillator model (4.5) neglected the dynamics of the amplitudes. Nevertheles these influence the real-space dynamics. It is known [29], that if the spectrum is shallow enough, the central limit theorem can be applied when calculating the velocity field from its Fourier modes. As a consequence, velocity fields with uncorrelated phases will show real-space Gaussian statistics. The condition on the spectrum is that it is not steeper

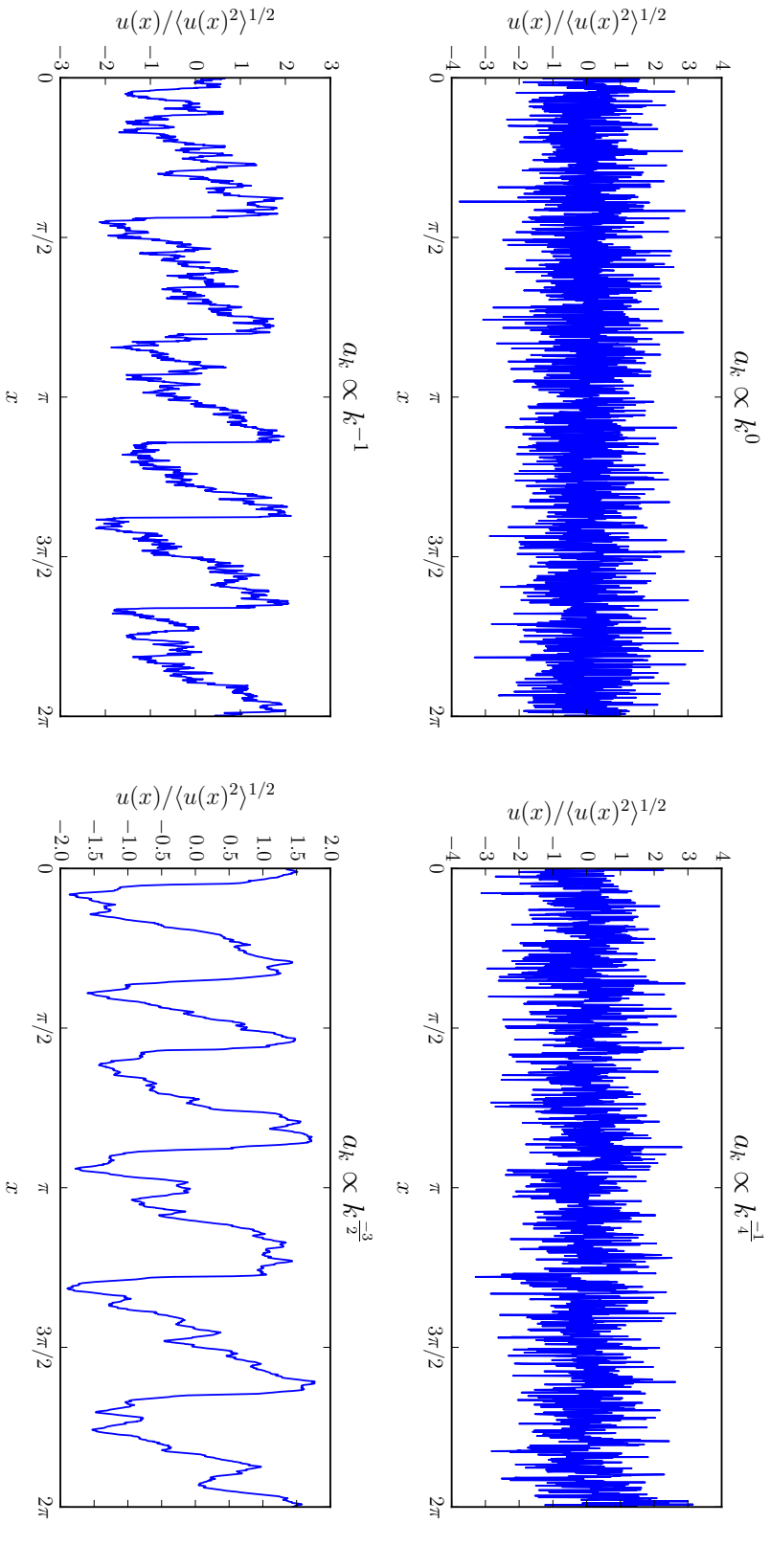

Figure 6.1.: Velocity profiles (4.10) are shown for different steepness of the spectra. For these cases the exponential cutoff was removed ($\beta = 0$ in (5.1)). Flat enough spectra produce Gaussian fields. For steeper spectra the velocity field tends to be dominated by the largest modes.

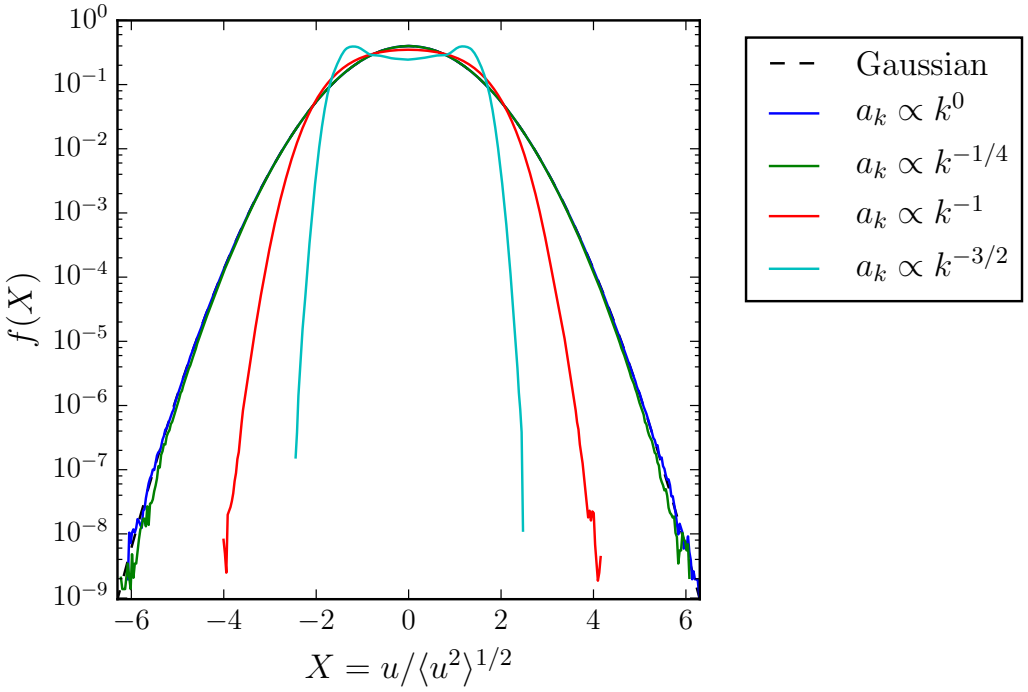

Figure 6.2.: Velocity field statistics for four different spectra. The spectra $a_k \propto k^0$ and $a_k \propto k^{-1/4}$ are flat enough to produce Gaussian statistics. The symmetric maxima at the highest steepness indicate the dominating contribution to the velocity field from its first modes (6.1). In general, velocity statistics remain sub-Gaussian.

than $a_k \propto k^{-1/2} \Leftrightarrow E_k \propto k^{-1}$.

Because we know that the coupled oscillator model has trivial one-oscillator statistics, a similar result must apply here, if non-trivial real-space statistics are to be observed. We will test this by setting $\beta = 0$ and $\alpha = 0, 1/4, 1, 3/2$ in the spectrum (5.1). In Figure 6.1, the typical velocity profile for these spectra is shown. Flat enough spectra produce Gaussian velocity fields. As the steepness increases the velocity field looses randomness and non-trivial statistics are observed.

The real-space PDFs were numerically obtained to quantitatively asses the statistics of these velocity fields. In Figure 6.2 we show the velocity PDFs for these spectra. Both the $a_k \propto k^0$ and $a_k \propto k^{-1/4}$ spectra are shallow enough produce Gaussian statistics. For steeper spectra the tails become sub-Gaussian. Additionally, if we further increase the spectrum's steepness, here by setting $a_k \propto k^{-3/2}$, the PDF shows two maxima symmetric with respect to zero. If the spectrum (5.1) is steep enough,

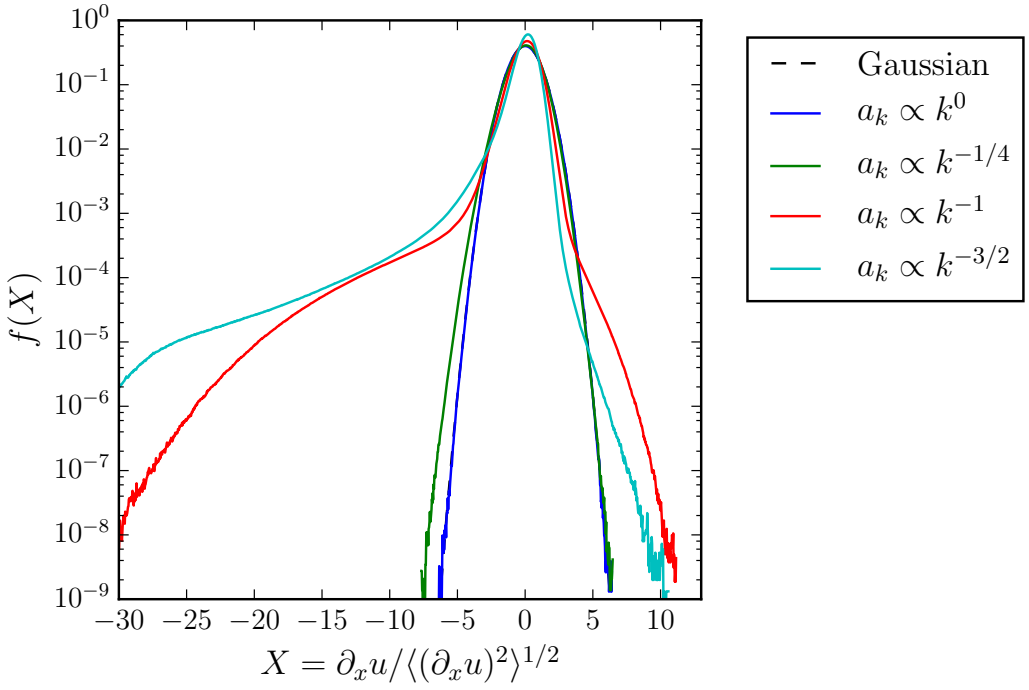

Figure 6.3.: Velocity gradient statistics for four different spectra. Note that $a_k \propto k^{-1/4}$ departs from Gaussianity, but notably less than the steeper spectra. The negative tails foretell the presence of negative shocks. Negative shocks are hallmark of Burgers systems [11].

the real-space velocity field (4.10) is dominated by the first term

$$u(t,x) \sim a_{k_0+1} \cos(\varphi_{k_0+1} + (k_0+1)\, x) + \mathcal{O}(a_{k_0+2}). \tag{6.1}$$

As we visually confirm from Figure 6.1, steeper spectra lead to a dominant contribution of the largest sinusoidal mode. This PDF with two symmetric maxima is typical of sinusoidal signals. This explains the behavior of the velocity PDF in Figure 6.2 for the steep spectrum.

Figure 6.3 shows the velocity gradient statistics for the same spectra. Increasing the steepness of the spectrum produces super-Gaussian negative tails. These tails signify the existence of negative shocks, just as in Burgers turbulence [9]. These shocks are clearly visible in the real-space velocity profiles in Figure 6.1. Note that the shocks are localized events, and they are hence not probed by the velocity statistics.

These observations can be quantified by looking at the PDFs' skewness and flatness. Recall that a Gaussian random variable has skewness zero and flatness three. By

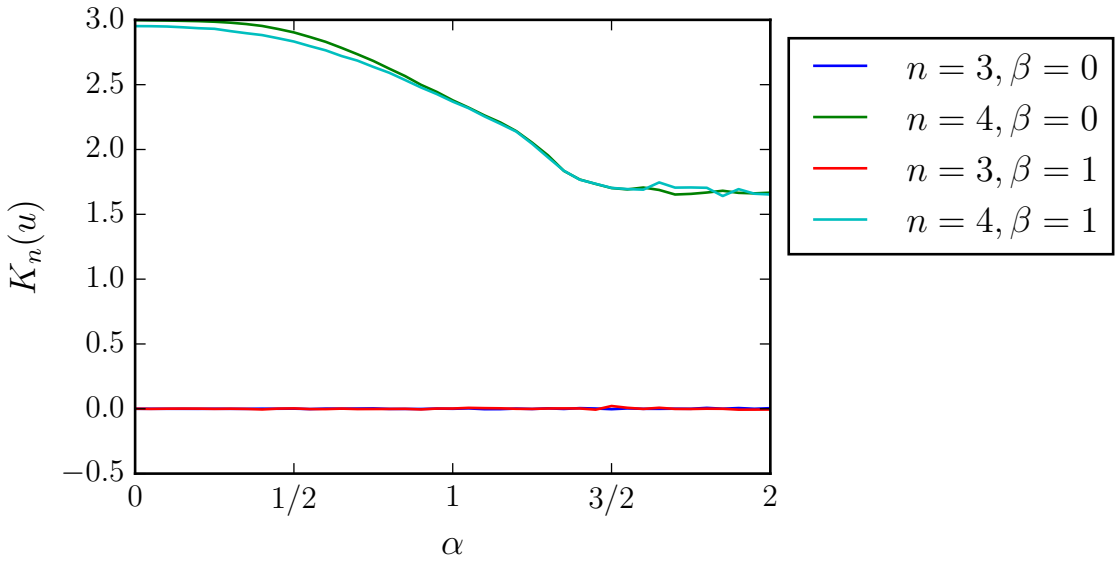

Figure 6.4.: Skewness and flatness of the velocity field $u(t, x)$ (4.10) for different spectra (5.1). The skewness indicates the symmetry of the PDF, whereas the flatness shows sub-Gaussian behavior.

comparing these values to the ones obtained from the velocity and gradient PDFs, the departure from Gaussianity can be quantitatively measured. For different choices of steepness, the velocity field's statistics were obtained, and are shown in Figure 6.4. The skewness remains zero for all choices of spectrum we looked at. On the other hand, by increasing the spectrum steepness the flatness decreases to around ~ 1.6 and seems to saturate there. This is a consequence of the sub-Gaussian tails, whereas zero-skewness indicates that the PDF is symmetric around the mean.

The velocity gradient was already shown to have PDFs with heavy negative tails. Both its skewness and flatness are shown in Figure 6.5 for the same spectra as for the velocity field. A more pronounced departure from Gaussianity is observed, which foretells the presence of extreme events in the small scales. Skewness is non-zero and remains negative. This indicates the prominence of the negative shocks. Skewness remains in the order of $\mathcal{O}(-10)$, whereas the flatness grows considerably to order of $\mathcal{O}(100)$. This is due to the fact that flatness is an even-order moment, so that negative and positive contributions do not cancel out.

It is notable that at $\alpha \sim 1.25$ both the skewness and flatness begin to decrease. This may be explained by considering that the dominating contribution to the real-space velocity field is, in the steep spectrum limit, a sinusoidal signal, as we already

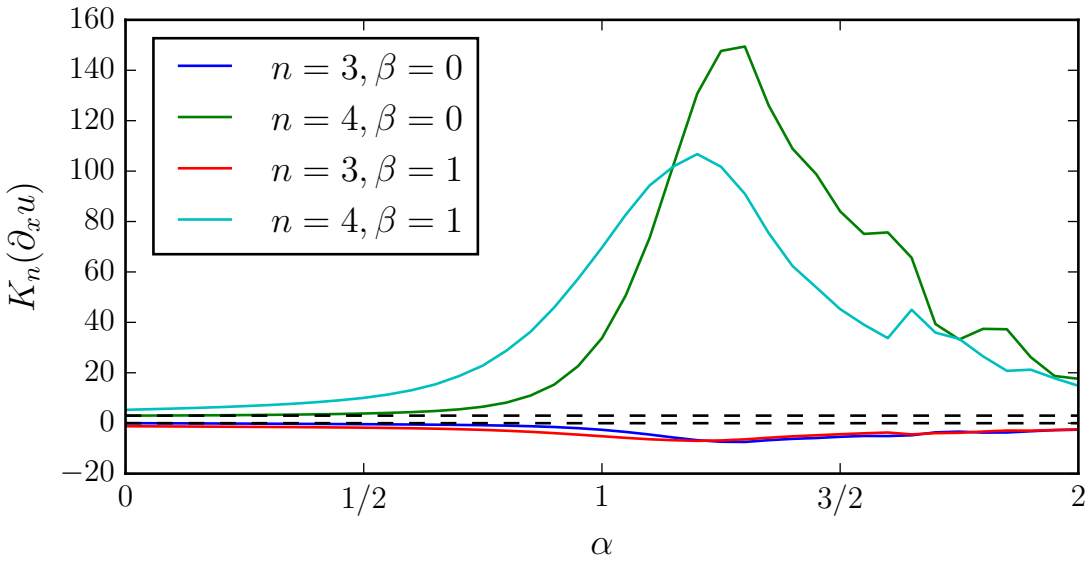

Figure 6.5.: Skewness K_3 and flatness K_4 of the gradient of the velocity field $\partial_x u(t, x)$ (4.11) for different spectra (5.1). The Gaussian values of skewness and flatness corresponding to zero and three are shown in dashed lines. The small scales depart notably from Gaussianity.

encountered in (6.1). This asymptotic approach to a sinusoidal behavior slowly normalizes flatness and skewness, as shocks become more gradual and symmetric.

An interesting observation from the velocity and gradient statistics is the following. The spectrum steepness at which the statistics deviate from Gaussianity is around $\alpha \sim 1/2$. This is clearly seen in the $\beta = 0$ case from Figures 6.4 and 6.5, where the statistics noticeably depart Gaussianity after $\alpha \sim 1/2$. This is precisely the expected result from the literature [29], and is very clearly exemplified here by the skewness and flatness of the velocity field and its gradient.

Finally, the one dimensional version of the velocity increment (3.5) is defined as

$$\delta_r u := u(t, x + r) - u(t, x). \tag{6.2}$$

As we commented in section 3.1, the velocity increment interpolates between the velocity and the gradient statistics, i.e. between large and small scales. We explore it for our usual choice of spectrum $\alpha = \beta = 1$. Both skewness and flatness of the velocity increment are shown in Figure 6.6.

Flatness of the velocity increment is very large for small increments, but quickly becomes sub-Gaussian with increasing the separation r. After $r \sim 0.211$ the flatness

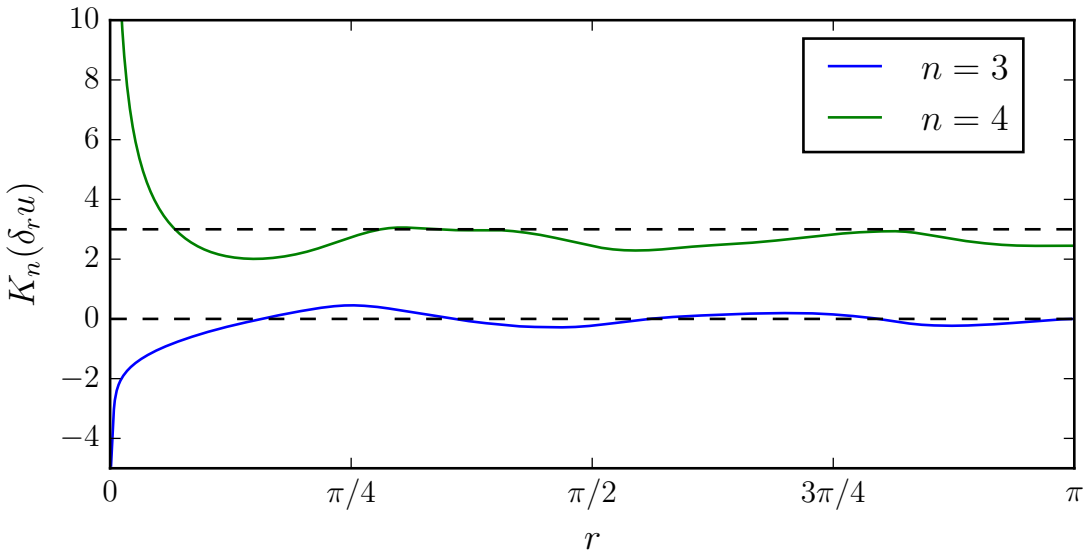

Figure 6.6.: Skewness K_3 and flatness K_4 of the velocity increment $\delta_r u$ as a function of r. The spectrum of the numerical implementation $\alpha = \beta = 1$ was used. The alternating skewness indicates a change in the symmetry of the PDF; this change is observed for the different separations r in Figure 6.7. Note that at $r \sim 3\pi/8$ and $r \sim 3\pi/4$ the velocity increments are close to normally distributed.

remains sub-Gaussian. This indicates that the super-Gaussian tails are exclusively found at the very small scales. At other scales sub-Gaussian tails are the norm.
The skewness is also minimal at the smallest scales, foretelling the presence of negative shocks. As the increment becomes bigger, the skewness returns to zero. As r increases further, the skewness oscillates around zero. This indicates that the PDF's symmetry is scale dependent. To illustrate this, the PDFs of several selected values of r are shown in Figure 6.6. Here we clearly observe the transition from heavy negative tails in the small scales to sub-Gaussian behavior at the large scales. Additionally, the dependence of the symmetry of the PDF on r is observable. As a final remark, note that the velocity increment is almost Gaussian at $r \sim 3\pi/8$ and $r \sim 3\pi/4$.
We have thus shown that a real-space velocity field obtained from the coupled oscillator model is intermittent. These results were obtained by directly integrating the oscillator model (4.5) and then applying an inverse discrete Fourier transform (4.10). In the last chapter we were able to reduce the study of triad statistics to one parameter per triad. This parameter completely describes the three-oscillator

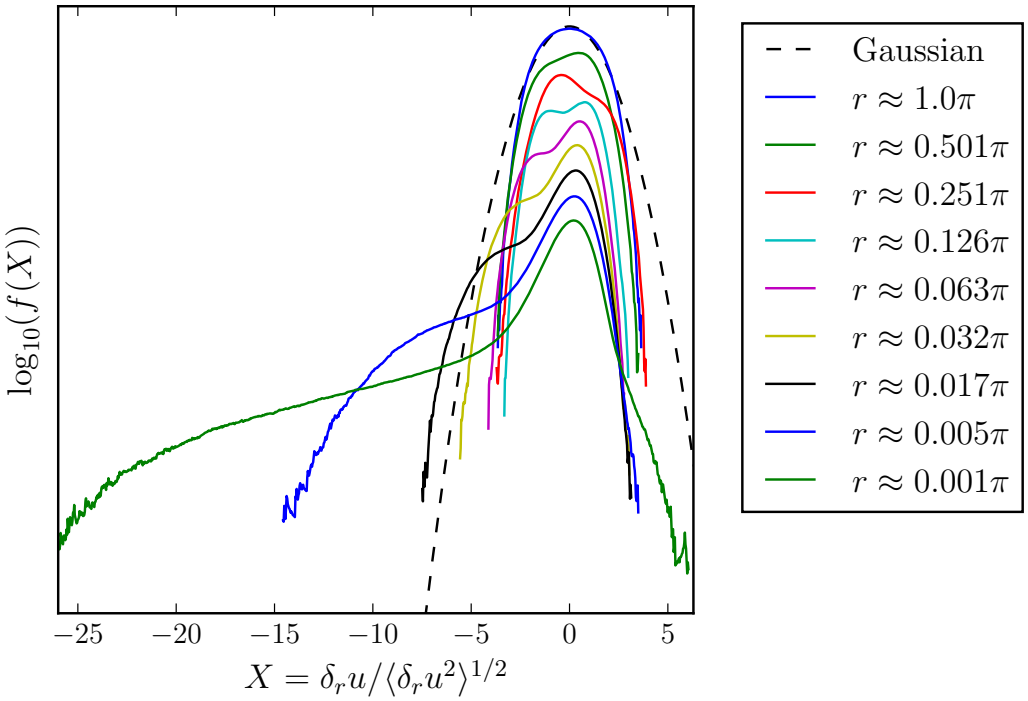

Figure 6.7.: Velocity increment PDFs for chosen values of the increment r. For clarity, an arbitrary offset is introduced between PDFs. Small increments show the typical super-Gaussian tails of gradient statistics. The larger increments reflect the sub-Gaussian tails of the velocity statistics.

coherence phenomena and each triad's statistics to a good approximation for most triads. This result in spectral space can be used to explain some of the real-space statistics explored in this section, and will be the topic of the next section.

6.2. Triad synchronization and real-space statistics

6.2.1. Single-point statistics

Some of the numerical observations presented in the last section can be explained with our knowledge of spectral space dynamics. We will denote averaged real-space fields as $\langle u \rangle$. This is understood as a space and time average, where the space average is taken first. Note, first of all, as a general result for fields of the form (4.10) or (4.11), that their first moment vanishes

$$\langle u(t,x) \rangle = 0 \quad \text{and} \quad \langle \partial_x u(t,x) \rangle = 0. \tag{6.3}$$

That is, as statistical variables $u(t,x)$ and $\partial_x u(t,x)$ are centered random variables. Furthermore, according to the Parseval identity (4.12) the second moment is fixed by the spectrum

$$\langle u(t,x)^2\rangle = \frac{1}{2N^2}\sum_{k=k_0+1}^{N} a_k^2\,, \tag{6.4}$$

$$\langle \partial_x u(t,x)^2\rangle = \frac{1}{2N^2}\sum_{k=k_0+1}^{N} k^2\, a_k^2\,. \tag{6.5}$$

Calculating the first two moments in real-space requires no knowledge on the oscillator statistics; the space average negates out all the time dependence. For the third moment the oscillator statistics will be relevant.

We will exemplify the process of averaging with the third moment of the velocity field. We start by writing the third power of the velocity field (4.10) as exponential functions and identifying the terms which are equal

$$\begin{aligned} u(t,x)^3 = \;& \frac{1}{8N^3}\sum_{k_1,k_2,k_3=k_0+1}^{N} a_{k_1}\, a_{k_2}\, a_{k_3} \\ & \times\Big[\exp[\mathrm{i}x(k_1+k_2+k_3)+\mathrm{i}(\varphi_{k_1}(t)+\varphi_{k_2}(t)+\varphi_{k_3}(t))] \\ & +3\exp[\mathrm{i}x(k_1+k_2-k_3)+\mathrm{i}(\varphi_{k_1}(t)+\varphi_{k_2}(t)-\varphi_{k_3}(t))]\Big] \\ & +\text{c.c.} \end{aligned} \tag{6.6}$$

Integrating over space leaves only the second exponential in the brackets

$$\begin{aligned} \frac{1}{2\pi}\int_{S^1}\mathrm{d}x\; u(t,x)^3 = \;& \frac{3}{8N^3}\sum_{k_1,k_2,k_3=k_0+1}^{N} a_{k_1}\, a_{k_2}\, a_{k_3}\delta_{k_1+k_2,\,k_3} \\ & \times\exp[\mathrm{i}(\varphi_{k_1}(t)+\varphi_{k_2}(t)-\varphi_{k_3}(t))] \\ & +\text{c.c.} \end{aligned} \tag{6.7}$$

The sum may be carried out, and by taking a time average we obtain the time and space averaged third-order moment of the velocity $\langle u^3\rangle$. For clarity the time and

space dependence will no longer be explicitly shown. We are thus led to

$$\begin{aligned}\langle u^3\rangle = \; & \frac{3}{8N^3}\sum_{k_1,k_2=k_0+1}^{N} a_{k_1+k_2}\, a_{k_1}\, a_{k_2} \\ & \times \langle \exp[\mathrm{i}(\varphi_{k_1}+\varphi_{k_2}-\varphi_{k_1+k_2})]\rangle \\ & +\text{c.c.}\end{aligned} \tag{6.8}$$

The average over the oscillators can be identified with the corresponding triad's first trigonometric moment

$$\left\langle \exp[\mathrm{i}\varphi_{k_1+k_2,\min\{k_1,k_2\}}]\right\rangle = \mathrm{i}R_{k_1+k_2,\min\{k_1,k_2\}}. \tag{6.9}$$

Recall, again, that all information contained in the triad PDF is also contained in the three-oscillator PDF. Hence, this triad parameter $R_{k,p}$ completely describes all three-oscillator coherence phenomena. The third-order moment of the velocity involves the three-oscillator statistics. Moreover, not all three-oscillator statistics, but only those forming triads, are taken into account. It is here that we first encounter the relationship between oscillator coherence and real-space statistics. Now, because the triads peak at $\pi/2$ taking complex conjugate leads to a vanishing third-order moment of the velocity field

$$\begin{aligned}\langle u^3\rangle = \; & \frac{3}{8N^3}\sum_{k_1,k_2=k_0+1}^{N} a_{k_1+k_2}\, a_{k_1}\, a_{k_2}\, \mathrm{i}\, R_{k_1+k_2,\min\{k_1,k_2\}} + \text{c.c} \\ = \; & 0.\end{aligned} \tag{6.10}$$

The gradient, on the other hand, has a non-vanishing third moment. Following a similar calculation as for the velocity field, we obtain

$$\begin{aligned}\langle \partial_x u^3 \rangle = & \frac{-3}{8\mathrm{i}N^3} \sum_{k_1,k_2=k_0+1}^{N} a_{k_1+k_2}(k_1+k_2)\, a_{k_1} k_1\, a_{k_2} k_2 \\ & \times \langle \exp[\mathrm{i}(\varphi_{k_1}+\varphi_{k_2}-\varphi_{k_1+k_2})]\rangle \\ & +\text{c.c.} \\ = & \frac{-3}{4N^3} \sum_{k_1,k_2=k_0+1}^{N} a_{k_1+k_2}\,(k_1+k_2)\, a_{k_1}\, k_1\, a_{k_2}\, k_2\, R_{k_1+k_2,\min\{k_1,k_2\}}.\end{aligned} \tag{6.11}$$

Here the relation between triad synchronization and gradient skewness is evident. We have reduced the study of triad synchronization to one parameter per triad $R_{k,p}$, whereby higher values of this parameter imply further departure from uniformly distributed, i.e. appearance of three-oscillator coherence events. This establishes a relation between the small-scale departure from Gaussianity, through skewness, and spectral space phase synchronization. That is, high $R_{k,p}$ corresponds to more common three-oscillator coherent events. At the same time, this parameter has a direct effect on the velocity gradient's skewness.
Note that we can explicitly write each triad's contribution to the gradient's skewness. In terms of triads, equation (6.11) reads

$$\langle \partial_x u^3 \rangle = \frac{-3}{2N^3} \sum_{k=2k_0+2}^{N} \sum_{p=k_0+1}^{\lfloor k/2 \rfloor} a_{k-p}\,(k-p)\, a_p\, p\, a_k\, k\, R_{k,p}. \tag{6.12}$$

This sums uniquely over all triads. Correspondingly, each triad's contribution to the gradient's skewness can be isolated as

$$[K_3(\partial_x u)]_{k,p} := \frac{-3\sqrt{2}\, a_{k-p}\,(k-p)\, a_p\, p\, a_k\, k\, R_{k,p}}{\left(\sum_{q=k_0+1}^{N} q^2\, a_q^2\right)^{3/2}}. \tag{6.13}$$

As we have previously seen, triads have a general dependence on the k index, i.e. their fastest member oscillator. Triads with higher k tend to have higher $R_{k,p}$ whereas lower k usually means a more uniformly distributed triad PDF. With this in mind,

we may sum the equation (6.13) scale by scale over the k index to obtain the total contribution to skewness per scale. In other words, we will look into the relative contribution

$$[K_3(\partial_x u)]_k := \frac{1}{K_3(\partial_x u)} \sum_{p=k_0+1}^{\lfloor k/2 \rfloor} [K_3(\partial_x u)]_{k,p}. \tag{6.14}$$

This relative skewness density is shown in Figure 6.8. Also shown is each triads' individual contribution (6.13) and the spectrum $k\, a_k$. We have set the exponential cutoff scale at $N/2$. Although the high k triads have higher $R_{k,p}$ their contribution is minimal because of the spectrum's steepness. It is hence a notable result in this system, that the major contribution to small-scale non-Gaussianity comes from triads in the lower part of the 'inertial' range, at $N/4 < k < N/2$.

6.2.2. Velocity increment statistics

The results presented in the last section can be extended to the velocity increment. The velocity increment interpolates between large and small scales, and it will help us further understand the effect of triad synchronization in real-space scale-dependent statistics. It is remarkable that we can find an expression for the velocity increment skewness and explicitly prove that it interpolates between velocity and gradient statistics.

As with the velocity and the gradient, the velocity increment's first moment vanishes. Its second moment is given by the spectrum and does not depend on oscillator statistics

$$\langle \delta_r u^2 \rangle = \frac{1}{N^2} \sum_{k=k_0+1}^{N} a_k^2 \, (1 - \cos(kr)). \tag{6.15}$$

The third moment follows in a similar way as for the velocity and its gradient. It involves similarly the triad $R_{k,p}$

$$\begin{aligned} \langle \delta_r u^3 \rangle = \; & \frac{3}{N^3} \sum_{k_1,k_2=k_0+1}^{N} a_{k_1}\, a_{k_2}\, a_{k_1+k_2}\, R_{k_1+k_2,\min\{k_1,k_2\}} \\ & \times \left[\frac{1}{2} \sin(r(k_1+k_2)) - \sin(k_2 r) \right]. \end{aligned} \tag{6.16}$$

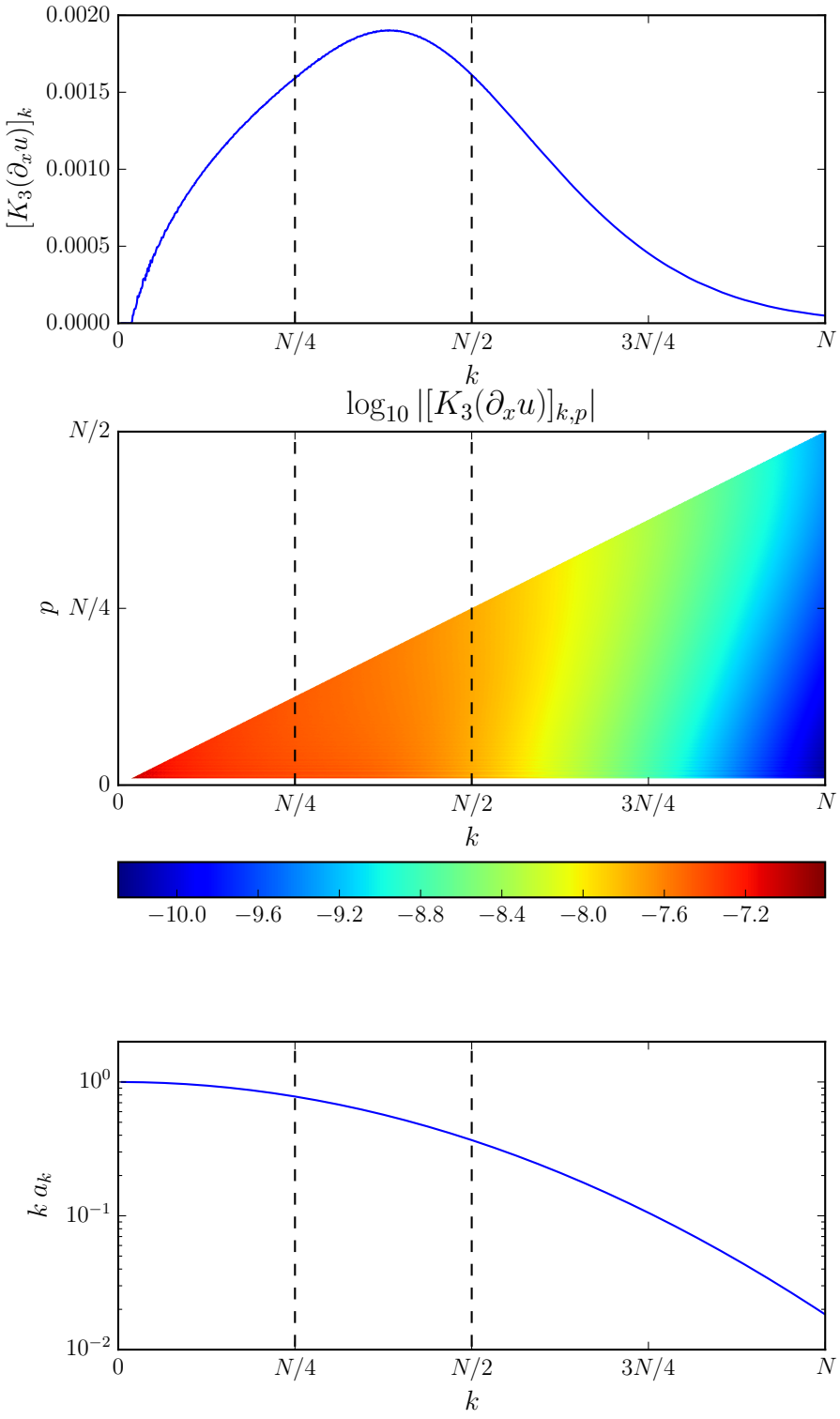

Figure 6.8.: The scale dependent contribution (6.14) (top) and the individual triad contribution (6.13) to the gradient's skewness (middle) are shown. The compensated spectrum $k\, a_k$ is also supplied (bottom). The main contribution for the skewness comes from triads in the intermediate range $N/4 < k < N/2$. Although high-k triads have higher peaked PDFs more (have bigger $R_{k,p}$) the spectrum steepness of the spectrum makes their contribution minimal.

This can also be rewritten in terms of individual triad contributions as

$$\begin{aligned}\langle \delta_r u^3 \rangle = \; & \frac{3}{N^3} \sum_{k=2k_0+2}^{N} \sum_{p=k_0+1}^{\lfloor k/2 \rfloor} a_k \, a_p \, a_{k-p} \, R_{k,p} \\ & \times \left[\sin(rk) - \sin(rp) - \sin(r(k-p)) \right] .\end{aligned} \tag{6.17}$$

As was done for the single-point statistics, each triad's contribution to the velocity increment skewness can be worked out. This reads

$$[K_3(\delta_r u)]_{k,p} = \frac{3 \, a_k \, a_p \, a_{k-p} \, \left[\sin(rk) - \sin(rp) - \sin(r(k-p)) \right]}{\left(\sum_{q=k_0+1}^{N} a_k^2 \, (1 - \cos(rq)) \right)^{3/2}} \, R_{k,p} \, . \tag{6.18}$$

Consequently, the full skewness is obtained by summing over all triads

$$K_3(\delta_r u) = \sum_{k=2k_0+2}^{N} \sum_{p=k_0+1}^{\lfloor k/2 \rfloor} [K_3(\delta_r u)]_{k,p}. \tag{6.19}$$

In turbulence one usually does not have a closed form for the velocity increment. Scaling laws may be valid in a certain range, but to have a system where functional form of a moment of the velocity increment is fully known yields a nice possibility of showing the continuous transition from gradient to velocity statistics. From the second and third moments of the velocity increment, the convergence to velocity statistics is rather straightforward

$$\lim_{r \to \pi} K_3(\delta_r u) = 0. \tag{6.20}$$

The limit $r \to 0$ will require some more work. In this limit the second moment of the velocity increment has the behavior

$$\langle \delta_r u^2 \rangle \sim r^2 \langle \partial_x u^2 \rangle + \mathcal{O}(r^4) \, , \; r \to 0. \tag{6.21}$$

For the third moment consider first the asymptotic behavior of the r-dependent sine functions. For small r they have the asymptotic form

$$\sin(rk) - \sin(rp) - \sin(r(k-p)) \sim \; -r^3 \frac{k \, p \, (k-p)}{2} + \mathcal{O}(r^5) \, , \; r \to 0. \tag{6.22}$$

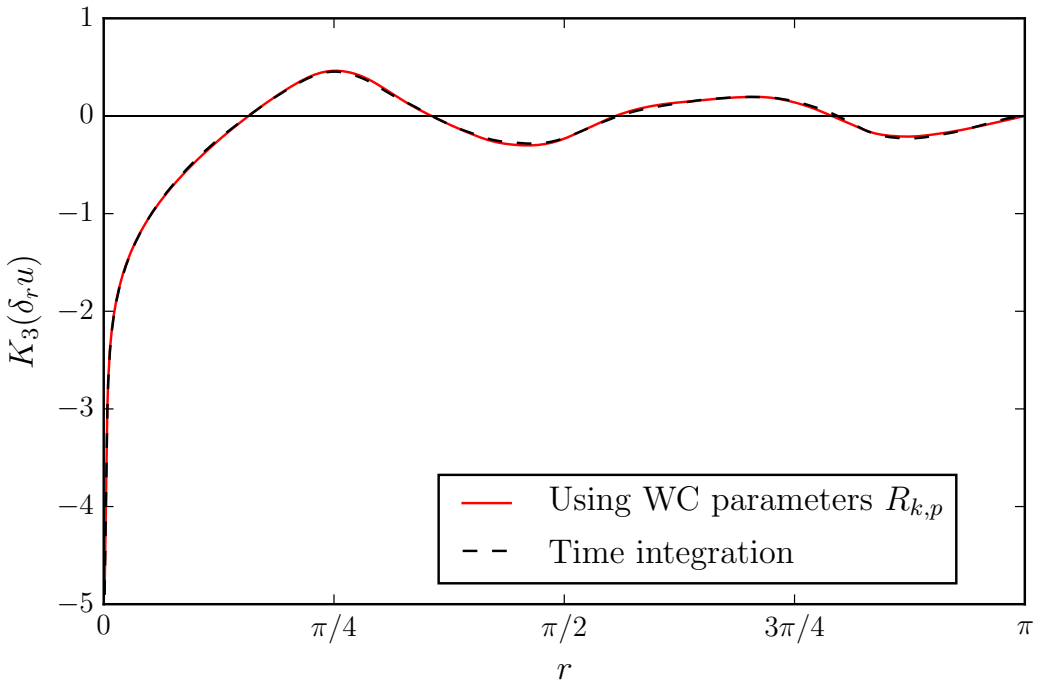

Figure 6.9.: Comparison of the velocity increment's skewness from numerical real-space data and from oscillator statistics as in equation (6.18).

Plugging this result into equation (6.17) and comparing with (6.12) gives us the asymptotic form

$$\langle \delta_r u^3 \rangle \sim r^3 \langle \partial_x u^3 \rangle + \mathcal{O}(r^5) \ , \ r \to 0. \tag{6.23}$$

Putting together equations (6.21) and (6.23) we obtain that the gradient and velocity increment skewness are asymptotic in the small r limit

$$K_3(\delta_r u) \sim K_3(\partial_x u) + \mathcal{O}(r^2) \ , \ r \to 0. \tag{6.24}$$

For completeness we will corroborate these real-space results by comparing equation (6.18) with the real-space numerical results. Using these two methods we produced Figure 6.9. Here the skewness obtained from equation (6.19) is compared with directly measured real-space skewness. As expected, the results are the same.
The relevance of these results is that by studying equation (6.18) each triad's contribution to the real-space skewness is isolated. That is, every possible three-oscillator combination forming a triad contributes uniquely to the skewness. Therefore, three-oscillator coherence events, parametrized by $R_{k,p}$, have a direct influence on the real-space scale-dependent statistics. As we will shortly see, higher moments re-

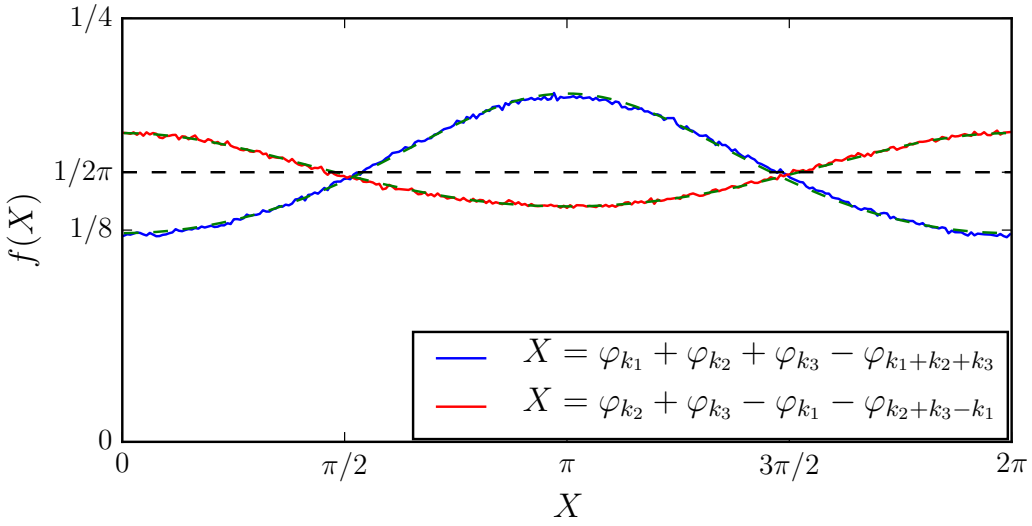

Figure 6.10.: PDFs f of different linear combinations of four oscillators. These linear combinations appear in the fourth-order moment of the velocity (6.25). Superimposed on green are WC fits, obtained from the first trigonometric moment of these linear combinations. Presented is the choice $k_1 = 320$, $k_2 = 160$, and $k_3 = 470$.

quire additional information on the many-oscillator statistics.

6.3. Higher-order moments

The next moment we can look at is the fourth moment. Proceeding in a similar fashion as for the lower moments, we obtain

$$\begin{aligned}\langle u(t,x)^4\rangle = \; & \frac{1}{4N^4}\sum_{k_1,k_2,k_3} a_{k_1}a_{k_2}a_{k_3} \\ & \times \Big[a_{k_1+k_2+k_3}\,\langle \exp[\mathrm{i}(\varphi_{k_1}+\varphi_{k_2}+\varphi_{k_3}-\varphi_{k_1+k_2+k_3})]\rangle \\ & + \frac{3}{4}a_{k_2+k_3-k_1}\,\langle \exp[\mathrm{i}(\varphi_{k_2}+\varphi_{k_3}-\varphi_{k_1}-\varphi_{k_2+k_3-k_1})]\rangle\Big] \\ & + \text{c.c.}\end{aligned} \tag{6.25}$$

The expression for the gradient follows in a similar way. The caveat here is that we have not yet developed a theory for the four-oscillator or higher-order statistics. Notice that the four-oscillator expected value can be rewritten as an average over

two triads

$$\begin{aligned}&\langle \exp[\mathrm{i}(\varphi_{k_1}+\varphi_{k_2}+\varphi_{k_3}-\varphi_{k_2+k_3-k_1})]\rangle = \\ &\langle \exp[\mathrm{i}(\varphi_{k_1}+\varphi_{k_2}-\varphi_{k_1+k_2})]\exp[\mathrm{i}(\varphi_{k_3}+\varphi_{k_1+k_2}-\varphi_{k_1+k_2+k_3})]\rangle\,.\end{aligned} \tag{6.26}$$

A possible way out would be to use the joint statistics with the correlation function factorization (4.24) and neglect the correlation function. However, in section 5.5 we argued based on the numerical data (Figure 5.17) that the correlation function is not unimportant. Moreover, it depends on which oscillator the two-triads have in common. Working with the four-oscillator statistics would therefore require more knowledge on the six-oscillator (two-triad) statistics. Consequently, with the information and theory we have developed until now, the fourth-order statistics cannot be tackled.

Nevertheless, a couple of numerical observations are worth mentioning. For a specific choice of four oscillators, the PDFs of such linear combinations are shown in Figure 6.10.These are linear combinations of oscillators as they appear in equation (6.25). The resulting PDFs peak either at π, or at 0. These PDFs are also very well described by a WC ansatz. That is, the first trigonometric moment of these linear combinations suffices to describe the PDF. This is an interesting numerical observation, as it reveals that the WC distribution also plays a role in the higher-order oscillator statistics. In future studies this observation and the α-stability of the WC distribution might play a role in deriving a theory for the higher-order statistics.

Finally, another strategy for describing the higher-order statistics could rely on the relation between the triads and the correlation function. Comparing equations (5.25) and (5.26) we are led to

$$f_3(\phi;k,p) = \frac{-\sum\limits_{\{k',p'\}}\Omega_{k,p,k',p'}\int_{S^1}\mathrm{d}\theta\cos\theta\, C_{3\times 3}(\phi,\theta;k,p,k',p')}{\tilde{\omega}_{k,p}\cos\phi}. \tag{6.27}$$

This is an exact relation between the correlation function and the triad PDF. If equation (6.25) could be recast as a relation involving the correlation function, then equation (6.27) might be used to describe these higher-order statistics in terms of the triad parameters.

It remains nevertheless remarkable that using the information on the parametriza-

tion of the triad PDFs results can be derived for the real-space statistics. Arguably similar results can be achieved without stating a theory for the triad PDFs, one needs only know the first trigonometric moment of the triads to obtain real-space skewness relations. The main achievement here is that a triad's first trigonometric moment completely describes its PDF. Additionally, on account of the translation symmetry we know that the three-oscillator and triad PDFs are equivalent. Hence this one parameter completely describes three-oscillator coherence events. It has both meanings of triad synchronization and real-space skewness to it. Recall that in turbulent fields intermittency is scale dependence of the statistics. This establishes the connection between real-space intermittency and Fourier phase coherence phenomena.

7. Summary, conclusions, and outlook

In this master's thesis we have presented a one-dimensional coupled oscillator model, which can be used to study Fourier phase dynamics in turbulent fluids. The model was derived from an inviscid Burgers equation, and its equations of motion read

$$\dot{\varphi}_k = \sum_{p=-N}^{N} \omega_{k,p} \ \cos(\varphi_p + \varphi_{k-p} - \varphi_k) \ , \quad k = 1, ..., N. \tag{4.5}$$

These equations retain the oscillator-oscillator coupling present in the spectral formulation of the Navier-stokes equation (3.4). They are nevertheless much simpler, and facilitate the study of oscillator coherent events. To better understand the relation between these oscillator-coherence phenomena and real-space intermittency was the main goal of this master's thesis.

The properties of the coupled oscillator system were derived in chapter 4. We explained how to obtain real-space fields from the oscillator model using the discrete Fourier transform and how to implement the equations of motion using the fast Fourier transform. Oscillators are coupled to one another in groups of three, as in the cosine in equation (4.5). Each triad has two indices, k and p, indicating the highest and lowest oscillator in the triad, respectively. We call such a set of three oscillators coupled in this way a triad $\varphi_{k,p}$. This leads to two dimensional representations, in which every triad can be uniquely presented (see e.g. Figures 4.1 and 4.2).

Because there are many more triads than oscillators, a triad basis is necessary when reformulating the dynamics in terms of triads. This avoids the introduction of spurious degrees of freedom when reformulating the system. Triad bases were explicitly derived for two different cases. The dynamics in terms of triads takes the form

$$\dot{\varphi}_{k,p} = \tilde{\omega}_{k,p} \cos(\varphi_{k,p}) + \sum_{\{k',p'\}} \Omega_{k,p,k',p'} \ \cos(\varphi_{k',p'}). \tag{4.15}$$

Here $\tilde{\omega}_{k,p}$ is the coupling of the triad to itself and $\Omega_{k,p,k',p'}$ are the coupling coefficients to all other triads. That is, they contain information regarding which triad is coupled to which others, and the corresponding coupling constants.
Afterwards, definitions for the one-oscillator PDF f_1, three-oscillator PDF $f_{1\times1\times1}$, and the triad PDF f_3 were introduced. Using the invariance of the oscillator system under the transformation

$$\varphi_k \to \varphi_k + kx_0\,, \quad \forall x_0 \in \mathbb{R}, \tag{4.6}$$

several results were derived for these PDFs. The one-oscillator PDFs are all uniform $f_1(\phi;k) = 1/2\pi\,\forall\,k$. Thre joint PDF of three oscillators forming a triad and the corresponding triad PDF have the same information. Hence, to speak of three-oscillator coherence phenomena is the same as to speak of triad accumulation at $\pi/2$. This identification allows us to work with triad PDFs, which are one-dimensional. In contrast, the three-oscillator PDFs are three dimensional.
A theory for the triad PDFs would describe the three-oscillator coherence events. A typical place to start is with the PDF equation. These are equations of conservation of probability fulfilled by PDFs. However, the triad PDF has the closure problem; it depends on the triad-triad statistics and is hence unclosed. We have thus no defining equations for the triad PDF. This motivates an alternative way of postulating a theory for the triad PDF. We proceeded by comparing the triad's equations of motion (4.15) to an array of Josephson junctions and a simpler cosine model resembling an Adler equation. This comparison led to an ansatz for the triad PDF. This ansatz is known as the Wrapped Stable and Uniform Mixture (WSM). This distribution was introduced in section 2.3.4, and it was shown that it has three free fit parameters. Each triad's PDF can then be described by the parameters $\mathbf{r}_{k,p} = r_{k,p}\exp[\mathrm{i}\Phi_{k,p}] \in \mathbb{C}$ and $C_{k,p} \in \mathbb{R}$.
These parameters must be fixed by the numerics. With this objective, the oscillator model was numerically integrated for $N = 1024$ oscillators, and in chapter 5 we presented numerical observations thereof. For the numerical integration the spectrum was set to

$$a_k = A\,|k|^{-\alpha}\,\exp\left[-\beta\,\left(\frac{k}{N/2}\right)^2\right], \tag{5.1}$$

with $\alpha = \beta = 1$. The amplitude A was set to one by time rescaling. First of all, the existence of a fixed point was reported. The system of coupled oscillators

(4.5) converges to the fixed point $\varphi_k = \pi/2$. This takes the form of a saw tooth function in real-space. This fixed point may be destabilized by removing the first k_0 oscillators from the oscillator system. A linear stability analysis was carried out, and we confirmed that setting the first $k_0 > 0$ oscillators to zero destabilizes the fixed point. With the spectrum fixed, and the first k_0 oscillators set to zero, time series were integrated. From these the different triad trigonometric moments were calculated. These are shown in Figure 5.6. This observation leads to a theory for the triad trigonometric moments

$$\hat{f}_n^{k,p} = C_{k,p}\, \mathrm{i}^n\, r_{k,p}^n\,, \quad n \in \mathbb{N}\,, \quad C_{k,p} \in \mathbb{R}^+, \quad |r_{k,p}| < 1. \tag{5.13}$$

This is equivalent to a WSM distribution for the triads. Knowing the two parameters $r_{k,p}$ and $C_{k,p}$ fully determines the triad's PDF. Larger $r_{k,p}$ means a triad PDF which peaks more strongly at $\pi/2$, whereas $C_{k,p}$ reflects the ratio of the angular dependence with respect to the uniform part of the distribution. Furthermore, these two parameters can be simultaneously shown for all triads in two-dimensional plots. Hence, the three-oscillator coherence phenomena can be read out of Figures 5.8 and 5.9.

Yet, a further simplification for the triad PDFs is possible. The simpler Wrapped Cauchy (WC) distribution for the triad PDFs can be used, while keeping error in the 5% margin. This simpler parametrization was introduced in section 2.3.3 and requires only one parameter per triad. A simplified theory for the triad trigonometric moments was hence proposed as

$$\hat{f}_n^{k,p} = \mathrm{i}^n\, R_{k,p}^n\,, \quad n \in \mathbb{N}\,, \quad |R_{k,p}| < 1. \tag{5.17}$$

This parametrization works very well for the majority of triads.

Reducing the study of triad PDFs to one parameter further simplifies the study of the system. For example, a Kuramoto-like order parameter may be defined. This parameter reads

$$R \exp(\mathrm{i}\Phi) \equiv \mathrm{i}\, \langle R_{k,p} \rangle_{k,p}\,. \tag{5.23}$$

With this order parameter, triads may be divided into faster or slower, by comparing their $R_{k,p}$ to the Kuramoto-like R. In this context faster is understood as representing more coherence events. The transition from slow to fast happens more or less at $k = N/2$. That is, the triad's highest oscillator, denoted by k, determines

if a triad is fast or slow. Additionally, fast triads are found after the Gaussian cutoff $k > N/2$.
The relation between oscillator coherence and real-space statistics was explored in chapter 6. The velocity increments were introduced in order to probe the scale-dependent statistics. These are defined as

$$\delta_r u := u(t, x + r) - u(t, x). \tag{6.2}$$

The velocity increment probes the velocity field $u(t, x)$ at different positions separated by r. The centered standardized moments of small increments converge towards the gradient statistics, whereas large r probe the velocity field's statistics. The main result from this chapter is isolating each triad's contribution to the third moment of the centered standardized velocity increment, i.e. the skewness, as

$$[K_3(\delta_r u)]_{k,p} = \frac{3\, a_k\, a_p\, a_{k-p}\, [\sin(rk) - \sin(rp) - \sin(r(k-p))]}{\left(\sum_{k=k_0+1}^{N} a_k^2\, (1 - \cos(kr)) \right)^{3/2}} R_{k,p}\,. \tag{6.18}$$

Summing over all triads, indexed by k and p, one obtains the full velocity increment skewness. Recall triad PDFs have the same information as three-oscillator PDFs. This means that the $R_{k,p}$ parameter completely describes the statistics of the three-oscillator coherence phenomena. Furthermore, this parameter also enters the real-space skewness (6.18). Hence the same parameter which completely describes the three-oscillator statistics also influences the velocity increment skewness. This establishes the relation between oscillator coherence phenomena and intermittency.

Future work may include developing a theory for the triad PDFs starting from first principles. Being able to describe triad PDFs as WC distribution gives the triad PDFs additional properties. They are invariant under convolutions with one another, i.e. the WC distribution is α-stable, and expectation values are analytic in the parameter $\mathbf{R}_{k,p}$. Additionally, the triad bases might provide a way to reduce all triad parameters to a minimal set, from which all others may be derived.
Moreover, an exact relation between the triad PDFs and the triad-triad correlation

function was found from the triad PDF equation. This relation reads

$$f_3(\phi;k,p) = \frac{-\sum\limits_{\{k',p'\}} \Omega_{k,p,k',p'} \int_{S^1} \mathrm{d}\theta \cos\theta \, C_{3\times 3}(\phi,\theta;k,p,k',p')}{\tilde{\omega}_{k,p}\cos\phi}. \tag{6.27}$$

The function $C_{3\times 3}$ is the triad-triad correlation function, and indicates the departure form statistical independence. This equation indicates that a first principles theory necessarily involves the higher-order statistics. These are, however, other alternatives to deriving a theory for the many-oscillator statistics. Consider the triad PDFs f_3 as described by either a WSM or a WC distribution. If higher-order statistics, for example real-space flatness, can be brought into the form of integrals over correlation functions as in (6.27), these may in turn be reformulated into triad trigonometric moments. In other words, the exact relations between low-order and high-order PDFs provided by the PDF equation may be used infer higher-order statistics from to the known triad PDFs.

Finally, from the side of coupled oscillators, the appearance of the WC distribution for the triads indicates that a study of this system with the Ott & Antonsen ansatz is in order. However, the fact that the oscillators are coupled in a very convoluted way is certainly a challenge. A way to deal with oscillators in a wide range of frequencies and non-trivially coupled to one another might lead to a further development of this ansatz. Finally, we worked here with ensemble averaged triad quantities, i.e. PDFs. Studying the time dynamics of the oscillators might lead to phenomena such as chimeras [43]. These are phenomena which have been observed in coupled oscillator models. They are characterized by dynamical phenomena in which parts of the system are synchronized while others remain incoherent. The tools and ideas developed here can simplify the study of temporal evolution of triads, and supply a starting point for further analysis in coupled oscillator systems with triad sinusoidal coupling.

A. First appendix

A.1. Numerical implementation

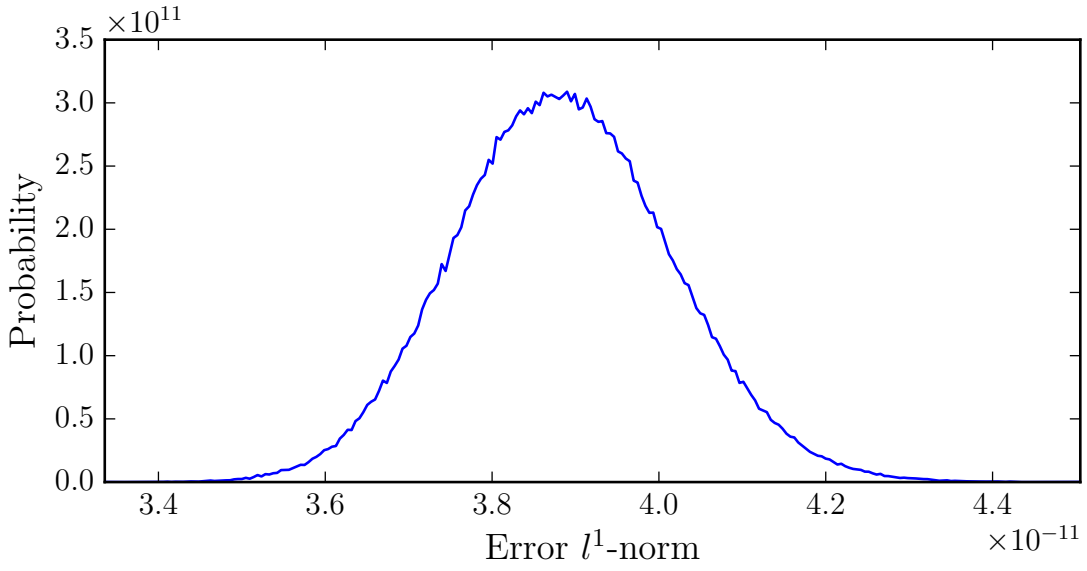

Figure A.1.: The accumulated l^1-error from the numerical FFT implementation is distributed with variance $\sigma = 1.69 \times 10^{-24}$ and mean 3.87×10^{-11}. The error per oscillator is hence of the order $\mathcal{O}(10^{-14})$.

Recall the original equation of the oscillator model (4.5). Directly implementing this sum we define a control implementation of this equation

$$\dot{\varphi}_k^{\text{control}} = \sum_{p=-N}^{N} \frac{-k\, a_{k-p}\, a_p}{a_k} \cos(\varphi_p + \varphi_{k-p} - \varphi_k)\,, \quad k = 1, ..., N. \tag{A.1}$$

As was introduced in chapted 5 in equation (5.1) the spectrum is implemented as

$$a_k = A\, |k|^{-\alpha}\, \exp\left[-\beta \left(\frac{k}{N/2}\right)^2\right]. \tag{A.2}$$

Calculating $\dot{\varphi}_k^{\text{control}}$ for all k is an operation of the order $\mathcal{O}(N^2)$. This can be optimized by use of the FFT algorithm. Equation (A.1) can be recast to (4.7), which explicitly shows the convolution

$$\frac{\mathrm{d}\varphi_k}{\mathrm{d}t} = \Re\left[\frac{-k\exp(-\mathrm{i}\varphi_k)}{a_k}\sum_{p=-N}^{N}(a_p\ \exp[\mathrm{i}\varphi_p])\,(a_{k-p}\ \exp[\mathrm{i}\varphi_{k-p}])\right]. \tag{A.3}$$

A convolution of two vectors $\underline{a}$ and $\underline{b}$ is defined as

$$(\underline{a} * \underline{b})_k = \sum_{p=-N}^{N} a_p\, b_{k-p}. \tag{A.4}$$

The vectors $\underline{a}$ and $\underline{b}$ are taken to have elements indexed by $i \in \{-N, ..., N\}$. Elements in the sum outside the defined index range $|i| > N$ are taken to be zero. The convolution itself $(\underline{a} * \underline{b})_k$ has its index in the range $k \in \{-N, ..., N\}$.
The FFT algorithm is of the order $\mathcal{O}(N \log N)$. The reason why the FFT algorithm reduces the cost of the convolution is that in real-space convolutions take the form of multiplication. Hence a convolution can be done by transforming to real-space, multiplying, and then taking the inverse transformation. This whole operation remains of order $\mathcal{O}(N \log N)$.

A.2. Numerical validation

To validate the numerical implementation (A.3) we set a flat spectrum. This weighs all oscillators equally and will highlight any numerical discrepancies in the implementation itself. Subsequently, values are randomly produced for the oscillators, and statistics we taken over the l^1-norm of the error

$$\text{Error} = \sum_{k=1}^{N} |\varphi_k^{\text{control}} - \varphi_k^{FFT}|. \tag{A.5}$$

For $N = 1024$, the accumulated l^1-error is distributed with variance $\sigma = 1.69 \times 10^{-24}$ and mean 3.87×10^{-11}. This means that the average error per oscillator is of the order $\mathcal{O}(10^{-14})$, which is of the order of numerical accuracy for double precision when exponential and trigonometric operations are involved.

For the time integration, a Runge-Kutta fourth-order scheme was implemented[1]. The time step Δt was chosen as to resolve the fastest time scales on the right hand side of (A.1). This is identical with the maximum element of the Jacobi matrix for all possible configurations of the oscillators. This is given by

$$\Delta t^{-1} = -\sum_{p=k_0+1}^{N-1-k_0} \omega_{N,p} \,. \tag{A.6}$$

We used random initial conditions for the oscillators and 10^5 time steps were taken as transient integration time.

A.3. Python class implementation

We now present a python class implementation of the oscillator model studied here. This allows us easily initialize and integrate systems for different sizes N, spectral parameters α, β, or the number of oscillators set to zero k_0. Integration is carried out with a Runge-Kutta fourth-order integration scheme. Both the control (A.1) and FFT (A.3) implementation of the equations of motion are included. This allows to confirm that the implementation is within numerical error. In this class are implemented functions that return the oscillators, the real-space velocity and the gradient. The eigenvalues of the Jacobi matrix at the current state can also be called. With all this at hand, time series may be integrated, and the oscillator and real-space statistics can be calculated.

[1]For basic numerical integration schemes in the context of turbulence we refer to appendix B in [34].

```
#Agustin Arguedas
#Version 02.11.17
#Implementation of the phase model.
#Can be used to integrate time series with
#a Runge-Kutta 4 integration scheme.
#Convolution in the equation of motion
#implemented using an FFT algorithm.
#Control iplementation of convolution
#also included, to control FFT implementation.
#

class Model:
    def __init__(self,N,ZeroOffset,alpha,beta):
        import numpy as np
        self.N=N#Number of oscillators
        self.ZeroOffset=ZeroOffset#k_0 number of oscillators set to zero
        self.alpha=alpha#Spectrum alpha
        self.beta=beta#Spectrum beta
        self.kcutoff = 1./2.*N#Gaussian kutoff at N/2
        self.phi=np.random.random(N)*2*np.pi-np.pi#Random initial conditions
        self.phi[0:self.ZeroOffset]=0.0#Set first k_0 oscillators to zero
        self.amp=1.0#spectrum amplitude. Gauged to 1
        self.klist=np.linspace(1,self.N,num=self.N,dtype='float64')#Udes to generate spectrum arrays
        self.acoeff =self.amp*np.abs(self.klist)**self.alpha
        *np.exp(-self.beta*(self.klist/self.kcutoff)**2.0)#Spectrum a_k
        self.omegak=-self.klist/self.acoeff#-k/a(k), appears in the control equation of motion
        self.acoeff[0:self.ZeroOffset]=0.0
        self.omegak[0:self.ZeroOffset]=0.0
        self.dt=10**-5#Set a starting value for the time step. Will be later changed by invoking set_timescale()
        self.acoeffR=np.concatenate(([0.0],self.acoeff))#Spectrum for the DFT
        self.acoeffG=np.linspace(0.0,self.N,num=self.N+1,dtype='float64')*1.0j*self.acoeffR#Spectrum for the DFT of the gradient
        self.klistExtended=np.linspace(-self.N,self.N,num=2*self.N+1,dtype='float64')#Udes to generate spectrum arrays
        self.acoeffExtended =self.amp*np.abs(self.klistExtended)**self.alpha*np.exp(-self.beta*(self.klistExtended/self.kcutoff)**2.0)#coefficient of oscillator convolution
        self.acoeffExtended[self.N-self.ZeroOffset:self.N+self.ZeroOffset+1]=0
        self.omegakExtended=np.where(self.acoeffExtended==0.0,0.0,-self.klistExtended/self.acoeffExtended)#coefficient of oscillator convolution


    def a(self,ak):#Spectrum as a function
        import numpy as np
        return np.where(np.abs(ak)<=self.ZeroOffset,0.0,np.where(np.abs(ak)>self.N,0.0,self.amp*np.abs(ak)**self.alpha*np.exp(-self.beta*(ak/self.kcutoff)**2.0)))

    def omega(self,ak,ap):#Omega coupling coefficients as a function
        import numpy as np
        return np.where(np.abs(ak)<=self.ZeroOffset,0.0,-ak/self.a(ak))*self.a(ap)*self.a(ak-ap)

    def set_timescale(self):#Set timescale
        import numpy as np
        self.dt=-1.0/np.sum(self.omega(self.N,np.linspace(self.ZeroOffset+1,self.N,num=self.N-self.ZeroOffset)))
```

```
        print("Time step set to "+str(self.dt)+".")

    def controlRHS(self,phi):#Straighforward implementation of the sum. For control
        import numpy as np
        phiNew=np.zeros(self.N,dtype='float64')
        phiNew[0:self.ZeroOffset]=0.0
        for kloop in range(self.ZeroOffset,self.N):
            for ploop in range(self.ZeroOffset,self.N-kloop-1):
                phiNew[kloop]+=2.0*self.acoeff[ploop]*self.acoeff[kloop+ploop+1]*np.cos(phi[ploop]+phi[kloop]-phi[kloop+ploop+1])
            for ploop in range(self.ZeroOffset,kloop-self.ZeroOffset):
                phiNew[kloop]+=self.acoeff[ploop]*self.acoeff[kloop-ploop-1]*np.cos(phi[ploop]+phi[kloop-ploop-1]-phi[kloop])
        phiNew=self.omegak*phiNew
        return phiNew

    def ODE(self,phi):#FFT implementation of the convolution in the equations of motion
        import numpy as np
        from scipy import signal
        phi=np.concatenate((-np.flipud(phi),np.zeros(1),phi))
        PConv=self.acoeffExtended*np.exp(1.0j*phi)
        Conv=signal.fftconvolve(PConv,PConv,mode='same')#np.convolve
        return (self.omegakExtended*np.abs(Conv)*np.cos(phi-np.angle(Conv)))[self.N+1:]

    def integrate(self):#Runke-Kutta 4 order integration scheme
        import numpy as np
        dt=self.dt
        phiOld=np.copy(self.phi)
        k1=self.ODE(phiOld)
        k2=self.ODE(phiOld+dt*k1/2.0)
        k3=self.ODE(phiOld+dt*k2/2.0)
        k4=self.ODE(phiOld+dt*k3)
        self.phi=phiOld+dt/6.0*(k1+2.0*k2+2.0*k3+k4)

    def compareRHS(self):#Compare the FFT and control implementations
        A=self.controlRHS(self.phi)
        B=self.ODE(self.phi)
        return A,B

    def Oscillators(self):#Return oscillators
        return self.phi

    def RealSpace(self):#Return real-space velocity profile
        import numpy as np
        aphi=np.concatenate(([0.0],self.phi))
        return np.fft.irfft(self.acoeffR*np.exp(aphi*1.0j))

    def Gradient(self):#Return real-space gradient profile
        import numpy as np
        aphi=np.concatenate(([0.0],self.phi))
```

```
    return np.fft.irfft(self.acoeffG*np.exp(aphi*1.0j))

def RealSpacePlot(self,title=''):#Plot current velocity profile
    import numpy as np
    import matplotlib.pyplot as plt
    titlesize=17
    labelsize=14
    ticksize=12
    x=np.linspace(0.0,2.0*np.pi,num=2*self.N,endpoint=False)
    RS=self.RealSpace()
    Norm=np.average(RS**2.0)**0.5
    fig = plt.figure(figsize=(6.,3.),facecolor = 'white')
    fig.subplots_adjust(top=0.96,bottom=0.18,left=0.12,right=0.99)
    ax=fig.add_subplot(111)
    ax.tick_params(labelsize=ticksize)
    ax.set_title(title,fontsize=titlesize)
    ax.set_xlabel(r'$x$', fontsize=labelsize)
    ax.set_ylabel(r'$u(x)/\langle u(x)^2\rangle^{1/2}$', fontsize=labelsize)
    ax.set_xticks([0,np.pi/2,np.pi,3*np.pi/2,2*np.pi])
    ax.set_xticklabels(["0","$\pi/2$","$\pi$","$3\pi/2$","$2\pi$"])
    ax.set_xlim([0.0,2.0*np.pi])
    ax.plot(x,RS/Norm)
    fig.savefig('RealSpace'+title+'.pdf',dpi=150)
    plt.show()

def EigenValues(self,last=False):#Returns sorted eigenvalues at current state. If last!=False returns only the EV with largest real part
    import numpy as np
    from numpy import linalg as LA
    ZO=self.ZeroOffset
    phi=np.copy(self.phi)
    phi=np.concatenate(([0.0],phi))
    N=self.N
    #Diagonal terms
    k=np.linspace(0.0,N,num=N+1,dtype='float64')
    klist=np.linspace(ZO+1,N,num=N-ZO,dtype='int32')
    plist=np.linspace(-N,N,num=2*N+1,dtype='int32')
    K,P = np.meshgrid(klist, plist, sparse=False, indexing='xy')
    kplist=K-P
    kplistSign=np.sign(kplist)
    kplist=np.where(np.abs(kplist)<=N,np.abs(kplist),0)
    JacobiDiag=np.sum(self.omega(k[K],np.sign(P)*k[np.abs(P)])*np.sin(np.sign(P)*phi[np.abs(P)]+kplistSign*phi[kplist]-phi[K]),axis=0)#np.flipud()
    #Non-diagonal terms
    K,Q = np.meshgrid(klist, klist, sparse=False, indexing='xy')
    JacobiMatrix=-2.0*self.omega(k[K],k[Q])*np.sin(phi[Q]+np.sign(K-Q)*phi[np.abs(K-Q)]-phi[K])-2.0*self.omega(k[K],k[np.where(K+Q<=N,K+Q,0)])*np.sin(phi[Q]+phi[K]-phi[np.where(K+Q<=N,K+Q,0)])
    klist=np.linspace(0,N-ZO-1,num=N-ZO,dtype='int32')
    JacobiMatrix[klist,klist]+=JacobiDiag
    EW=LA.eigvals(JacobiMatrix)#Eigenvalues vals
    EW=np.sort(np.real(EW))
```

```
        if last==False:
            return EW
        else:
            return EW[-1]
```

B. Second appendix

B.1. A simple cosine model

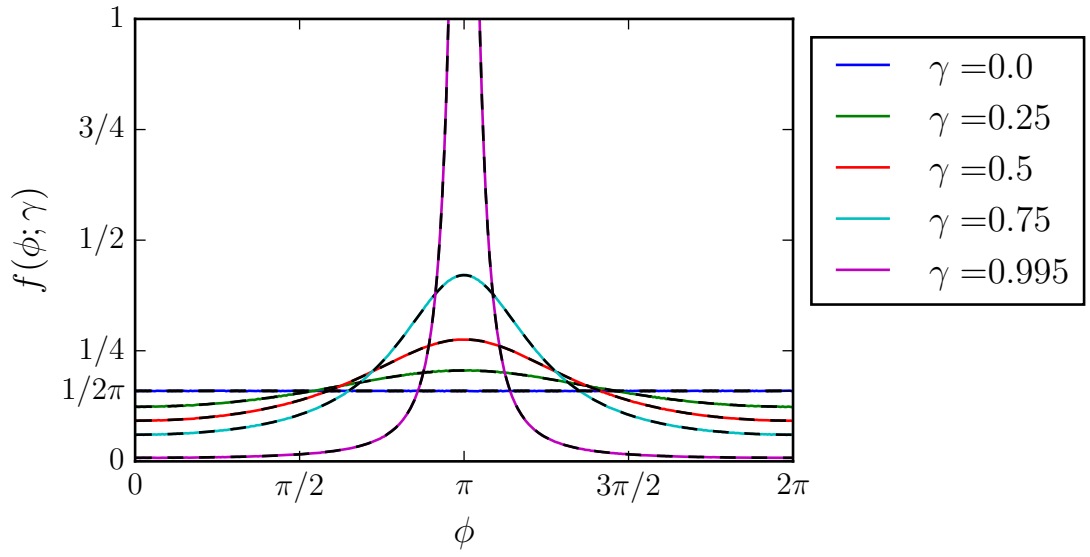

Figure B.1.: Numerical PDFs for model (B.1) for different choices of γ. The numerical PDFs perfectly reproduce the analytic result for the PDF.

In this appendix we will present a very simple ordinary differential equation for a variable φ. This variable's PDF will be derived as a function of the parameter γ. This shall serve as a simple example of deducing a variable's PDF from its dynamics. Consider a simple dynamical system given by

$$\dot{\varphi} = 1 + \gamma \cos\varphi\,, \quad \gamma \in [0, 1). \tag{B.1}$$

This is a simpler version of the Adler equation [23]. In the case $\gamma = 0$ the system has the solution $\varphi(t) = \varphi(t_0) + t - t_0$. In the range $\gamma \in (0, 1)$ the variable φ has linear growth with superimposed oscillations. Both these cases are described by an

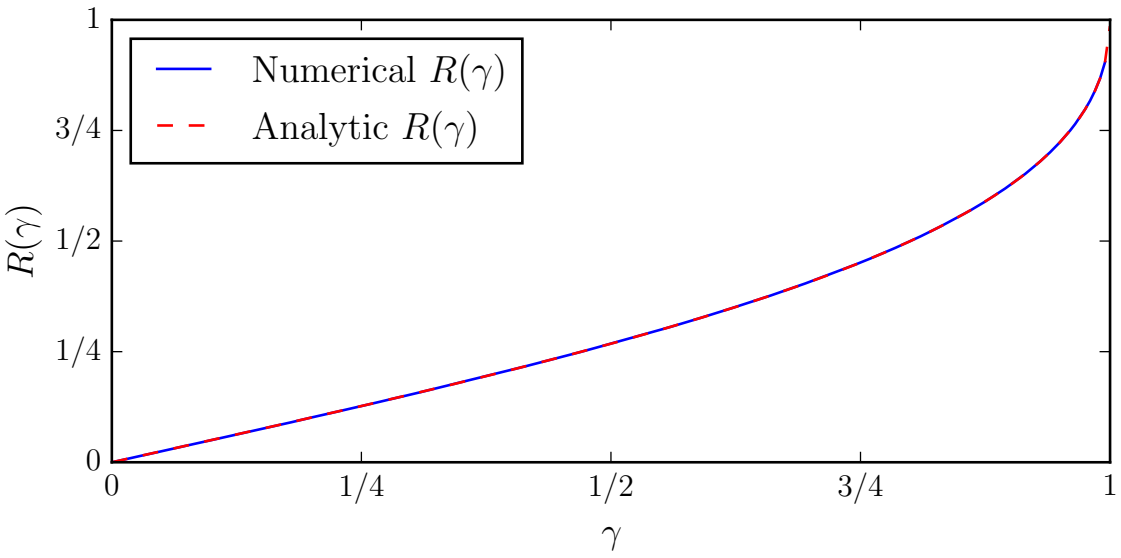

Figure B.2.: Numerically calculated amplitudes of the first trigonometric moment $R(\gamma)$ are compared to the analytic result (B.9).

analytic solution. This solution is implicitly given by

$$t - t_0 = \frac{2}{\sqrt{1-\gamma^4}} \arctan\left[\sqrt{\frac{1-\gamma^2}{1+\gamma^2}} \tan\left(\frac{\varphi(s)}{2}\right)\right]\Bigg|_{s=t_0}^{s=t}. \tag{B.2}$$

On the other hand, if $\gamma \geq 1$ the fixed point $\cos\varphi = -1$ can be reached from any initial condition $\varphi(t_0) \in \mathbb{R}$. In this case therefore convergence to this fixed point is assured.

As we see, the variable $\varphi(t)$ is not chaotic. It possesses nevertheless a PDF $f(\phi;\gamma)$ parametrized by γ. The cases $\gamma = 0$ and $\gamma \geq 1$ are simple, as they have an uniformly distributed and δ-distributed PDF, respectively. For the intermediate case we will derive the form of the PDF.

Let the fine-grained PDF $\hat{f}$ and the PDF f of φ be defined as

$$\hat{f}(t,\phi;\gamma) := \delta(\phi - \varphi(t)) \quad \text{and} \quad f(\phi;\gamma) := \langle \delta(\phi - \varphi(t)) \rangle. \tag{B.3}$$

This PDF has a probability conservation equation. PDF equations can be derived as follows. We start from the fine-grained PDF and take a time derivative. Next we

use the sifting property of the δ-distribution to obtain

$$\partial_t \hat{f}(t,\phi;\gamma) = -\partial_\phi[\hat{f}(t,\phi;\gamma)(1+\gamma\cos\phi)]. \tag{B.4}$$

Finally averaging yields the PDF equation

$$\partial_t f(\phi;\gamma) = -\partial_\phi\left[f(\phi;\gamma)(1+\gamma\cos\phi)\right]. \tag{B.5}$$

Because f is stationary we have a PDF of the form

$$f(\phi;\gamma) = \frac{K(\gamma)}{1+\gamma\cos\phi}. \tag{B.6}$$

In this case because no joint statistics are involved, the PDF equation yields a condition for the PDF. The identity

$$\begin{aligned}\frac{1}{1+\gamma\cos\phi} \equiv\ & \frac{1-\sqrt{1-\gamma^2}}{\gamma^2+1+\sqrt{1-\gamma^2}} \\ & \times\left[1+\sum_{n\in\mathbb{N}}\left[\frac{1-\sqrt{1-\gamma^2}}{\gamma}\right]^n \exp[\mathrm{i}n(\pi-\phi)]+\text{c.c.}\right],\end{aligned} \tag{B.7}$$

is valid for $-1 < \gamma < 1$, and it can be verified by use of the geometric series. The normalization of the PDF will fix $K(\gamma)$. With this identity the normalization condition on (B.6) clearly leads to

$$K(\gamma) = \frac{1}{2\pi}\frac{\gamma^2+1+\sqrt{1-\gamma^2}}{1-\sqrt{1-\gamma^2}}. \tag{B.8}$$

Additionally, with use of this identity we can identify the PDF of φ as a WC distribution with first trigonometric moment

$$\mathbf{R}(\gamma) = \frac{1-\sqrt{1-\gamma^2}}{\gamma}\exp[\mathrm{i}\pi]. \tag{B.9}$$

The form of the PDF (B.6) with $K(\gamma)$ as in (B.8) as well as its identification as a WC distribution with first moment (B.9) are numerically verified in Figures B.1 and B.2. In the first figure numerical PDFs are compared with the analytic result, and in the second figure the analytic formula for the first trigonometric moment is compared with the numerically computed first moment.

We have hence analytically shown and numerically verified that the process (B.1) leads to a WC distributed PDF where the relation between the parameter γ and the first trigonometric moment is exactly known.

C. Third appendix

C.1. Ott & Antonsen reduction in an array of coupled Josephson junctions

The time-independent behavior of an array of Josephson junctions can be reduced to a system of coupled oscillators [53]

$$\dot{\varphi}_k(t) = \Omega + a\ \cos\varphi_k(t) + \frac{1}{N}\sum_{p=1}^{N}\cos\varphi_p(t)\ , \quad k = 1, .., N\ , \quad a, \Omega \in \mathbb{R}. \tag{C.1}$$

Following [35], we take the thermodynamic limit $N \to \infty$. In this limit the system is described by a circular PDF $f(t, \phi)$. The quantity $f(t, \phi)d\phi$ tells us the amount of oscillators in the range $[\phi, \phi + d\phi]$. This PDF has a continuity equation of the form

$$\partial_t f(t, \phi) + \partial_\phi[f(t, \phi)v(t, \phi)] = 0, \tag{C.2}$$

where v is a velocity field. It is a continuum version of the original oscillators' equation (C.1) and has the form

$$v(t, \phi) = \Omega + a\cos\phi + \Re(\mathbf{R}). \tag{C.3}$$

As is common in oscillator systems, $\mathbf{R} \in \mathbb{C}$ is the first trigonometric moment of the oscillator ensemble

$$\mathbf{R}(t) = R(t)\exp[\mathrm{i}\Phi(t)] = \int_{S^1} \mathrm{d}\phi\ f(t, \phi)\ \exp[\mathrm{i}\phi]. \tag{C.4}$$

Using a WC distribution ansatz for the PDF fixes all trigonometric moments through the first one. The PDF takes the form

$$f(t, \phi) = \frac{1}{2\pi}\left[1 + \sum_{n\in\mathbb{N}}\mathbf{R}(t)^n\exp[-in\phi] + \text{c.c.}\right]. \tag{C.5}$$

Plugging equations (C.5) and (C.3) into equation (C.2) yields then equations of motion for the first trigonometric moment

$$\frac{\mathrm{d}\mathbf{R}(t)}{\mathrm{d}t} = \mathrm{i}\left[\frac{a}{2}(\mathbf{R}(t)^2 + 1) + \mathbf{R}(t)\left[\Omega + \Re(\mathbf{R}(t))\right]\right]. \tag{C.6}$$

In terms of $R(t)$ and $\Phi(t)$, these equations of motion constitute a two-dimensional closed system. This means that the low-dimensional synchronization behavior of (C.2) is parametrized in the thermodynamic limit with a PDF given by a WC distribution. Additionally, a consequence of the closure of these equatios is that if the initial conditions for a system of oscillators is found in the manifold parametrized by PDFs of this form, time evolution will not take the PDF out of this manifold. For further analysis we refer to [35].

Bibliography

[1] Daniel M. Abrams, Rennie Mirollo, Steven H. Strogatz, and Daniel A. Wiley. Solvable model for chimera states of coupled oscillators. *Phys. Rev. Lett.*, 101:084103, Aug 2008. URL https://doi.org/10.1103/PhysRevLett.101.084103.

[2] Juan A. Acebrón, L. L. Bonilla, Conrad J. Pérez Vicente, Félix Ritort, and Renato Spigler. The Kuramoto model: A simple paradigm for synchronization phenomena. *Rev. Mod. Phys.*, 77:137–185, Apr 2005. URL http://dx.doi.org/10.1103/RevModPhys.77.137.

[3] G.B. Arfken and H.J. Weber. *Mathematical Methods for Physicists*. Elsevier, 2005. ISBN 9780120885848. URL https://www.elsevier.com/books/mathematical-methods-for-physicists-international-student-edition/arfken/978-0-12-088584-8.

[4] M. Argentina and P. Coullet. A generic mechanism for spatiotemporal intermittency. *Physica A: Statistical Mechanics and its Applications*, 257(1):45 – 60, 1998. ISSN 0378-4371. URL https://doi.org/10.1016/S0378-4371(98)00213-1.

[5] J. Bak and D.J. Newman. *Complex Analysis*. Undergraduate Texts in Mathematics. Springer New York, 2010. ISBN 9781441972880. URL https://doi.org/10.1007/978-1-4419-7288-0.

[6] E. Balkovsky, G. Falkovich, I. Kolokolov, and V. Lebedev. Intermittency of burgers' turbulence. *Phys. Rev. Lett.*, 78:1452–1455, Feb 1997. URL https://doi.org/10.1103/PhysRevLett.78.1452.

[7] Lasko Basnarkov and Viktor Urumov. Phase transitions in the Kuramoto model. *Phys. Rev. E*, 76:057201, Nov 2007. URL https://doi.org/10.1103/PhysRevE.76.057201.

[8] J. Bec and U. Frisch. Probability distribution functions of derivatives and increments for decaying Burgers turbulence. *Phys. Rev. E*, 61:1395–1402, Feb 2000. URL https://doi.org/10.1103/PhysRevE.61.1395.

[9] Jérémie Bec and Konstantin Khanin. Burgers turbulence. *Physics Reports*, 447(1):1 – 66, 2007. ISSN 0370-1573. URL https://doi.org/10.1016/j.physrep.2007.04.002.

[10] T. Bohr, M.H. Jensen, G. Paladin, and A. Vulpiani. *Dynamical Systems Approach to Turbulence*. Cambridge Nonlinear Science Series. Cambridge University Press, 2005. ISBN 9780521017947. URL https://doi.org/10.1017/CBO9780511599972.

[11] S. A. Boldyrev. Burgers turbulence, intermittency, and nonuniversality. *Physics of Plasmas*, 5(5):1681–1687, 1998. URL https://doi.org/10.1063/1.872836.

[12] J.M. Burgers. *The Nonlinear Diffusion Equation: Asymptotic Solutions and Statistical Problems*. SpringerLink : Bücher. Springer Netherlands, 2013. ISBN 9789401017459. URL https://doi.org/10.1007/978-94-010-1745-9.

[13] Miguel D. Bustamante, Brenda Quinn, and Dan Lucas. Robust energy transfer mechanism via precession resonance in nonlinear turbulent wave systems. *Phys. Rev. Lett.*, 113:084502, Aug 2014. URL https://doi.org/10.1103/PhysRevLett.113.084502.

[14] Michele Buzzicotti, Luca Biferale, Uriel Frisch, and Samriddhi Sankar Ray. Intermittency in fractal Fourier hydrodynamics: Lessons from the burgers equation. *Phys. Rev. E*, 93:033109, Mar 2016. URL https://doi.org/10.1103/PhysRevE.93.033109.

[15] Michele Buzzicotti, Brendan P. Murray, Luca Biferale, and Miguel D. Bustamante. Phase and precession evolution in the Burgers equation. *The European Physical Journal E*, 39(3):34, Mar 2016. ISSN 1292-895X. URL https://doi.org/10.1140/epje/i2016-16034-5.

[16] Lawrence C. Cheung and Tamer A. Zaki. An exact representation of the nonlinear triad interaction terms in spectral space. *Journal of Fluid Mechanics*, 748:175–188, 2014. URL https://doi.org/10.1017/jfm.2014.179.

[17] Hayato Chiba and Isao Nishikawa. Center manifold reduction for large populations of globally coupled phase oscillators. *Chaos: An Interdisciplinary Journal of Nonlinear Science*, 21(4):043103, 2011. URL https://doi.org/10.1063/1.3647317.

[18] Internal communication. Numerical data provided by Christian Lalescu at the Max Planck Institute for Dynamics and Self-Organization. Date 30.10.2017.

[19] Charles R. Doering. The 3D Navier-Stokes problem. *Annual Review of Fluid Mechanics*, 41(1):109–128, 2009. URL https://doi.org/10.1146/annurev.fluid.010908.165218.

[20] J. Andrzej Domaradzki and Robert S. Rogallo. Local energy transfer and nonlocal interactions in homogeneous, isotropic turbulence. *Physics of Fluids A: Fluid Dynamics*, 2(3):413–426, 1990. URL https://doi.org/10.1063/1.857736.

[21] U. Frisch and A.N. Kolmogorov. *Turbulence: The Legacy of A. N. Kolmogorov*. Cambridge University Press, 1995. ISBN 9780521457132.

[22] Uriel Frisch, Anna Pomyalov, Itamar Procaccia, and Samriddhi Sankar Ray. Turbulence in noninteger dimensions by fractal Fourier decimation. *Phys. Rev. Lett.*, 108:074501, Feb 2012. URL https://doi.org/10.1103/PhysRevLett.108.074501.

[23] Punit Gandhi, Edgar Knobloch, and Cédric Beaume. Dynamics of phase slips in systems with time-periodic modulation. *Phys. Rev. E*, 92:062914, Dec 2015. URL https://doi.org/10.1103/PhysRevE.92.062914.

[24] Toshiyuki Gotoh. Inertial range statistics of Burgers turbulence. *Physics of Fluids*, 6(12):3985–3998, 1994. URL https://doi.org/10.1063/1.868388.

[25] Toshiyuki Gotoh. Probability density functions in steady-state Burgers turbulence. *Physics of Fluids*, 11(8):2143–2148, 1999. URL https://doi.org/10.1063/1.870106.

[26] S. Heinz. *Statistical Mechanics of Turbulent Flows*. Springer, 2003. ISBN 9783540401032. URL https://doi.org/10.1007/978-3-662-10022-6.

[27] S.R. Jammalamadaka and A. Sengupta. *Topics in Circular Statistics*. Series on multivariate analysis. World Scientific, 2001. ISBN 9789812779267. URL http://www.worldscientific.com/worldscibooks/10.1142/4031.

[28] Gao Jian, Xu Can, Sun Yuting, and Zheng Zhigang. Order parameter analysis for low-dimensional behaviors of coupled phase-oscillators. *Scientific reports*, (6):30184, 2016. URL http://dx.doi.org/10.1038/srep30184.

[29] Javier Jimenez. Turbulent velocity fluctuations need not be Gaussian. *Journal of Fluid Mechanics*, 376:139–147, 1998. URL http://dx.doi.org/10.1017/S0022112098002432.

[30] Robert H. Kraichnan. The structure of isotropic turbulence at very high Reynolds numbers. *Journal of Fluid Mechanics*, 5(4):497–543, 1959. URL https://doi.org/10.1017/S0022112059000362.

[31] Y. Kuramoto. *Chemical Oscillations, Waves, and Turbulence*. Springer Series in Synergetics. Springer Berlin Heidelberg, 1984. ISBN 9783642696893. URL http://dx.doi.org/10.1007/978-3-642-69689-3.

[32] Carlo R. Laing. The dynamics of chimera states in heterogeneous Kuramoto networks. *Physica D: Nonlinear Phenomena*, 238(16):1569 – 1588, 2009. ISSN 0167-2789. URL http://doi.org/10.1016/j.physd.2009.04.012.

[33] P.L. Lions. *Mathematical Topics in Fluid Mechanics: Volume 1: Incompressible Models*. OUP Oxford, 2013. ISBN 9780199679218.

[34] P. Manneville. *Instabilities, Chaos and Turbulence*. ICP fluid mechanics. Imperial College Press, 2010. ISBN 9781848163928. URL http://www.worldscientific.com/worldscibooks/10.1142/p642.

[35] Seth A. Marvel and Steven H. Strogatz. Invariant submanifold for series arrays of Josephson junctions. *Chaos: An Interdisciplinary Journal of Nonlinear Science*, 19(1):013132, 2009. doi: 10.1063/1.3087132. URL https://doi.org/10.1063/1.3087132.

[36] Seth A. Marvel, Renato E. Mirollo, and Steven H. Strogatz. Identical phase oscillators with global sinusoidal coupling evolve by Moebius group action. *Chaos: An Interdisciplinary Journal of Nonlinear Science*, 19(4):043104, 2009. URL https://doi.org/10.1063/1.3247089.

[37] L. Moriconi. Instanton theory of Burgers shocks and intermittency. *Phys. Rev. E*, 79:046324, Apr 2009. URL https://doi.org/10.1103/PhysRevE.79.046324.

[38] B. P. Murray and M. D. Bustamante. Energy flux enhancement, intermittency and turbulence via Fourier triad phase dynamics in 1D Burgers equation. *ArXiv e-prints*, May 2017. URL http://adsabs.harvard.edu/abs/2017arXiv170508960M.

[39] Alan C. Newell, David A. Rand, and David Russell. Turbulent transport and the random occurence of coherent events. *Physica D: Nonlinear Phenomena*, 33(1):281 – 303, 1988. ISSN 0167-2789. URL https://doi.org/10.1016/S0167-2789(98)90022-7.

[40] Koji Ohkitani and Shigeo Kida. Triad interactions in a forced turbulence. *Physics of Fluids A: Fluid Dynamics*, 4(4):794–802, 1992. URL https://doi.org/10.1063/1.858296.

[41] R. Örlü, A. Talamelli, M. Oberlack, and J. Peinke. *Progress in Turbulence VII: Proceedings of the iTi Conference in Turbulence 2016*. Springer Proceedings in Physics. Springer International Publishing, 2017. ISBN 9783319579344. URL https://doi.org/10.1007/978-3-319-57934-4.

[42] Edward Ott and Thomas M. Antonsen. Low dimensional behavior of large systems of globally coupled oscillators. *Chaos: An Interdisciplinary Journal of Nonlinear Science*, 18(3):037113, 2008. URL http://dx.doi.org/10.1063/1.2930766.

[43] Mark J Panaggio and Daniel M Abrams. Chimera states: coexistence of coherence and incoherence in networks of coupled oscillators. *Nonlinearity*, 28(3):R67, 2015. URL http://stacks.iop.org/0951-7715/28/i=3/a=R67.

[44] Arthur Pewsey. The wrapped stable family of distributions as a flexible model for circular data. *Computational Statistics & Data Analysis*, 52(3):1516–1523, 2008. ISSN 0167-9473. URL https://doi.org/10.1016/j.csda.2007.04.017.

[45] Arkady Pikovsky and Michael Rosenblum. Partially integrable dynamics of hierarchical populations of coupled oscillators. *Phys. Rev. Lett.*, 101:264103, Dec 2008. URL https://doi.org/10.1103/PhysRevLett.101.264103.

[46] Arkady Pikovsky and Michael Rosenblum. Dynamics of globally coupled oscillators: Progress and perspectives. *Chaos: An Interdisciplinary Journal of Nonlinear Science*, 25(9):097616, 2015. URL https://doi.org/10.1063/1.4922971.

[47] Arkady Pikovsky, Michael Rosenblum, and Jürgen Kurths. *Synchronization: A Universal Concept in Nonlinear Sciences*. Cambridge Nonlinear Science Series. Cambridge University Press, 2001. URL http://dx.doi.org/10.1017/CBO9780511755743.

[48] S.B. Pope. *Turbulent Flows*. Cambridge University Press, 2000. ISBN 9780521598866. URL http://www.cambridge.org/de/academic/subjects/physics/nonlinear-science-and-fluid-dynamics/turbulent-flows?format=PB&isbn=9780521598866.

[49] J. M. Reynolds-Barredo, D. E. Newman, P. W. Terry, and R. Sanchez. Fourier signature of filamentary vorticity structures in two-dimensional turbulence. *EPL (Europhysics Letters)*, 115(3):34002, 2016. URL http://stacks.iop.org/0295-5075/115/i=3/a=34002.

[50] Michael Rosenblum and Arkady Pikovsky. Self-organized quasiperiodicity in oscillator ensembles with global nonlinear coupling. *Phys. Rev. Lett.*, 98:064101, Feb 2007. URL https://doi.org/10.1103/PhysRevLett.98.064101.

[51] Ashis Sengupta and Chandranath Pal. On optimal tests for isotropy against the symmetric wrapped stable circular uniform mixture family. *Journal of Applied Statistics*, 28(1):129–143, 2001. URL http://dx.doi.org/10.1080/02664760120011653.

[52] Steven H. Strogatz. From Kuramoto to Crawford: exploring the onset of synchronization in populations of coupled oscillators. *Physica D: Nonlinear Phenomena*, 143(1):1 – 20, 2000. ISSN 0167-2789. URL https://doi.org/10.1016/S0167-2789(00)00094-4.

[53] Kwok Yeung Tsang, Renato E. Mirollo, Steven H. Strogatz, and Kurt Wiesenfeld. Dynamics of a globally coupled oscillator array. *Physica D: Nonlinear Phenomena*, 48(1):102–112, 1991. ISSN 0167-2789. URL https://doi.org/10.1016/0167-2789(91)90054-D.

[54] V. Venkatakrishnan, M.D. Salas, and S.R. Chakravarthy. *Barriers and Challenges in Computational Fluid Dynamics*. ICASE LaRC Interdisciplinary Series in Science and Engineering. Springer Netherlands, 2012. ISBN 9789401151696. URL https://doi.org/10.1007/978-94-011-5169-6.

[55] Fabian Waleffe. The nature of triad interactions in homogeneous turbulence. *Physics of Fluids A: Fluid Dynamics*, 4(2):350–363, 1992. URL https://doi.org/10.1063/1.858309.

[56] Chaoqing Wang and Nicolas B. Garnier. Continuous and discontinuous transitions to synchronization. *Chaos: An Interdisciplinary Journal of Nonlinear Science*, 26(11):113119, 2016. URL https://doi.org/10.1063/1.4968016.

[57] Michael Wilczek, Haitao Xu, Nicholas T Ouellette, Rudolf Friedrich, and Eberhard Bodenschatz. Generation of lagrangian intermittency in turbulence by a self-similar mechanism. *New Journal of Physics*, 15(5):055015, 2013. URL http://stacks.iop.org/1367-2630/15/i=5/a=055015.

[58] Michael Wilczek, Dimitar G. Vlaykov, and Cristian C. Lalescu. *Emergence of Non-Gaussianity in Turbulence*, pages 3–9. Springer International Publishing, Cham, 2017. ISBN 978-3-319-57934-4. URL https://doi.org/10.1007/978-3-319-57934-4_1.

[59] M Wolfrum, S V Gurevich, and O E Omelchenko. Turbulence in the Ott-Antonsen equation for arrays of coupled phase oscillators. *Nonlinearity*, 29(2):257, 2016. URL http://stacks.iop.org/0951-7715/29/i=2/a=257.

In principio erat Verbum,
et Verbum erat apud Deum,
et Deus erat Verbum.
Hoc erat in principio apud Deum.
Omnia per ipsum facta sunt,
et sine ipso factum est nihil,
quod factum est;
in ipso vita erat,
et vita erat lux hominum,
et lux in tenebris lucet,
et tenebrae eam non comprehenderunt.

Et Verbum caro factum est
et habitavit in nobis;
et vidimus gloriam eius,
gloriam quasi Unigeniti a Patre,
plenum gratiae et veritatis.

Acknowledgments

I would like to thank the Max Planck Research group on the Theory of Turbulent Flows for allowing me to work with them during my Master's thesis phase. Taking me in to their scientific life at the institute gave me the opportunity to work firsthand with professional and highly capable scientists. Additionally, I am thankful for their feedback on my work and assistance in presenting it eloquently. I would most specially like to thank my thesis supervisor Dr. Michael Wilczek for his support and very useful advice.
I also would like to thank the colleagues at the University of Rome 'Tor Vergata', Luca Biferale and Michele Buzzicotti, and at the University College Dublin, Miguel Bustamante and Brendan Murray, for useful discussions.
Finally, I would like to express the utmost gratitude to my friends and family. One does not study for vainglory. Nor because it is and end in and of itself. It is rather because one finds in oneself the gifts and talents which may be nurtured by this human endeavor and thus put to the disposition of others.

Erklärung Ich versichere hiermit, dass ich die vorliegende Arbeit ohne fremde Hilfe selbstständig verfasst und nur die von mir angegebenen Quellen und Hilfsmittel verwendet habe. Wörtlich oder sinngemäß aus anderen Werken entnommene Stellen habe ich unter Angabe der Quellen kenntlich gemacht. Die Richtlinien zur Sicherung der guten wissenschaftlichen Praxis an der Universität Göttingen wurden von mir beachtet. Eine gegebenenfalls eingereichte digitale Version stimmt mit der schriftlichen Fassung überein. Mir ist bewusst, dass bei Verstoß gegen diese Grundsätze die Prüfung mit nicht bestanden bewertet wird.

Göttingen, den January 11, 2018

(José-Agustín Arguedas-Leiva)